Production, Characterization and Testing of Tempered Martensite Assisted Steels (TMAS) obtained via Subcritical Annealing of Cold Rolled TRIP Steels

By

Vikram Jayaraman

A Thesis Submitted to the Faculty of Graduate Studies and Research in Partial Fulfillment of the Requirements for the Degree of Master of Engineering

Department of Mining, Metals and Materials Engineering

McGill University

Montreal, Canada

January 2007

Your file Votre référence
ISBN: 978-0-494-32597-1
Our file Notre référence
ISBN: 978-0-494-32597-1

Abstract

The requirement for lighter, safer and fuel efficient cars has created a major stir in the steel research society to develop advanced automotive steels. Since there is a trade off between strength and ductility, most of the conventional high strength steels do not address the strength-formability combination. With the realization of the TRIP phenomenon first in austenitic stainless steels, a new generation of advanced steels called TRIP steels were realised with an inexpensive and easier to process C-Mn-Si chemistry. TRIP or **TR**ransformation **I**nduced **P**lasticity is a phenomenon where the timely strain induced transformation of Retained Austenite (RA) to Martensite locally strengthens the steel at the point of plastic instability, causing failure by necking to be postponed and shifted elsewhere along the steel. This phenomenon repeated over and over again allows increased levels of strength and ductility, prior to fracture.

In current TRIP grades, the retained austenite particles present have to posses certain characteristics such as, optimum carbon concentration, optimum grain size and morphology etc. in order to account toward mechanical properties. Such limiting characteristics in turn minimize the processing window and make TRIP processing expensive and difficult to control. In this work, it is suggested that Tempered Martensite Assisted Steels (TMAS) obtained from TRIP steels via subcritical annealing of cold rolled TRIP steels may potentially replace TRIP steels. Relationship between the retained austenite volume fractions and mechanical properties was developed for TRIP steels. The effect of variation of retained austenite on tempered martensite volume fraction in TMAS, which in turn affect the mechanical properties was also investigated in depth. Results indicate that tempered martensite particles in TMAS do not have any limiting factors as in the case of RA in TRIP steels, in order to contribute toward enhancement of mechanical properties. Results also indicate that TMAS offers better strength levels compared to TRIP steels for same the level of formability.

Retained austenite volume fractions in TRIP steels were measured through XRD. Cold rolling of the samples was done in a laboratory scale rolling machine. The microstructures were analysed using conventional and color etching techniques. A new color etching technique for viewing all the four major phases in TRIP steel was developed in this work. The mechanical properties of both TRIP and TMAS were assessed by shear punch testing. And finally, the relationship between tempered martensite volume fraction and TMAS properties was developed and was compared to TRIP properties.

Résumé

L'exigence pour des véhicules plus légers, sécuritaires et économiques a engendré le développement d'aciers avant-gardistes pour l'industrie automobile. Étant donné qu'il y a un compromis entre l'augmentation de la résistance et la ductilité, la majorité des aciers conventionnels à haute résistance ne satisfont plus à la condition d'une bonne combinaison de résistance et de formabilité. Avec la réalisation du phénomène TRIP (**TR**ansformation **I**nduced **P**lasticity) premièrement dans les aciers inoxidables austénitiques, une nouvelle génération d'aciers TRIP ont été conçus avec un procédé non coûteux et simple contenant les éléments C-Mn-Si. Le phénomène TRIP s'explique par le fait que la déformation instantanée, qui induit la transformation de l'austenite retenue (RA, Retained Austenite) en martensite, renforce l'acier au moment de l'instabilité plastique et de ce fait repousse la rupture par striction à une plus grande déformation. Ce phénomène répété plusieurs fois permet d'augmenter la résistance et la ductilité avant la rupture.

Les particules d'austénite retenue présentes dans les aciers TRIP actuels doivent, afin d'améliorer les propriétés mécaniques, posséder certaines caractéristiques telles que une concentration optimale de carbone, une taille de grains et une morphologie optimales etc. Ces limitations minimisent à leur tour la flexibilité d'opération et rendent la fabrication des aciers TRIP coûteuse et difficile à contrôler. Dans ce travail, il est suggéré que les aciers TMAS (Tempered Martensite Assisted Steels, Aciers Assistés par la Martensite Revenue) obtenus à partir des aciers TRIP laminés à froid et revenus à une température sous-critique pourraient éventuellement remplacer les aciers TRIP. Une relation entre la fraction volumique de l'austénite retenue et les propriétés mécaniques a été développée pour les aciers TRIP. De plus, l'idée selon laquelle la variation de l'austénite retenue affectant la fraction volumique de la martensite revenue dans les aciers TMAS qui à son tour affecte les propriétés mécaniques a profondément été analysée. Les résultats indiquent que les particules de martensite revenue dans les aciers TMAS ne sont pas un facteur limitant, comme c'est le cas dans les aciers TRIP, à la contribution de l'amélioration des propriétés mécaniques. Les résultats ont aussi démontré que les aciers TMAS offrent des niveaux de résistance supérieurs comparés aux aciers TRIP pour des degrés équivalents de formabilité.

Les fractions volumiques d'austénite retenue dans les aciers TRIP ont été mesurées à l'aide de la diffraction par rayons-X. Le laminage à froid a été effectué sur une machine à échelle de laboratoire. Les microstructures ont été analysées à l'aide de techniques d'attaques chimiques conventionnelles et par codage de couleur. Une nouvelle technique d'attaque chimique par codage de couleur qui permet de distinguer les quatre phases majeures des

aciers TRIP a aussi été développée. Les propriétés mécaniques des aciers TRIP et TMAS ont été obtenues à l'aide d'essais à poinçon de cisaillement. Et finalement, la relation entre la fraction volumique de la martensite revenue et les propriétés des aciers TMAS a été développée et ensuite comparée aux propriétés des aciers TRIP.

Acknowledgements

I would like to extend my sincere gratitude to my thesis supervisor, Prof. Stephen Yue for giving me the opportunity to work toward this AUTO 21 NEW Generation Steels (NGS) project. I would also like to thank him for his unconditional support and technical expertise throughout the course of this project. In addition, I would like to express my gratitude to AUTO 21 for extending financial support to this project.

I am grateful to Dr. Elhachmi Essadiqi of Materials Technology Laboratory, CANMET, Ottawa for providing the experimental steels and offering valuable guidance during the course of this project. I would also like to thank Dr. Abdel Elwazri, Dr. Faramarz Zarandi, Dr. Rocco Varrano and Mr. Edwin Fernandez for their help with sample preparation and testing. I would also like to use this opportunity to express my sincere gratitude to Mr. Roman Huppee and Mr. Francesco Mariani for reviewing and proof reading my thesis work.

And many thanks to my fellow graduate students, especially, Geoff, Geremi, Sean, Umu and Jinbo for making my time here in McGill most fruitful and memorable. Last but not the least, I would like to extend my sincere gratitude and appreciation to my family without whose help I would not have been able to travel across two different oceans and pursue advanced degree here at McGill University.

Table of Contents

List of Figures

List of Tables

CHAPTER 1

Introduction

The requirement for safer and lighter cars has brought about extensive research and development in advanced automotive steels spectrum. The discovery and exploitation of TRIP (**TR**ansformation **I**nduced **P**lasticity) assisted multiphase steels in the recent past has led to a balance of strength and ductility which is a significant improvement over other competitive materials such as dual phase steel, Interstitial Free (IF) steel, Al and Mg based alloys. Among the aforementioned automotive materials TRIP steels offer the best performance and have been the focus of research for many years now.

With controlled thermo-mechanical processing of TRIP steels, high values of tensile strength (above 1200 MPa) and ductility (20 to 55%) can be achieved. Such an exceptional balance of strength and ductility in these steels is attributed to its multiphase microstructure, consisting of retained austenite and bainite dispersed in a matrix of ferrite. The high ductility and strength achieved in these steels are due to the transformation of metastable retained austenite to martensite during straining. The phenomenon of transformation of metastable retained austenite into martensite during straining is termed as Strain Induced Transformation (SIT). This transformation is accompanied by a volume expansion and results in a localized increase of the strain hardening coefficient during straining, thereby delaying necking and increasing total elongation [1].

Conventional low alloyed TRIP steels contain substantial levels of Si (usually more than 1%), in order to retain austenite in the final microstructure by prohibiting cementite formation during cooling [2]. Unfortunately, high Si additions result in a very strong surface oxide layer which is difficult to remove and pose severe surface problems during hot dip galvanizing. This results in poor paintability and also accounts for corrosion issues during service [3].

Since aluminum works in many ways similar to Si and does not contribute to any galvanizing problems it was introduced in lieu of silicon in TRIP steels. Replacement of Al by Si in TRIP steels reduced a number of coating and galvanizing problems and they are used in a wide variety of automotive applications [3].

However, the quest for stronger, lighter and easy to fabricate materials is keeping steel researchers on their toes till date. With design and safety restrictions getting more stringent with time, the need for more stronger and crashworthy material without compromising formability has increased considerably. Steel researchers are working towards creating new steel grades that would push the strength-formability boundary set by the TRIP steels. Figure 1.1 is a schematic representation of automotive steels placed relative to each other on the basis of their mechanical properties. One can notice that TRIP steels show an exceptional balance of strength and ductility compared to other contemporary automotive steels. However, contemporary steel researchers focus on creating new steel grades whose mechanical properties will be encompassed by the area above the TRIP steels, indicated by the oval region in the diagram. Such new steels would posses excellent strength-ductility balance and would be the favored choice for automotive applications.

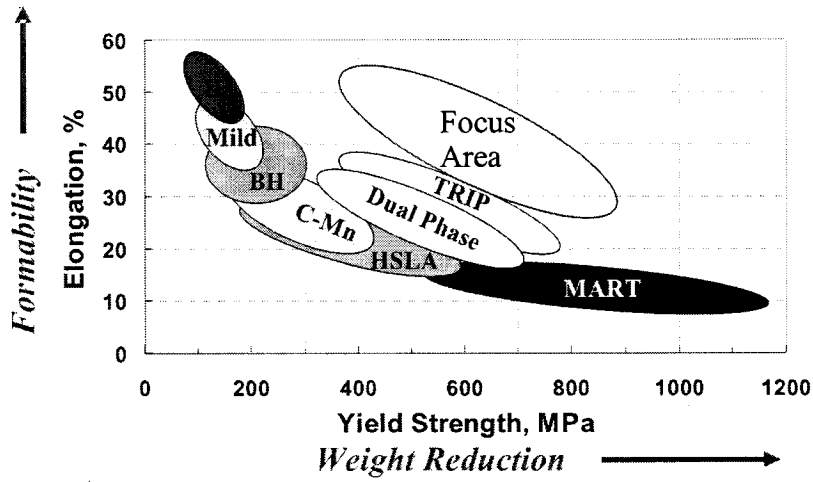

Figure 1.1 Schematic representation of strength/formability balance of all automotive steels

In contrast to recent studies on TRIP steels, which concentrate on achieving the desired mechanical properties only by altering the alloy chemistry and thermo-mechanical parameters, this work tries to put forward a new approach to utilize TRIP steels to produce a new steel grade called Tempered Martensite Assisted Steels (TMAS). TMAS is obtained via cold rolling a TRIP steel, thus creating strain induced martensite and subsequently subcritically annealing the structure to produce tempered martensite, recrystallized ferrite and bainite. The main crux of the project, then, was to develop a microstructure with martensite particles *not* obtained by quenching, since quenching brings in quenching issues such as internal stresses, warping and so on. Through such a novel method, this work tries to push the stringent strength-formability boundary set by TRIP steels.

Previous work by Jeong et al [4] on subcritical heat treatment of cold rolled Al containing TRIP steel was based on one TRIP microstructure and hence one retained austenite and one tempered martensite volume fraction. This study on the other hand aims at elucidating the influence of the variation of retained austenite and tempered martensite

volume fraction on microstructure and mechanical properties of TRIP and TMAS, respectively.

Chapter 2 presents a brief literature review on the processing and characteristics of TRIP steels. Topics included are TRIP steel basics, processing of TRIP steels, effect of alloying elements, characteristics of retained austenite. Efforts were also taken to introduce Tempered Martensite Assisted Steels (TMAS) to the reader since very little or no information is available on them.

Chapter 3 illustrates and describes the instrumentation and experimental setup utilized for processing TRIP and TMAS. The setup for characterization of microstructures and mechanical properties are also included.

Chapter 4 describes the experimental procedures and techniques utilized during the course of the investigation. TRIP annealing and subcritical annealing treatments were performed in radiant furnaces. Cold rolling was performed on a laboratory scale cold rolling mill. Mechanical properties were measured by shear punch technique and sample microstructures were characterized by optical microscopy and image analysis. Finally, the RA characteristics were determined by X-ray diffraction.

Chapter 5 presents the experimental results of the work. The effect of TRIP annealing parameters on the retained austenite volume fraction, retained austenite volume fraction on final properties of the TRIP steel, TRIP microstructure on SIT transformation are presented in this chapter. Finally, the effect of cold rolling of TRIP steels, subcritical annealing of the cold rolled structure, TMAS microstructural evolution and effect of tempered martensite volume fraction on final properties of TMAS is also presented.

The results are discussed in Chapter 6 and finally, the conclusions of this work are presented in Chapter 7.

CHAPTER 2

Literature Review

Classical quenched and tempered steels have long been used for high strength applications, especially in automotive and aerospace sector. Quenched and tempered steels exhibit exceptional strength values, but this increase in strength is brought about at the cost of uniform elongation [5]. Figure 2.1 shows engineering stress-strain curves of a number of automotive steels. One can notice from the Figure that with increasing strength levels, there is a significant decrease in the uniform elongation.

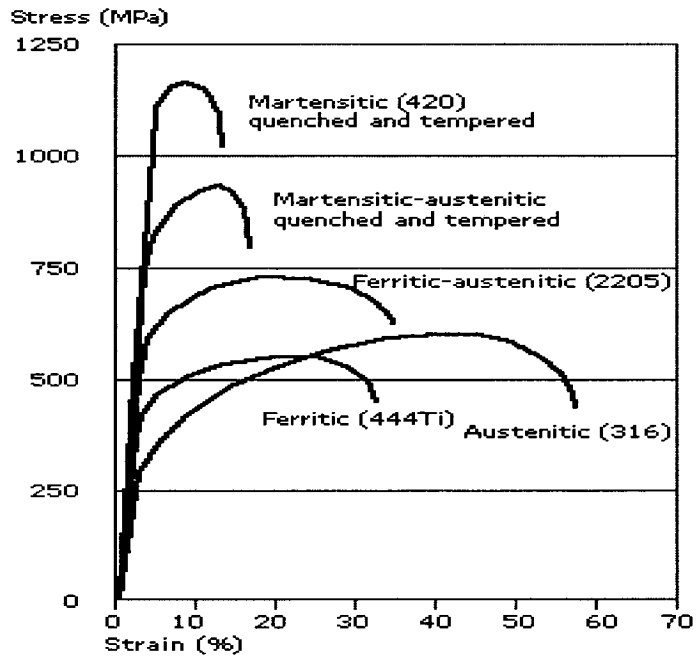

Figure 2.1 Engineering stress-strain curves of various steels [5]

Zackay et al [6] stated that the loss of uniform elongation is due to an inadequate strain hardening rate produced by dislocation interaction to compensate for the increased stress at the neck region. Such inability to prevent plastic instability results in low uniform and total elongation and hence, formability, keeping the use of high strength steels such as martensitic 420 to a minimum in automotive sector.

Extensive research was carried out to overcome this inherent problem with high strength steels, and the results indicated that the best way to tackle this issue was to find a way to produce obstacles harder than dislocation tangles to delay the onset of necking. Further, these obstacles have to be produced during deformation to strike a balance between plastic instability and strain hardening in the unstable region. Zackay et al [6] suggested that martensite plates would fulfill the first requirement and they can also be formed from metastable retained austenite during deformation, thus serving the second requirement.

The mechanism by which metastable retained austenite transforms to martensite is called Strain Induced Transformation (SIT) and the phenomenon by which the strength and ductility of the steel increases during deformation is called Transformation Induced Plasticity (TRIP). Steels that exhibit the TRIP phenomena are termed as TRIP steels and their high strength leads to better crash/dent resistance, weight reduction and improved fuel efficiency. Their high formability leads to better aesthetic shapes and design at a favorable cost; thus they are of high interest to today's automotive sector [7].

2.1 TRIP Steel Processing

TRIP steels are processed in two varieties, as hot rolled and cold rolled and annealed. A brief description on the two varieties is given below.

2.1.1 As hot rolled TRIP steels

As hot rolled TRIP steels are produced by following the Thermomechanical Processing (TMP) route shown in Figure 2.2.

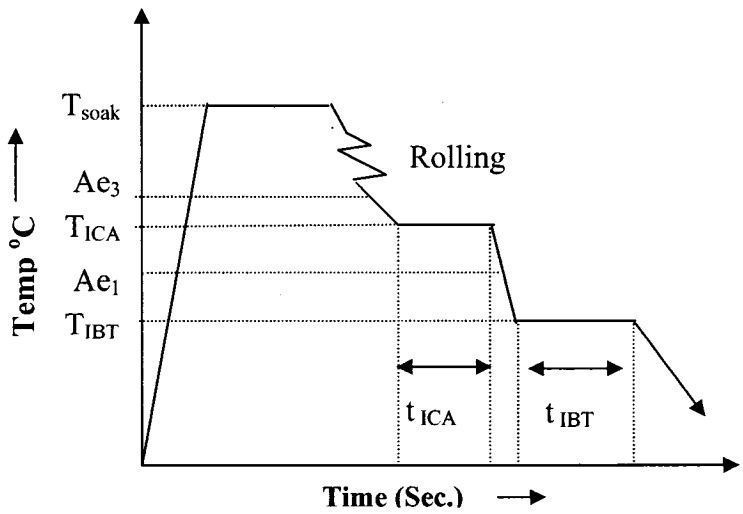

Figure 2.2 Hot Band TRIP steel processing [7]

In hot band TRIP processing, the slabs are first reheated and soaked at a well chosen high temperature T_{SOAK}, well into the austenite regime, followed by roughing and finishing deformation at decreasing temperature. The deformation is contained in the austenite region for maximum reduction in thickness and uniform deformation. Then, the material is Intercritically Annealed (ICA) at T_{ICA} for some time t_{ICA}. Where, T_{ICA} is higher than Ae_1 (the end of the austenite transformation) and lesser than Ae_3 (the start of the austenite transformation). The material is then rapidly cooled to a temperature T_{IBT} ~300-500°C for the Isothermal Bainitic Transformation (IBT). At T_{IBT}, much of the intercritical austenite transforms to bainitic ferrite (preferably) or bainite (undesirably). Also, during the rapid cool from T_{ICA} to T_{IBT}, little of the intercritical austenite transforms to ferrite or pearlite. The material is coiled at this isothermal bainite transformation temperature. The coil is then cooled to room temperature, and some of the austenite is still retained, leading to a complex microstructure consisting of intercritical ferrite, epitaxial ferrite, bainite/bainitic ferrite, retained austenite, and perhaps small amounts of pearlite or martensite [8].

In the laboratory, the isothermal bainite transformation is usually done for a stipulated amount of time, termed t_{IBT} to simulate coiling and obtain a multiphase microstructure.

2.1.2 Cold Rolled and Annealed

The cold rolled and annealed method is conveniently used for producing sheets of thinner gauge and the sheets can be processed through either continuous annealing line or continuous hot dip galvanizing lines that contain a proper section for performing the isothermal bainite transformation [9, 10]. The processing path is shown Figure 2.3. The material is hot rolled in the austenite range, then cooled to room temperature (resulting in a ferrite + pearlite structure). The material is cold-rolled at this point to desired thickness. The steel is then reheated in the galvanizing lines to T_{ICA}. During this intercritical anneal, which is typically >~60 seconds austenite will form. This results in an $\alpha+\gamma$ intercritical structure, which is then cooled rapidly to the isothermal bainite hold at T_{IBT}. The steel sheets emerging out from the galvanizing line has the TRIP microstructure.

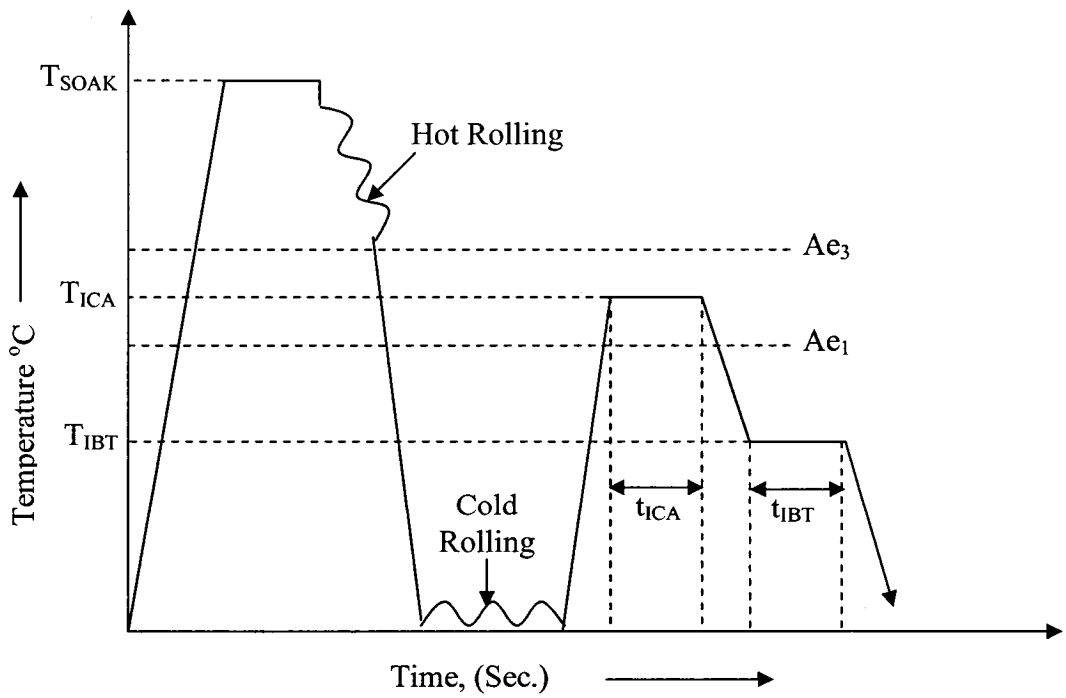

Figure 2.3 CAL/CGL TRIP steel sheet processing [9]

2.2 Microstructural Evolution during TRIP annealing

2.2.1 Intercritical Annealing:

The main objective of the intercritical annealing is to introduce a two-phase ($\alpha+\gamma$) microstructure which is eventually converted into the TRIP microstructure. There are three important parameters of this stage; intercritical annealing temperature, time and cooling rate to the bainite holding temperature. Any change in the above parameters will vary the amount of retained austenite and its stability against strain-induced transformation.

The optimum intercritical annealing temperature for TRIP steels in general has been a subject of debate for some years. Mahieu et al [11] and Chen et al [12] suggested that a temperature where there is a 50:50 split of austenite to ferrite volume fraction as the optimum intercritical temperature. Other researchers such as Zhao et al [13] advocate 70:30 ratio of austenite to ferrite volume fraction for optimum final properties. On the other hand, Sakuma et al. [14], Jacques et al [15] and Hanzaki et al [16] found that a lower temperature just above the Ae_1 temperature, would lead to optimum retained austenite fraction and the best combination of strength and ductility. By combining these propositions one can ascertain that the optimum intercritical annealing temperature lies between the 50:50 temperature and Ae_1 temperature. In general, a higher intercritical annealing temperature leads to more austenite with lower carbon concentration, and vice versa [17]. This is shown in Figure 2.4 for 0.16C-1.5Mn-0.4Si TRIP steel.

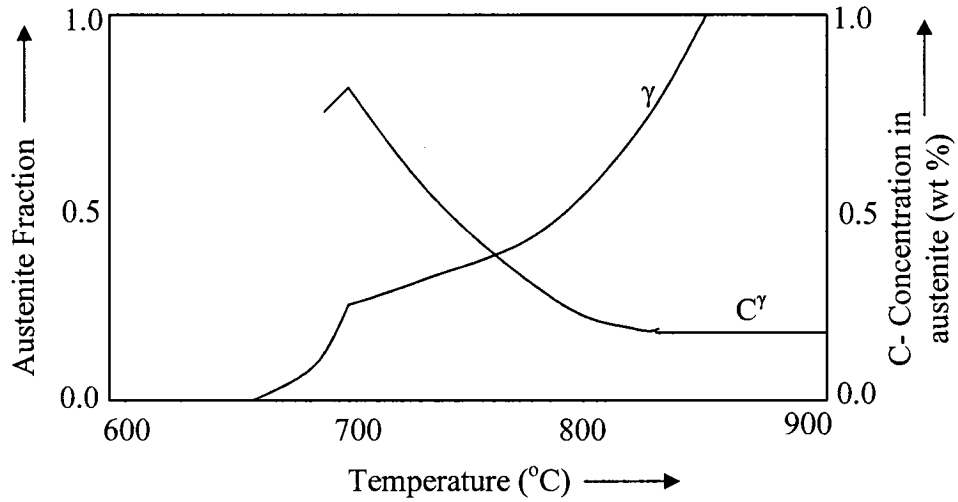

Figure 2.4 Temperature dependence of austenite volume fraction and carbon concentration in austenite (Cγ, in wt %) in 0.16C-1.5Mn-0.4Si steel, calculated from ortho-equilibrium thermodynamic analysis [14].

Increasing the intercritical annealing temperature close to A_{e3} temperature increases the austenite volume fraction. However, such high intercritical austenite volume fraction does not guarantee high retained austenite volume fraction in the final TRIP microstructure. The final retained austenite volume fraction is a strong function of, (i) the size of intercritical austenite and (ii) the carbon content of the austenite at the intercritical temperature. The smaller the austenite size, the better the chance of retention because the possibility of finding a nucleation site for ferrite is small; increasing C content increases the stability of austenite by increasing hardenability.

At higher intercritical temperatures the size of the intercritical austenite increases and the carbon content of the austenite decreases, and both increase the martensite start (M_s) temperature of austenite. Both the factors promote the formation of martensite during cooling to the isothermal bainite transformation regime. On the other hand, when the annealing temperature is decreased close to the Ae_1, the nucleation of austenite dominates over the growth, so the size of austenite particle is small and the carbon concentration in austenite approaches the maximum equilibrium state, resulting in an increased possibility of retention of austenite [18]. But, too low a temperature, close to

Ae_1 or insufficient holding time at this temperature can result in an unrecrystallized microstructure and undissolved cementite, the latter may result in not enough austenite formed for subsequent bainitic transformation [19].

Figure 2.5 shows the kinetics of austenite phase formation. As expected the austenite kinetics are much more strongly influenced by temperature rather than time.

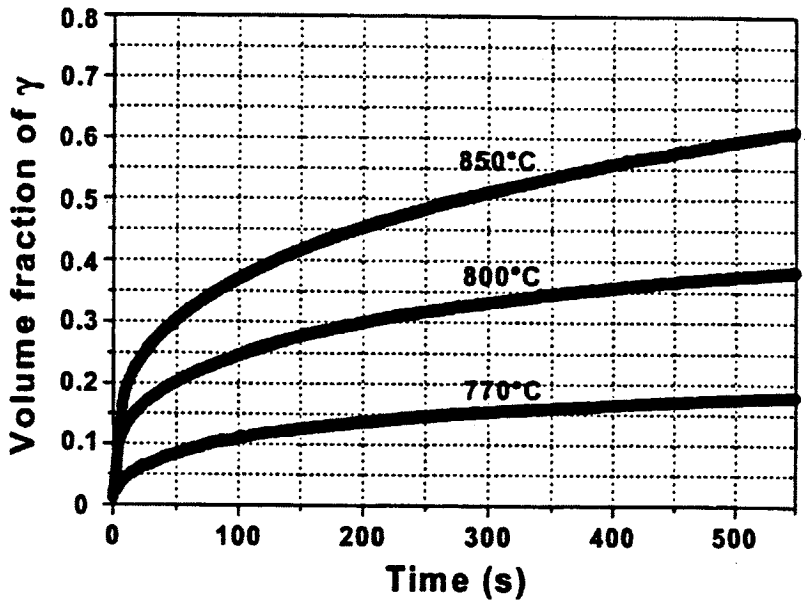

Figure 2.5 Kinetics of the austenite phase formation at different ICA temperatures for the 1.7% Al C-Mn-Al [19]

Pichler et al. [20] studied the effect of intercritical annealing temperature on retained austenite volume fraction and final properties by keeping all other parameters such as cooling rate and isothermal bainitic transformation temperature constant. He determined that there exists only a minor impact on the microstructure, and by increasing the ICA temperature only the shape of the retained austenite changes to a more plate like appearance, while its content remained almost unaffected.

2.2.2 Cooling Rate

Generally, in industrial situations, the range of cooling rates available in Continuous Annealing Lines (CAL) is defined by the line speed, quenching and isothermal bainitic transformation temperature. Coldren et al. [21] reported that a there was no significant influence of the cooling rate on the microstructure of 0.16C-1.5Mn-1.5Si TRIP above 10°K s^{-1}. However, at 10°K s^{-1} there was a significant decrease in retained austenite when isothermal bainite temperatures were <450 °C (Figure 2.6), presumably because there was less austenite retained immediately after attaining the isothermal bainite temperature. This resulted in a slight increase in total elongation with a slight decrease in yield and tensile strength for the investigated TRIP steel.

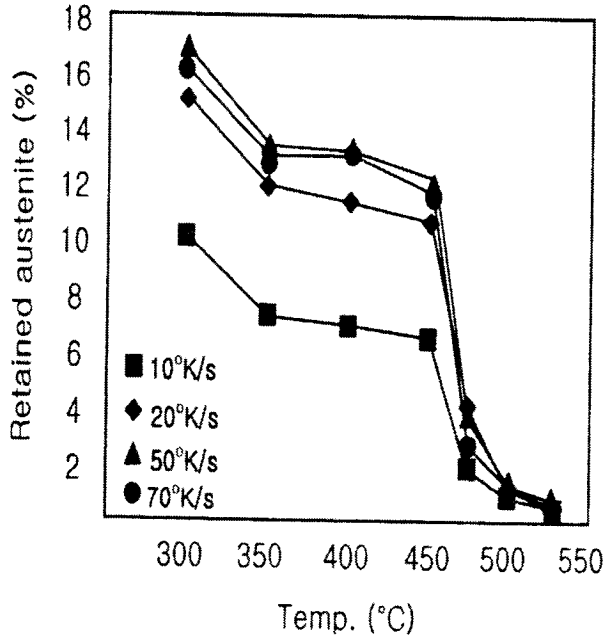

Figure 2.6 Influence of Isothermal bainitic transformation temperature and cooling rate on the final retained austenite volume fraction [21]

2.2.3 Isothermal Bainitic Transformation (IBT)

One of the most important steps during the processing of TRIP steels is the enrichment of carbon in austenite due to bainitic ferrite formation and prevention of cementite precipitation. A detailed investigation on the transformation of intercritical austenite during bainite formation was carried out by Chen et al [22]. Figure 2.7 is a schematic representation of the isothermal transformation process.

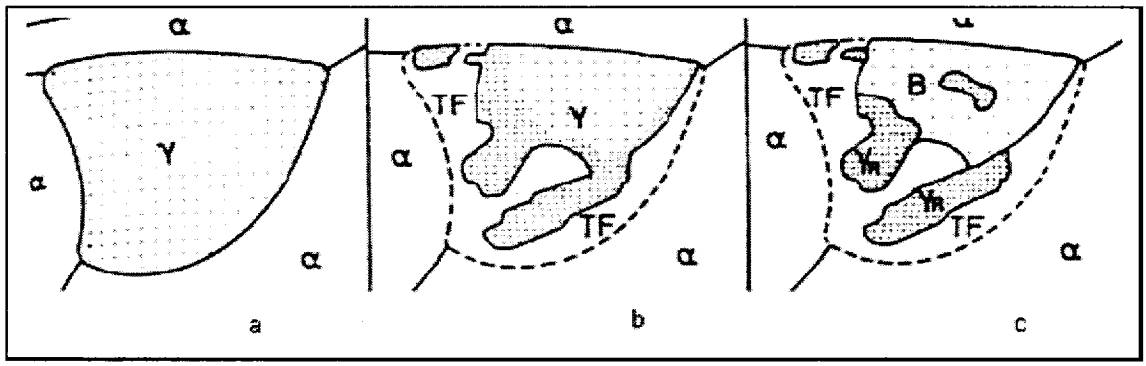

Figure 2.7 Schematic representation of transformation of intercritical austenite to epitaxial ferrite (TF), bainite (B) and retained austenite [22]

Chen et al [22] also reported that the intercritical austenite when quenched to the bainite temperature and held, becomes unstable and starts to transform to epitaxial ferrite by rejecting carbon into the surrounding metastable austenite, as shown in Figure 2.7. The increasing black dots in Figure 2.7b and 2.7c represent carbon segregation. As time passes, the unstable intercritical austenite starts transforming to bainitic ferrite as shown in Figure 2.7c. Extensive carbon segregation in the remaining austenite results in increased austenite stability which in turn reduces the Ms temperature of such enriched austenite below room temperature. Such highly enriched intercritical austenite is retained in the final microstructure as retained austenite. The steel is then air cooled to room temperature, leading to a final microstructure of intercritical ferrite, epitaxial ferrite, bainitic ferrite, retained austenite and little or no martensite.

According to Traint et al. [23], at high bainite temperatures, coarse bainite formation and a tendency toward carbide formation is observed. This plunders the carbon concentration from the intercritical austenite, resulting in reduction and stability of room temperature retained austenite. At low temperatures the transformation kinetics is quite slow and the transformation may not be completed. Thus, there is an optimum bainite temperature that would yield an optimum retained austenite volume fraction with a good stability. This optimum temperature has been found to be 400°C for most conventional TRIP

steels. However, it is not clear as to how this is affected by the cooling rate to the isothermal bainite temperature.

In general, the isothermal transformation in the bainite regions promotes the retention of austenite and the degree of austenite retention is usually the result of two competing phenomena, namely, the decomposition of austenite to bainite and decomposition of enriched austenite to carbide. The result of this competition leads to an observed maximum of retained austenite fraction at some intermediate temperature (350°C in this work). Hanzaki et al [24] and Chiro et al [25] have done extensive work in identifying the possible location of retained austenite in steels chemically similar to the one used in this work using color etching techniques. According to them, during the isothermal annealing stage, bainitic structure formed from the decomposition of two phase austenite starts to encapsulate the remaining austenite, enriching it with excess carbon. This bainite structure encapsulating the retained austenite resists the shear strains that accompany the martensite formation. As a result, the retained austenite particles become increasingly stabilized to SIT. The size and morphology of this bainitic structure depends on the isothermal annealing temperature. Bouet et al [26] showed that with increasing isothermal annealing temperature the thickness of the bainite platelets increased and its morphology became less acicular. He associated this change in morphology to low diffusion rate of carbon in front of the bainitic ferrite-austenite interface. Consequently, it was shown that the coarse bainitic structures encompassed lesser amount of retained austenite compared to fine bainitic structures formed at low isothermal temperatures. This was corroborated with the findings of Hanzaki et al [27] who observed low austenite retention at higher isothermal where the retained austenite phase had a film like morphology situated between the lamellas of coarse bainitic ferrite.

Vaisilakos et al [28] reported that for 0.18C-0.02Si-1.4Mn-1.58Al TRIP steel, at low bainite temperatures, the amount of austenite retained is significantly higher than those retained at higher bainite temperatures, which is in accordance to the findings of Bouet et al [29]. Figure 2.8 shows the influence of isothermal bainite transformation holding

temperature and time over the final retained austenite volume fraction. It was also showed that if the bainitic hold time is not long enough to finish the bainitic transformation of unstable intercritical austenite, the remaining austenite transforms to martensite during secondary cooling to room temperature, which was in accordance to the findings of other researchers [30, 31, 32]. However, if the holding time is too long, the unstable intercritical austenite converts completely to bainite and carbides, thus becoming more of dual phase ferrite-bainite steel. This would suggest that there is an optimum hold time for a given temperature, but this is not observed in Fig. 2.8.

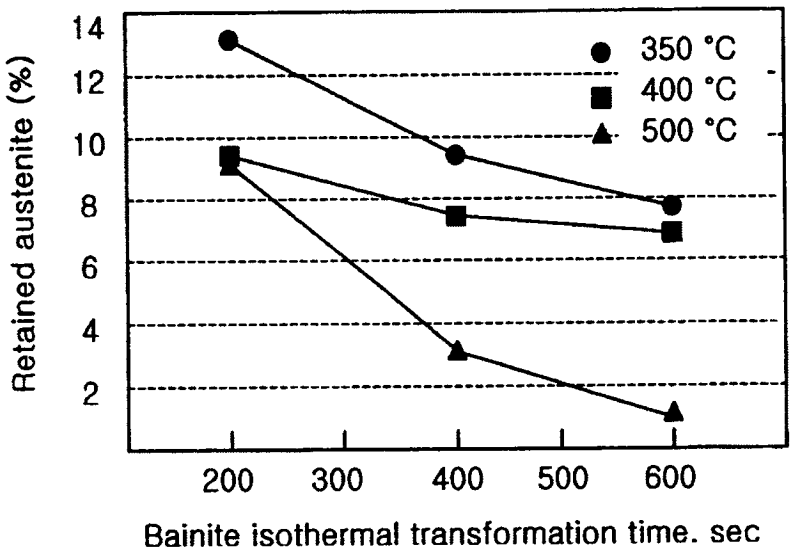

Figure 2.8 Influence of isothermal bainite transformation hold time on the final retained austenite volume fraction [32]

2.3 Effects of alloying elements

The major alloying elements found in low alloy TRIP steels are represented in Table 2.1. A brief introduction to the influences and drawbacks caused by the addition of alloying elements is also represented in the table. Figure 2.9 represents the fashion in which these alloying additions affect various phase transformation.

Table 2.1 Effects of alloying elements in low alloy TRIP steels [33]		
Alloying Element	**Effects/Influence**	**Possible Problems**
C (0.15 – 0.3)	• Austenite stabilizer. • Determines retained austenite stability.	• Weldablity. • Toughness reduction.
Mn (0.15 – 2.00)	• Austenite stabilizer. • Retards pearlite formation.	• Mn segregation in the form of bands in microstructure.
Si (0.1 – 1.50)	• Retards cementite formation.	• Poor surface. • Poor galvanizability.
Al (0.08 – 2.00)	• Retards cementite formation.	• Castablity.
P (0.01 - 0.30)	• Retards cementite formation.	• Toughness reduction. • Segregation issues.
Nb (0.04)	• Grain refinement. • Increases carbon in retained austenite. • Reduces Ms temperature.	• Carbide formation.
Cr, Mo (0.4)	• Retards pearlite formation.	• Carbide formation.
V (0.06)	• Precipitation hardening.	

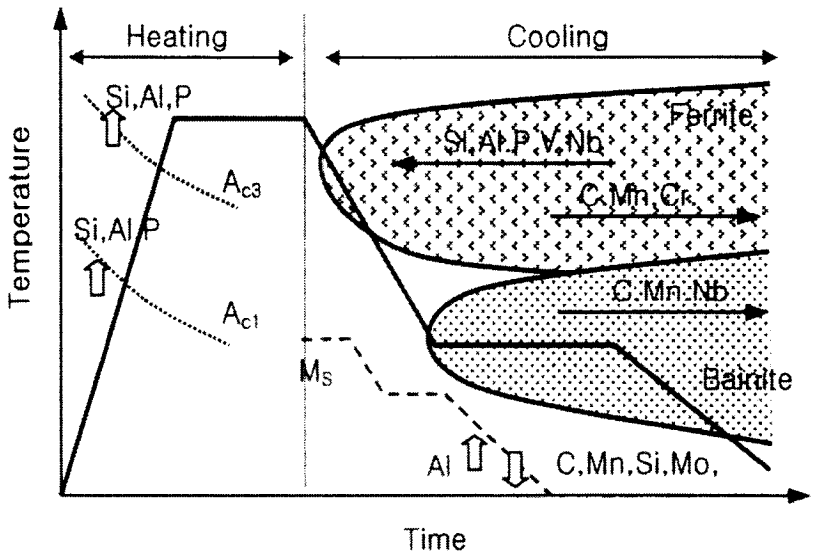

Figure 2.9 Influence of alloying elements on phase transformations [33]

Certain alloying elements such as C, Mn, Cr, Ni etc. have a direct effect on austenite retention and therefore a direct influence on TRIP properties. Other elements such as Si and P have an indirect effect via control of the carbide formation. However, they all have the same outcome. When added in sufficient quantities, a significant level of austenite is retained to room temperature by effectively lowering the Ms (Martensite transformation start temperature) and M_f (Martensite transformation finish temperature) temperatures to a marked degree.

The direct effect of elements such as C, Mn, Ni, Cr and N on TRIP mechanical properties were identified by Ludwigson et al [34]. They reported that elements such as C, Mn, Ni, Cr and N decrease the Ms temperature by solid solution strengthening of the intercritical austenite. Of these elements, interstitial C and N strengthened both austenite and any martensite derived from it to the greatest degree. Substitutional elements such as Mn, Ni, and Cr on the other hand, had much smaller effects on plastic flow behavior than the interstitial elements. Results from other researchers have also shown that strengthening of the austenite by solid solution hardening [35], and the increase in elastic constants of the austenite [36, 37, 38], hinders both the nucleation as well

as the growth of martensite. Since martensite follows a shear mechanism, strengthening elements in austenite solid solution offer a physical barrier to its progression, thereby limiting or even eliminating its occurrence [39, 40].

Elements that have an indirect effect on austenite retention are responsible for postponing pearlite and cementite formation; both thermodynamically and kinetically, increasing potential ferrite formation and austenite saturation with carbon. These elements include Si, Mo, Cr. Mn and Ni and they postpone cementite formation by their affinity for C and also contribute toward hardenability of the steel [41, 42].

In this work, the major alloying elements of interest are C, Al, Si and Mn. Their effects on the equilibrium and kinetics of the system are dealt individually below.

2.3.1 Effect of Aluminum and Silicon

As discussed before, both aluminum and silicon are ferrite formers. Their major role in TRIP steels is to retard the formation of carbides during bainite transformation by reducing the activity of carbon [43]. Figure 2.10 shows how the addition of Si shifts the CCT curve of a 0.2%C-1.0%Si-1.5%Mn TRIP steel favorably to inhibit pearlite formation during cooling leaving carbon in solution for austenite enrichment. One can also observe from the Figure that an increase in Si content by 1.0% not only inhibits pearlite formation but also increases the bainite window, which renders the processing of TRIP steels easier by increasing the range of cooling rates. Aluminum is being considered as a promising alternate for silicon since it does not pose any surface problems during galvanizing. It has been cited in literature that aluminum, though as good as silicon in inhibiting carbide precipitation, offers small solid solution strengthening effect (25 MPa), compared to silicon (83 MPa). Hence it is detrimental to the strength-ductility balance of the steel when it substitutes for Si completely [44, 45, 46].

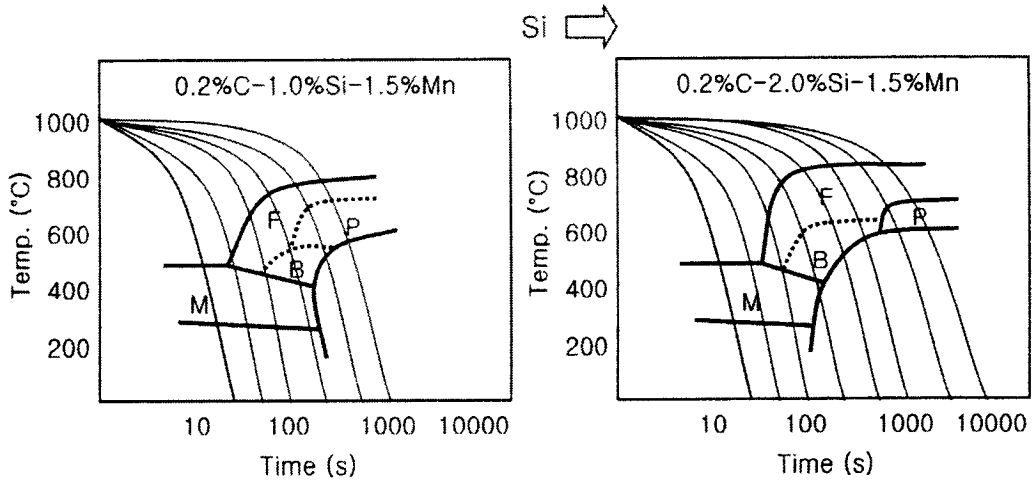

Figure 2.10 Change in CCT curve as function of Si level [47]

2.3.2 Effect of Carbon

Carbon is an austenite stabilizer and it is generally accepted that it is the most potent in increasing the hardenability among all the alloying elements. It has also been established that the carbon content in austenite solid solution strongly influences the retention of austenite [48]. Increasing the carbon content restricts the growth of polygonal ferrite and increases the fraction of granular bainite in the microstructure, widely affecting the UTS and ductility of the steel [49], Figure 2.11. Also, it has been shown that the transition temperature from upper to lower bainite decreases with increasing carbon content. Chiro et al. [50] reported that

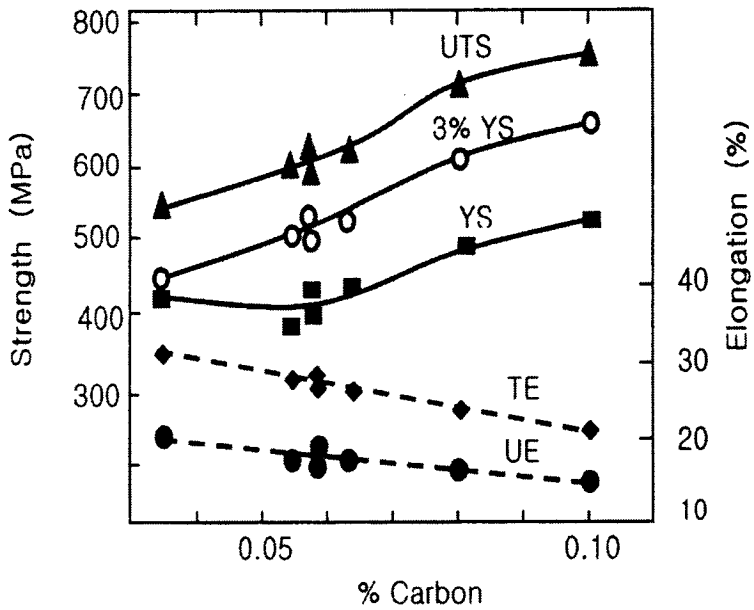

Figure 2.11Effect of carbon content on the mechanical properties of hot rolled dual phase steel [48]

with increasing carbon content, the UTS and the retained austenite volume fraction of the TRIP steel increased.

2.3.3 Effect of Manganese

Manganese, similar to carbon, is an austenite stabilizer. It reduces both the Ae_3 and Ae_1 transition temperatures, and reduces the width of the intercritical region, thereby stabilizing the austenite over a wider temperature and carbon compositional range [52]. It has also been reported that it lowers the activity coefficient of C and N, and postpones carbide formation, thereby increasing the solubility of the cementite in austenite [52, 53].

Additionally, with respect to CCT curves, an increase in Mn content by 0.5% in 0.2C-1.5Si-1.5Mn TRIP steel increases the processing window for generating optimum ferrite and retained austenite by reducing the cooling rates needed to avoid pearlite. This is shown in Figure 2.12.

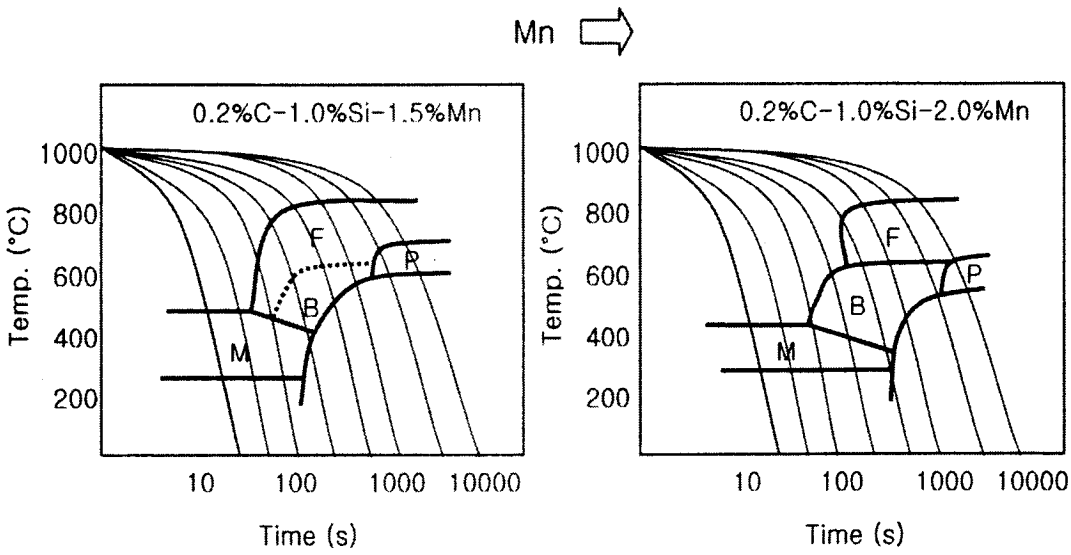

Figure 2.12 Change in CCT curve as function of Mn level [54]

2.4 Retained Austenite Characteristics

The straightforward way to quantify RA stability is through the Ms temperature [55]; the lower the Ms temperature, the higher the stability. This in turn depends on the carbon content of the steel. With regard to strain induced transformation, stability of the retained austenite is also profoundly affected by its morphology, the phases surrounding it, deformation temperature and strain rate [57]. Only morphology and effect of other phases surrounding RA will be covered in this section since these are the two parameters explored in this thesis.

2.4.1 RA Morphology and Effect of Surrounding Phases

Sugimoto et al [58] processed a 0.17C-1.41Si-2.00Mn steel to produce three different retained austenite morphology. "Type I" produced austenite islands in ferrite and/or bainite matrix and/or between ferrite-bainite junction. "Type II" produced narrow austenite films along bainite lath boundaries and "type III" produced acicular austenite islands in a ferritic matrix. Compared to the other two types, the type II steel (Figure 2.13) exhibited poor mechanical properties, especially elongation. This was attributed to high hydrostatic pressure exerted on the retained austenite films by the surrounding phases in the type II steels.

Nishiyama et al [59] stated that the hydrostatic pressure basically compresses the atoms, and thus their atomic orbital, modifying their transformation behavior and consequently lowering the Ms temperature of the steel. Sugimoto et al [60] proposed that the hydrostatic pressure exerted by the surrounding phases in Type III and Type II are 900 MPa and 1560 MPa, respectively. They associate such high hydrostatic pressures of film like Type II RA to the thickness and stiffness of the surrounding bainitic ferrite platelets. Such stiff surrounding platelets in case of Type II and stiff surrounding phases in case of Type III resist the volume expansion that accompanies the martensitic transformation and consequently inhibits the SIT or retained austenite.

Also, when accounting for compositional differences, Sugimoto et al. [60] estimated the type II Ms to be 70-110°C lower than the other materials. The martensitic transformation is a shear transformation, and the back-stress exerted by the surrounding phases makes the shearing of the retained austenite particle inherently difficult. As a result, the transformation is suppressed to lower Ms temperature values and a higher driving force (proportional to undercooling) is required to overcome the imposed stress by shearing. As a result, the retained austenite in the type II steel will be overly stable, resulting in the poor observed elongations. The steel is thus not a TRIP-steel, despite its large fraction of retained austenite.

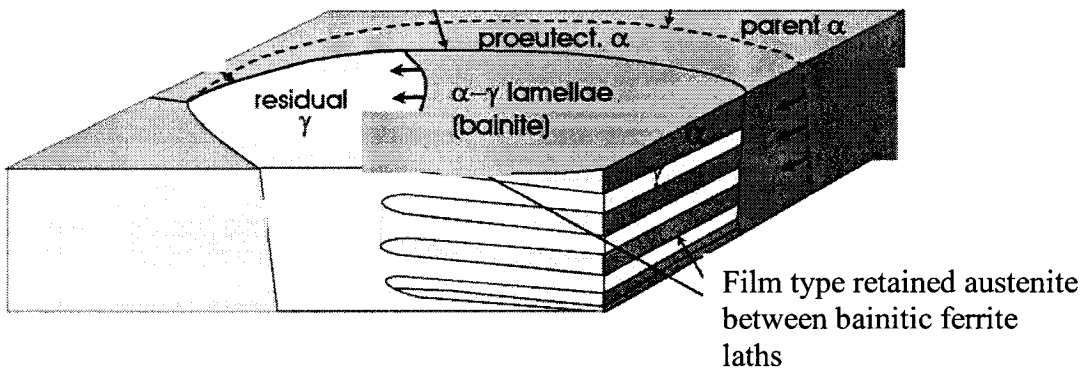

Figure 2.13 Typical Type II TRIP microstructure model, α (bainite) - Bainitic Ferrite, γ – Retained Austenite, α - Ferrite [59].

2.5 Subcritical Annealing or Tempering

In strict metallurgical terminology, tempering or subcritical heat treatment is a process by which hardened steels are heated and held for certain time at a temperature lower than the Ae_3 temperature in order to relieve internal stresses and reduce brittleness, and cooled subsequently to room temperature [61]. Tempering treatment lowers hardness, strength and wear resistance of the steel marginally but compensates for the loss in strength by restoring toughness and ductility. Occasionally, tempering can also strengthen certain high alloy steels due to the formation of certain alloy carbides. Such strengthening is termed as secondary hardening [62].

The concept of tempering is usually used in context with high strength martensitic steels, but in recent years, a few researchers [63] have experimented with tempering of advanced high strength steels such as dual phase and TRIP steels. Speich et al., [64] reported the changes in microstructure and mechanical properties of ferrite-martensite dual phase steel after tempering at two temperatures of 200 and 650°C. Tempering at 200°C for 1 hour resulted in carbide precipitation in both ferrite and martensite phases. Most of the carbide precipitation was observed at interlath or inter-plate boundaries of the martensite. Tempering at 650°C resulted in lowering of dislocation density in ferrite phase and precipitation of coarse carbide particles in the martensite phase.

Waterschoot et al. [65] proposed the strengthening mechanism of low temperature aging in dual phase steel as 1) the formation of a Cottrell atmosphere, 2) the precipitation of the interstitial carbon of the initial matrix stage, and 3) the strengthening stage due to the contribution from the tempering of martensite phase.

Meyer et al. [66] recently suggested the mechanism of microstructural changes during the bake hardening (temperature) process of TRIP steel, after which yield strength increases to a significant degree by 100MPa. This paint baking process involves aging of ferrite (ferritic matrix and bainitic ferrite) and a low temperature tempering of residual martensite, which involves carbon segregation and precipitation and decomposition of

retained austenite to bainite or martensite. The effects of bake hardening on mechanical properties are shown in Figure 2.14.

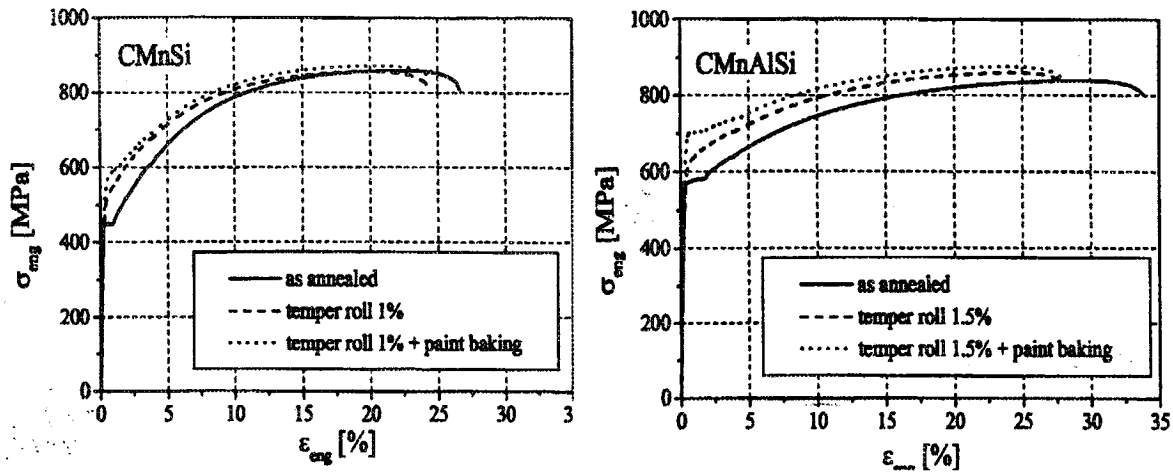

Figure 2.14 Change in Yield Strength of C-Mn-Si and C-Mn-Si-Al TRIP steels before and after paint baking [66].

In recent years, Jeong et al [67] proposed a novel treatment involving tempering, to process cold rolled TRIP steels. In this process, hot rolled TRIP steel with TRIP microstructure is cold rolled to produce strain induced martensite, work hardened ferrite and bainite in the microstructure and then subcritically annealed to produce tempered martensite, recrystallized ferrite and bainite. Jeong et al [67] cold rolled an Al containing TRIP steel samples and subcritically annealed them at temperatures ranging from 200 to 600°C for 1 hour and characterized their mechanical properties and microstructure. Figure 2.15 is the engineering stress-strain curves for a number of cold rolled-subcritically annealed Al TRIP steels. For the purpose of simplicity and easy understanding, all TRIP steels with TRIP microstructures that are cold rolled and subcritically annealed at a temperature lesser than Ae_1 temperature will be henceforth denoted as Tempered Martensite Assisted Steels (TMAS). It is to be noted by the reader that the term TMAS is coined by the author of this work and does not correspond to any commercial grade steel in the past or present.

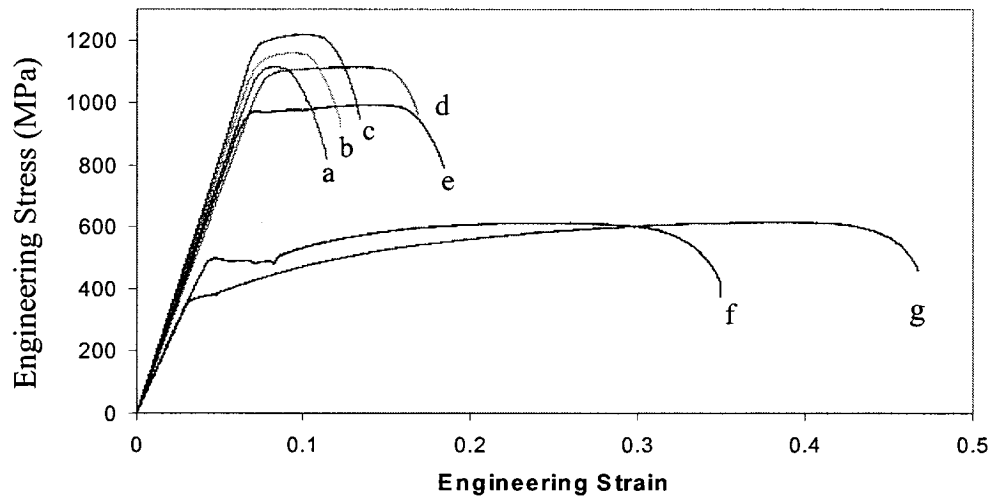

Figure 2.15 Stress-strain curves of a) as cold rolled, b) subcritically heat-treated at 200°C, c) subcritically heat-treated at 300°C, d) subcritically heat-treated at 400°C, e) subcritically heat-treated at 500°C, f) subcritically heat-treated at 600°C and g) cold rolled and TRIP annealed samples [67].

It can be observed from Figure 2.15 that the cold rolled Al TRIP steel subcritically annealed at high temperatures show better total elongation compared to the ones annealed at lower temperature. Jeong et al [68] associates such softening of the steel to recrystallization and decomposition of martensite as ferrite + cementite mixture during high temperature tempering treatment. It was reported that when samples of cold rolled Al TRIP steel that were subcritically annealed at 600°C showed strength values higher than conventional TRIP steels and their total elongation values were closer to conventional TRIP ductility. This improved ductility and toughness, with a good combination of strength is due to the presence of tempered martensites distributed in a recrystallized ferritic matrix. Figure 2.16 is the strength and total elongation Al TMAS as a function of tempering temperature.

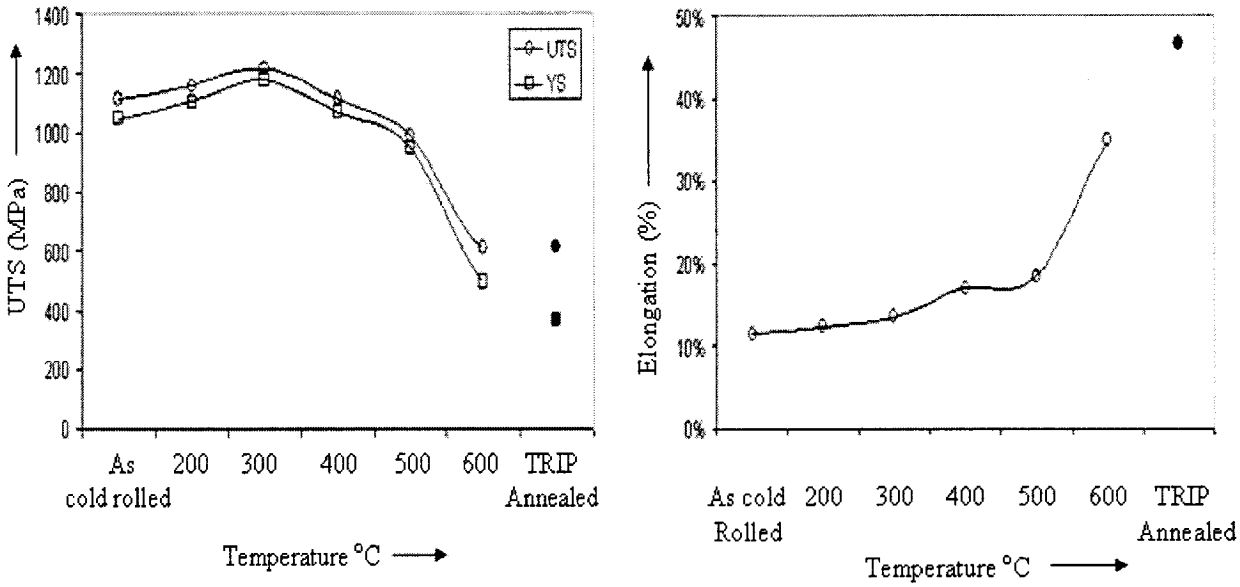

Figure 2.16 Strength and Total Elongation of 0.16-1.5Mn-2Al TMAS as a function of tempering temperature [68].

The slight increase in strength after a low temperature tempering treatment of 300°C is due to the decomposition of high carbon martensite into epsilon carbide and low carbon martensite. The tempering stage where increase in strength is observed is called first stage of tempering or low temperature tempering. The epsilon carbides formed are very fine in size and contribute to steel strength in the form secondary strengthening particles. The marginal increase in the ductility is due to relief of internal stresses and recovery [68].

Traint et al [69] suggested a procedure to evaluate crashworthiness of advanced automobile steels, displayed in terms of mass-related energy absorption. The mass-related energy absorption is calculated by dividing the energy dissipated during deformation by mass of the deformed part of the sample. This mass-related energy absorption is a property which refers to the crash behavior of the entire component, largely depending on material strength and thickness. This in turn means material thickness of the automotives steel can be compensated by increasing the strength of the steel. Pichler et al [70] was able to bring down the material thickness by approximately

20% by substituting TRIP 600 steel for H 320 LA HSLA steel. This is shown in Figure 2.17.

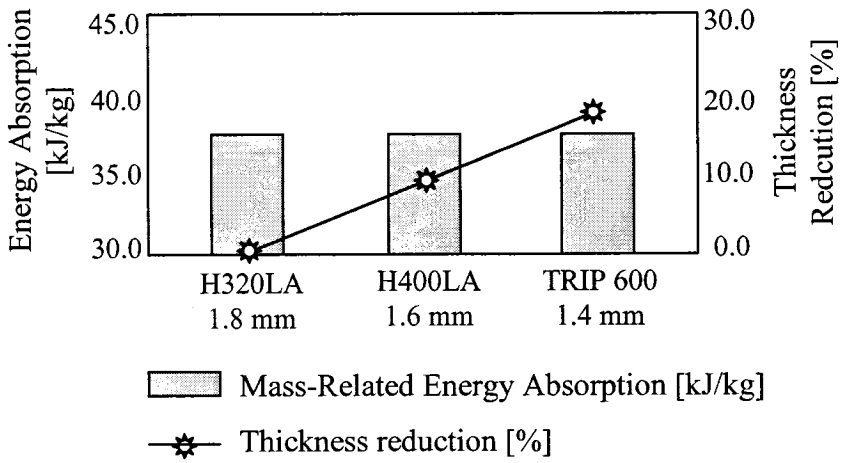

Figure 2.17 Mass-related energy absorption factors for different automotive steels of varying thickness [70]

Since TMAS exhibits a good combination of strength and formability one can assume that TMAS can offer competitive crashworthiness than most of the conventional high strength steels, for a given sheet thickness.

CHAPTER 3

Instrumentation and Experimental Setup

This work attempts to elucidate the influence of retained austenite volume fraction on mechanical properties and microstructures of Al and Si alloyed TRIP steels. This work also attempts to observe how such variation in RA affect the final tempered martensite volume fraction present in TMAS, and subsequent properties.

This chapter focuses on describing and illustrating the instrumentation and experimental setups utilized for steel processing, mechanical property and microstructure characterization. The setup is classified as follows,

1. Heat Treatment.
2. Cold Rolling.
3. Material Characterization
4. Mechanical Properties Assessment.

3.1 Heat Treatment

3.1.1 TRIP and Subcritical Annealing

The first of the two stage TRIP annealing treatment was carried out in either horizontally or vertically mounted radiant furnace. In the case of subcritical annealing treatment, the horizontally mounted furnace was used.

3.1.1.1 Horizontally Mounted Radiant Furnace

The horizontal radiant furnace, developed by Research Incorporated, is equipped with a 16KW power supply and comprises of four tungsten filaments. The filaments generate the required heat. Four mirror finished elliptical reflectors of aluminum; positioned symmetrically about the center of the furnace, reflect the radiant heat toward the center of the sample and anvil. The control of furnace temperature is achieved through a 386 microprocessor temperature controller developed by Micristar. The specimen is held in one of the two grips located at either ends, and kept in contact with a K-type thermocouple to monitor and control the temperature. The heating rate and holding time are all pre-programmed in the 386 microprocessor before the start of the actual experimentation. The sample is heated inside a quartz tube filled with protective argon atmosphere to avoid decarburization. Controlled cooling rates (in the case of quenching) can be achieved by forcing either He or Ar gas radially through the quartz tube through a cylindrical shaped gas nozzle attached to the muzzle of the furnace.

In the case of TRIP annealing, once the samples are intercritically annealed they are manually transferred to a salt bath kept at isothermal bainite transformation temperature for isothermal bainitic transformation, the second stage of TRIP annealing. In the case of subcritical annealing, once the sample is subcritically annealed it is removed from the furnace and air cooled to room temperature.

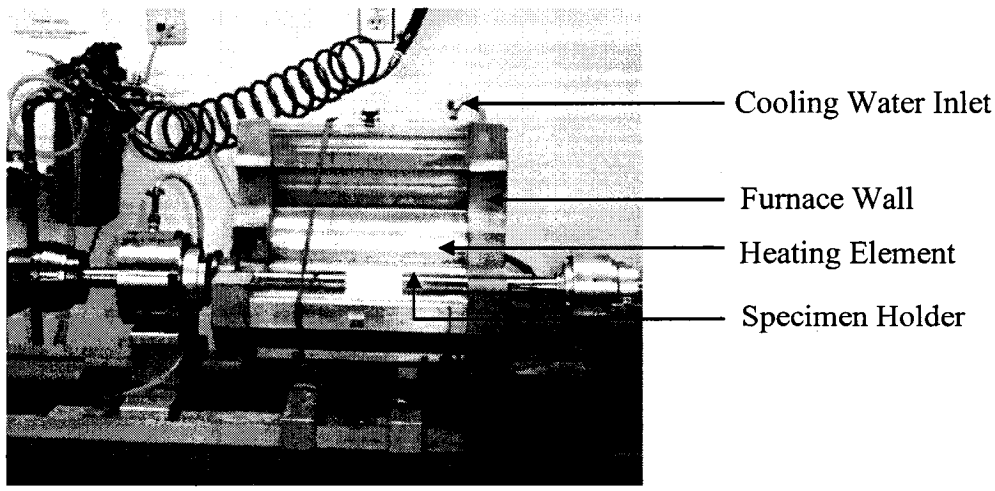

Figure 3.1 Horizontally mounted radiant furnace.

3.1.1.2 Vertically Mounted Radiant Furnace:

The vertically mounted radiant furnace is similar to the horizontal radiant furnace in operation, arrangement, heating elements used and cooling. This furnace in an integral unit of the MTS hot compression machine equipped with a 486 microprocessor controlled temperature monitoring system. Similar to the horizontal furnace, parameters such as hearting rate, holding time and cooling rates can be programmed.

The sample is placed on top of the lower compression anvil placed in contact with a thermocouple located inside a quartz tube filled with argon gas. The other anvil is moved up and away from the furnace zone, since no compression is involved. The top of the furnace is covered with a ceramic tile to minimize heat loss and intrusion of ambient atmosphere. This setup is shown in Figure 3.2. By means of a lever, the sample on the lower anvil can be removed for quenching through a hole in the lower support. This sample is then transferred to either a salt bath or other quenching medium through an aluminum chute. This method allows for high cooling rates by which samples can be quenched within 1 second.

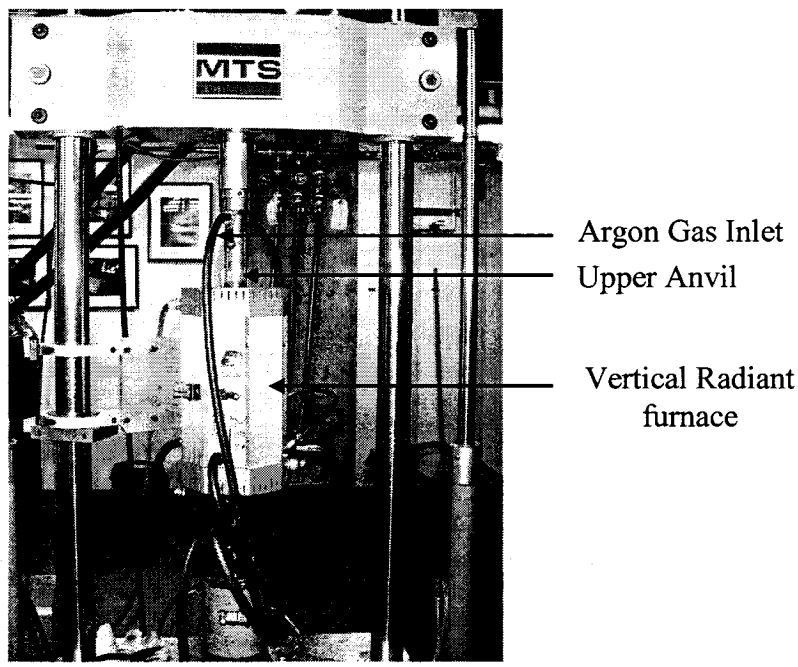

Figure 3.2 Vertical radiant furnace.

3.1.1.3 Salt Bath for Isothermal Bainite Transformation

The second stage of the TRIP annealing treatment, isothermal bainite transformation (IBT), is carried out in a molten salt bath maintained at the required IBT temperature. The salt bath has two concentric cylindrical layers, salt pot and the heating zone. The molten salt is contained in the salt pot and is placed inside the heating zone with heating elements running circumferentially. The temperature in both the heating zone and salt pot are monitored and controlled by microprocessors. The top and bottom portion of the unit are shielded by insulation to avoid heat loss. The hood of the salt bath is connected to an exhaust duct that removes the fumes instantaneously. Figure 3.3 represents the salt bath setup.

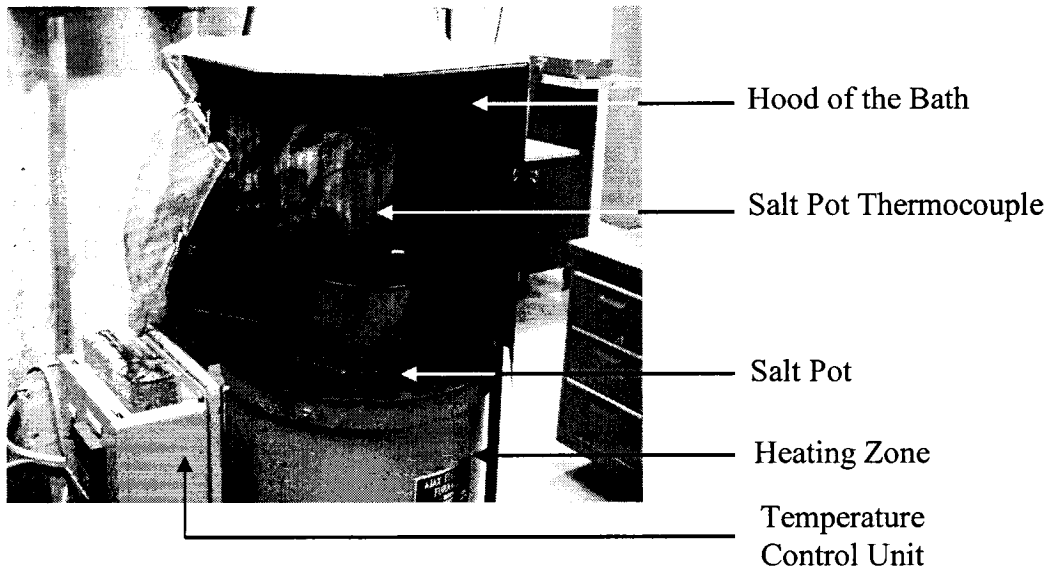

Figure 3.3 Salt Bath Setup for Isothermal Bainite Transformation

3.2 Cold Rolling

All the cold rolling operations were performed with a STANAT laboratory scale cold rolling mill. The rolls are made of hardened high alloy steel. The mill consists of a power unit to drive the rolls, platform to feed and receive the sample and a roll gap control wheel to control roll gap. A wooden pusher was used to feed the samples into the rolls. Each complete revolution of the roll gap control wheel reduces the roll gap by

0.1 mm. External cooling of the rolls was not necessary, since the experiments were carried out in batch process and actual rolling time was very small for any extensive roll heating. Figure 3.4 is the cold rolling setup. The samples for cold rolling were 1 cm wide, and 4 cm long with varying thickness for different steel.

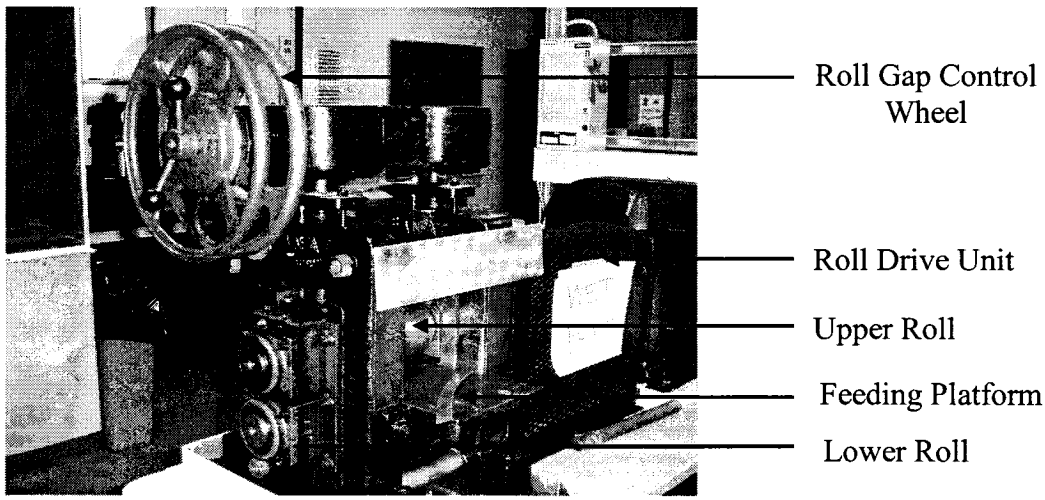

Figure 3.4 Laboratory Scale STANAT Cold Rolling Mill

3.3 Material Characterization

3.3.1 X-Ray Diffraction

Analysis via X-ray diffraction for the TRIP annealed samples was carried out using a Philips PW 1710 X-ray diffractometer with Cu-Kα radiation source. The X-ray wavelength utilized was 1.54 Å (Kα1 = 1.540598 Å, Kα2= 1.544426 Å). X-ray diffraction tests were run using an accelerating voltage of 40 kV, a source current of 20 mA. The diffracted X-ray count versus 2θ angle was measured over a range of 60 to 105 degrees with a scan rate of 0.1 °/ 3s. The X-ray diffractometer and the space for sample insertion can be seen in Figure 3.5. Care was taken to ensure the samples were placed perfectly horizontal on the specimen holder to avoid any inadvertent shift in X-ray peaks.

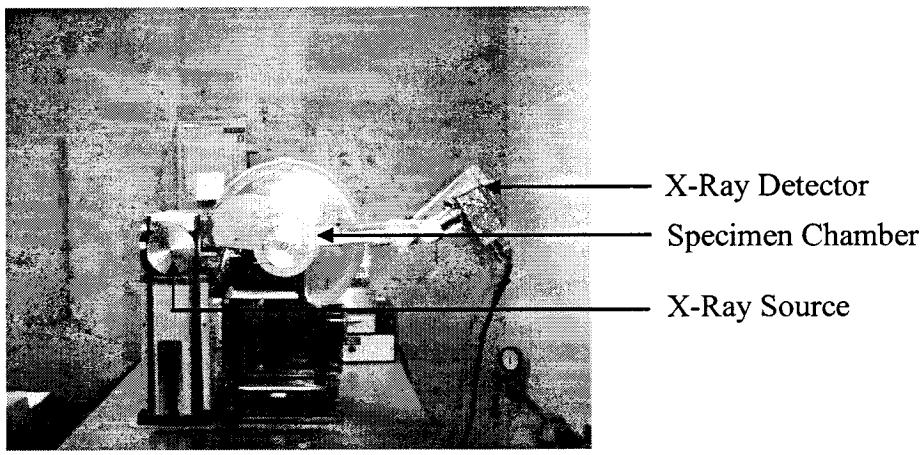

Figure 3.5 Philips PW X-ray Diffractometer

3.3.2 Optical Metallography

Qualitative microstructural examination of TRIP and TMAS samples were performed using optical metallography. The samples were cut along the axis of interest, such as rolling, transverse and normal direction, and mounted in bakelite and/or carbon for further polishing to expose fresh unaltered metal surface. Figure 3.6 is a schematic representation of a metallographic sample.

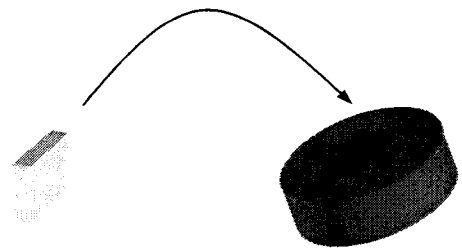

Figure 3.6 Sample for optical and electron metallography

Samples for optical metallography were ground using 60,120, 240, 400, 600 grit SiC papers in sequence and then polished with 9, 3 and 1 micron diamond paste suspension

prior to etching and analyses. The microstructures were revealed using etches that will be described in the next chapter.

3.4 Mechanical Properties

3.4.1 Shear Punch

Given the limited availability of the experimental steel, it was not technically feasible to prepare samples for conventional tensile testing, which requires a relatively substantial amount of material. As a result, shear punch testing [53, 54] was used. This test is based on a blanking operation common to sheet metal forming.

The shear punch test studies were performed on a computerized Materials Testing System (Model 810) with a load cell of 25 kN capacity (reduced range of ± 2.5 kN with an accuracy ± 1% of the range) and a linear variable differential transformer for continuous monitoring punch head displacement using a data acquisition system. The equipment is a specially designed apparatus consisting of an aligned upper and lower housing containing a flat cylindrical punch and a die, respectively, as shown in Figure 3.7. The material selected for both the punch and die was A2 air hardened tool steel (RC 58).

The central axes of the punch and die were exactly aligned in the upper and lower housing, respectively. The sheet material for testing was fastened tightly onto the die surface and aligned above the die orifice with a screwed on washer so as to prevent the specimen from moving during punching and avoid premature fracture. The flat tipped punch drives through the specimen, shearing a circular disk from the material through the die, bringing the test to an end. During the entire course of the test, the computer system records the load vs. displacement data.

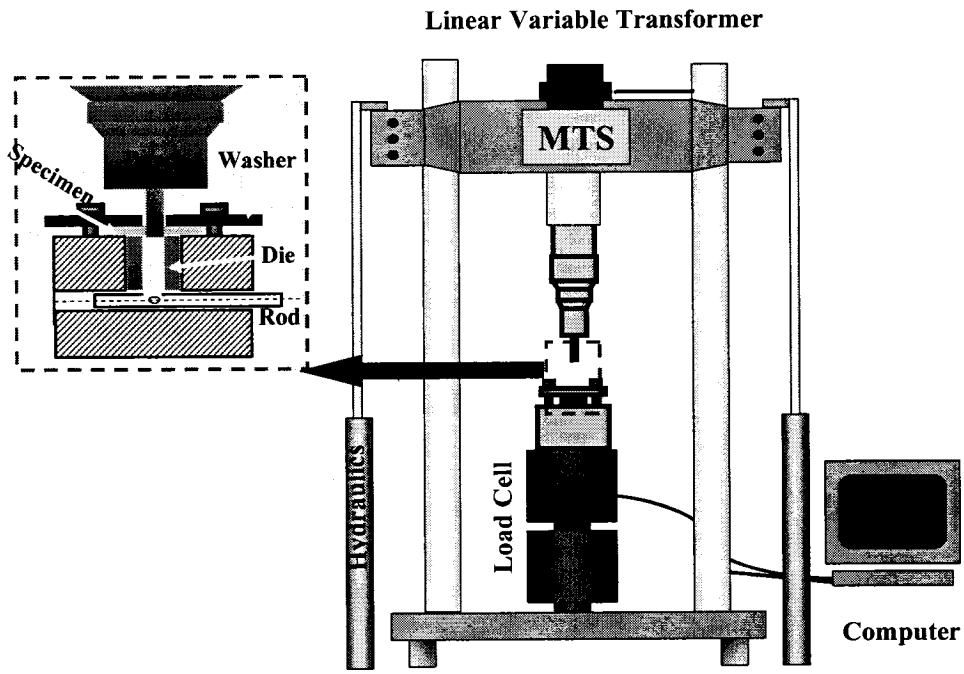

Figure 3.7 Shear Punch Testing Setup

3.4.2 Specimen Preparation for Shear Punch

To obtain the required final geometrical size, the shear punch specimens were rough ground from bulk material into cuboids of dimension 1 cm wide, 2-4 cm long and 0.1 cm thick, using a 60 and/or 120 grit SiC paper. The surfaces of sample were subsequently ground on successively finer SiC paper 320, 400 and 600-grit to assure a uniform surface finish and a thickness of 350 to 400 micrometers. Figure 3.8 is a schematic representation of a shear punch sample.

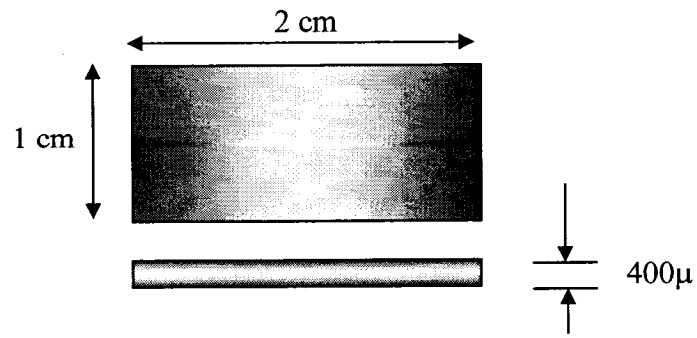

Figure 3.8 Schematic representation of a typical shear punch sample

CHAPTER 4

Experimental Procedures

4.1 Materials

Retained austenite present in TRIP steels has to possess a few characteristics, such as optimum grain size, optimum carbon concentration and suitable morphology, to optimize the mechanical properties [71, 72, 73]. Deviation from such optimum characteristics renders the retained austenite either too high or too low in stability and prevents it from undergoing a useful SIT during deformation, resulting in poor mechanical properties.

However, the major focus of this work is to determine whether Tempered Martensite Assisted Steels (TMAS) can be created by processing a multiphase TRIP steel and have properties better or equal to conventional TRIP steels.

Two steels, an Al containing TRIP steel and a classic Si TRIP steel were processed for this purpose. The chemical composition of the steels is given in Table 4.1.

Table 4.1 Experimental Steels Chemical Composition (Wt. %)

Steel	*C*	*Si*	*Mn*	*Al*	*Mo*	*Nb*	*Ti*
AL	0.16	0.017	1.57	2.00	0.064	0.008	0.003
CL	0.17	1.53	1.50	0.03	0.046	0.008	0.022

The main differences between the AL and CL steels are the Si and the Al concentrations. AL steel is the one that has aluminum as the major TRIP alloying element, while CL is the classic TRIP steel with silicon as the major TRIP alloying element. Both AL and CL steels were prepared and cast at CANMET (Ottawa). The AL steel was received in 2 conditions; 1) hot rolled TRIP annealed and 2) as hot rolled condition. The CL steel was received as hot rolled.

The hot rolled AL and CL steel were rolled from ingots (127 mm thick x 152 mm breadth x 203 mm long) into 13 mm plates, after reheating at a temperature of 1230°C. The plates were further sectioned along the longitudinal axis into strips approximately 120 mm wide. The hot rolled and TRIP annealed AL steel samples were thermomechanically processed from an ingot (127 mm thick x 152 mm breadth x 203 mm long) into strips (130 mm width x 280 mm length x 4.65 mm thick). The steel ingot was first reheated at 1225°C and then reduced by a 7 pass hot rolling through the intercritical region to the desired thickness and bainite treated at 380°C for 10 minutes to achieve the TRIP microstructure. CANMET reported an initial retained austenite volume fraction of 9.2% with a carbon concentration of 1.5%. The Al containing TRIP steel used in this work is similar to the one used by Jeong et al [74].

4.2 Processing Route

The TRIP steels were both thermomechanically and mechanically processed with the expectation of achieving the desired results. The processing route employed to create TMAS by processing the TRIP steels is shown schematically in Figure 4.1.

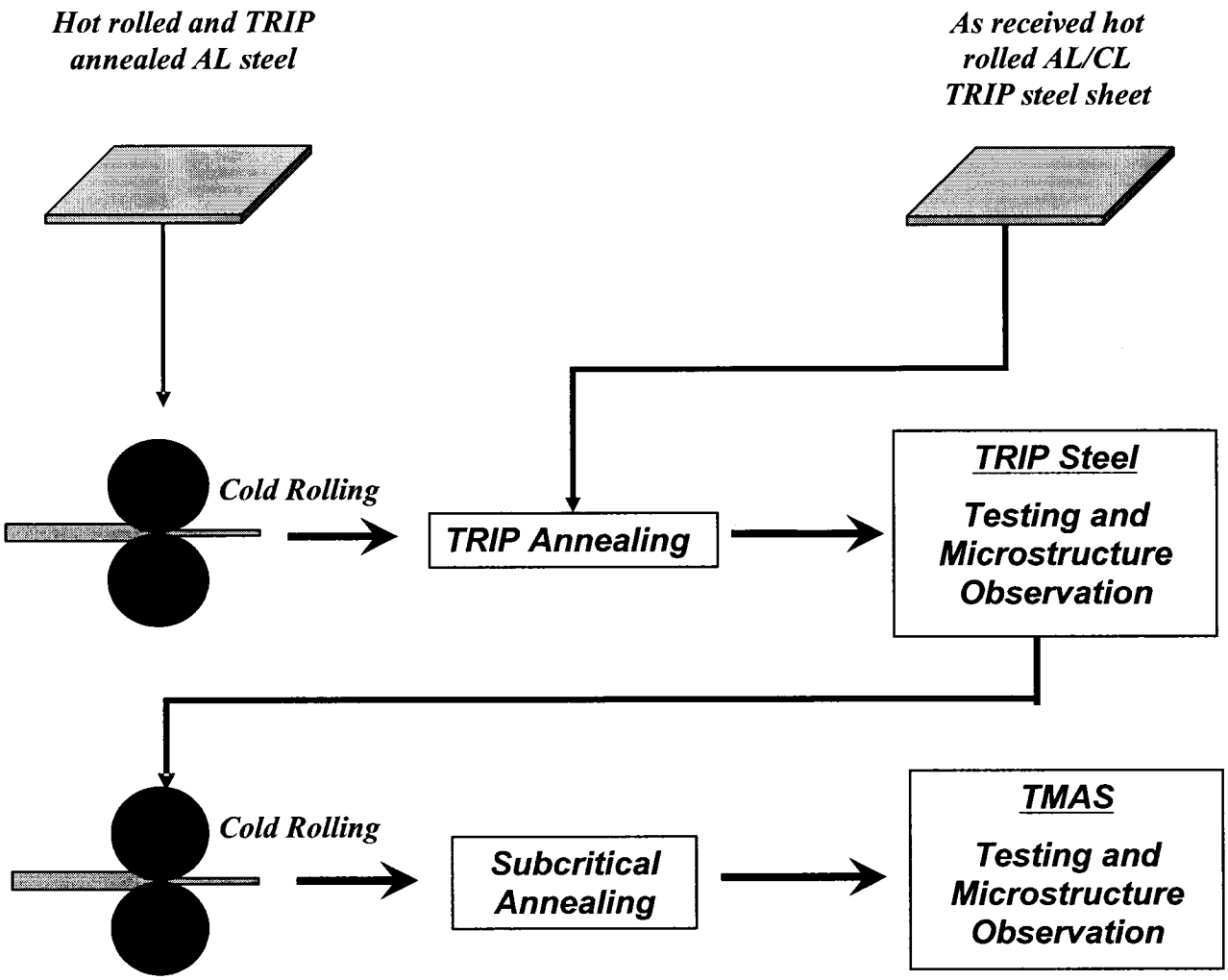

Figure 4.1 Schematic representation of TMAS processing route.

Since the initial microstructure is known to have a strong effect on the final properties of the steel, the initial TRIP microstructure of the hot rolled TRIP annealed AL steel was altered by cold rolling before processing them into TMAS. This cold rolling operation was designed to transform all the retained austenite into martensite by Strain Induced Transformation (SIT). As a result, this cold rolled steel has SIT martensite, work hardened bainite and ferrite in the initial microstructure, in contrast to the as hot rolled AL/CL steel sheets, which have ferrite + pearlite in the initial microstructure. This difference in the initial microstructure was expected to alter the final properties of the TMAS obtained from TRIP steels containing them.

The cold rolled TRIP steels mentioned above, and the hot rolled AL/CL steels were then TRIP annealed to achieve a TRIP microstructure of retained austenite and bainite dispersed in a matrix of ferrite. Both of these TRIP steels were then cold rolled and subcritcally annealed to create TMAS. It should be noted that this double cold rolling procedure performed on one of the specimens is not intended as an industrial processing route, but as a laboratory way to generate very different TMAS structures. Mechanical testing was performed on both TRIP steel and TMAS to assess mechanical properties and to establish relationships between structure and property.

As mentioned earlier, TMAS are produced via cold rolling of TRIP steels with TRIP microstructure which transforms all RA into martensite by Strain Induced Transformation (SIT) and also work hardens the ferritic matrix. When these cold rolled structures are subcritically annealed subsequently, all the martensite present starts to temper into tempered and the ferritic matrix undergoes recrystallization. Such steels, containing tempered martensite and bainite dispersed in a ferritic matrix are called TMAS.

The parameters used during the aforementioned multistage processing are discussed in detail in the forthcoming paragraphs in this chapter.

4. 3 Heat Treatments

4.3.1 TRIP Annealing

For the purpose of convenience, the abbreviations C(AL), H(AL) and H(CL) will be used for cold rolled and TRIP annealed AL TRIP steel, hot rolled and TRIP annealed AL TRIP steel and hot rolled and TRIP annealed CL TRIP steel, respectively.

All three C(AL), H(AL) and H(CL) TRIP steels were TRIP annealed to generate the TRIP microstructure. This process is schematically represented in Figure 4.2. The TRIP annealing parameters used for the steels are described in Tables 4.2, 4.3 and 4.4.

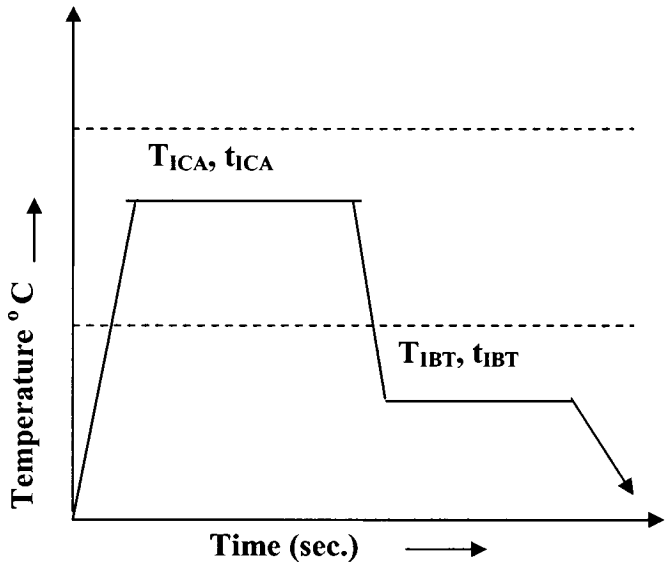

Figure 4.2 Schematic representation of TRIP annealing treatment.

Table 4.2 - TRIP Annealing Parameters for C(AL) TRIP Steel				
Cycle	**Intercritical Annealing Temperature T_{ICA} (°C)**	**Intercritical Annealing Time t_{ICA} (Sec.)**	**Bainite hold temperature T_{IBT} (°C)**	**Bainite hold time t_{IBT} (Sec.)**
A(I)*	830	300,350,450,550	400	240
C1	890	350	400	240
V	865	900	335	240
*I = 1, 2, 3, 4, ...n.				

Table 4.3 - TRIP Annealing Parameters for H(AL) TRIP Steel				
Cycle	**Intercritical Annealing Temperature T_{ICA} (°C)**	**Intercritical Annealing Time t_{ICA} (Sec.)**	**Bainite hold temperature T_{IBT} (°C)**	**Bainite hold time T_{IBT} (Sec.)**
HA(I)*	830	300,350,450,550	400	240
HC(1,2)	890, 865	350	400	240
*I = 1, 2, 3, 4, ...n.				

Table 4.4 - TRIP Annealing Parameters for H(CL) TRIP Steel				
Cycle	**Intercritical Annealing Temperature T_{ICA} (°C)**	**Intercritical Annealing Time t_{ICA} (Sec.)**	**Bainite hold temperature T_{IBT} (°C)**	**Bainite hold time t_{IBT} (Sec.)**
CL-2T	800	300	455	600
CL-3T	800	300	455	300
CL-4T	800	300	455	240
CL-5T	800	300	400	240
CL-6T	800	300	390	240
CL-7T	800	300	365	240
CL-8T	800	300	350	240
CL – 9T	800	300	300	240

The intercritical annealing temperatures used for the AL steels were deduced from the works of previous researchers [74, 75], according to which, at intercritical temperatures of 830, 865 and 890°C the microstructure is approximately 28% austenite + 72% ferrite, 41% austenite + 59% ferrite and 45% austenite + 55% ferrite respectively. The bainite temperatures used for AL steel were also deduced from literature [76], wherein they provide optimum retained austenite volume fraction and mechanical properties.

The intercritical annealing temperature utilized for CL steel was deduced from equation 4.1., which is the temperature at which there is 50% austenite [77].

$$ICA = (Ac_1 + Ac_2)/2 \quad \text{..... (4.1)}$$

Where, ICA, Ae_1 and Ae_2 are Intercritical Annealing Temperature, Lower Critical Temperature and Upper Critical Temperature during cooling, respectively. The critical temperatures were calculated using Andrew's equation [78], shown in equations 4.2 and 4.3. The evaluated value was 806°C, but was rounded off to 800°C, as seen in Table 4.4. Bainite hold time and temperature were deduced from best performing parameters observed in literature [79, 80]. The heating rate at which the samples were heated into the intercritical region kept close to 1.1°C/sec.

$$Ac_1 (\square) = 723 - 10.7Mn - 16.9Ni + 29.1Si + 16.9Cr + 290As + 6.38W \ldots.(4.2)$$

$$Ac_3 (\square) = 910 - 203\sqrt{C} - 30Mn - 20Cu - 15.2Ni - 11Cr - 700P \ldots\ldots (4.3)$$
$$+ 44.7Si + 31.5Mo + 104V + 460Al + 13.1W + 120As$$

All C(AL), H(AL) and H(CL) TRIP steels were cold rolled to give a 69% reduction in thickness after the TRIP annealing treatment. As mentioned earlier, this operation was expected to transform all the retained austenite (RA) into martensite.

4.3.2 Subcritical Annealing

The post cold rolling heat treatment, namely the subcritical annealing, was performed on cold rolled steel samples in the horizontal radiant furnace. The heat treatment parameters used are shown in table 4.5. The samples were heated into the subcritical region at a heating rate of 1.1°C/sec. The subcritical annealing temperature was chosen with due consideration to Jeong et al's [81] work, wherein the samples subcritically annealed at 500°C showed good combination of strength and ductility.

Table 4.5 Subcritical Heat Treatment Schedule

Heat Treatment	Heat treatment condition
Subcritical heat treatment	500°C for 1 hour

4.4 Microstructural Observation

Considering the strong effect of microstructures on mechanical properties of steel, it is imperative to perform precise metallographic examination for property enhancement. In this work, microstructures were revealed by etching the freshly prepared steel surface with three major etching solutions, they are;

1. 2% Nital.

2. LePera solution.
3. 10% sodium metabisulphite solution.

1. 2% Nital: Nital is basically a solution of nitric acid in ethanol and, the prefix 2% indicates the amount of nitric acid in the solution. Nital is predominantly used to etch steel for its ability to differentiate pearlite, cementite network and martensite from ferrite and also to differentiate the ferrite boundaries. This solution was used to examine the starting microstructure of as hot rolled AL/CL TRIP steel containing ferrite + pearlite, cold rolled TRIP steels and TMAS containing tempered martensite, bainite and ferrite. The freshly prepared surface was exposed to the etching solution for 2 to 7 seconds and washed immediately with water and ethanol to remove any traces of residual etchant from the sample surface before commencement of any microscopic observation.

2. LePera: Classical etching solutions, such as Nital used for microstructure investigation of steel allow the simultaneous observation of only a limited number of phases. Such techniques serve little use for observing multiphase microstructure such as the TRIP structure. However, a number of phases can be observed by their relative colors in the LePera color etching technique. LePera color etching solution is a solution of 5% $Na_2S_2O_5$ (sodium metabisulfite) + 4% $(NO_2)_3C_6H_2OH$ (Picric Acid) + 4% Nital mixed in a ratio of 5:5:1. The specimens were exposed to the etching solution for 10 to 20 seconds before microscopic examination. This technique stains ferrite both blue and/or grey, bainite appears dark brown and, martensite and retained austenite appear white. The reagents have to be mixed freshly; any delay in etching for more than 20 seconds renders the etching technique futile.

3. 10% sodium metabisulphite (SMB, $Na_2S_2O_5$): This is similar to LePera etching in principal. This etching solution preferentially tints the phases present and makes it possible to observe multiphase microstructures simultaneously with ease. In reality, 10% sodium metabisulphite (SMB) solution is seldom used alone. First the specimens are pre-etched for 2 to 5 seconds in 2% Nital followed by a 20 second

etch in 10% sodium metabisulfite. Under this technique, ferrite appears grey and/or blue, bainite appears dark brown, martensite appears black and retained austenite appears white. Unlike the LePera etch, where retained austenite and martensite appear as the same tint, this technique can differentiate retained austenite from martensite. This quality makes this etching technique a suitable candidate for quantitative metallographic analysis.

4.5 Retained Austenite and Tempered Martensite Measurement

The retained austenite volume fraction and its C content were measured using X-ray diffraction. Equation 4.6 was suggested by Meyer et al [82] which quantifies RA by comparing the relative X-ray intensities from ferrite and austenite phases. Figure 4.3 is a typical XRD diffraction pattern for TRIP steels.

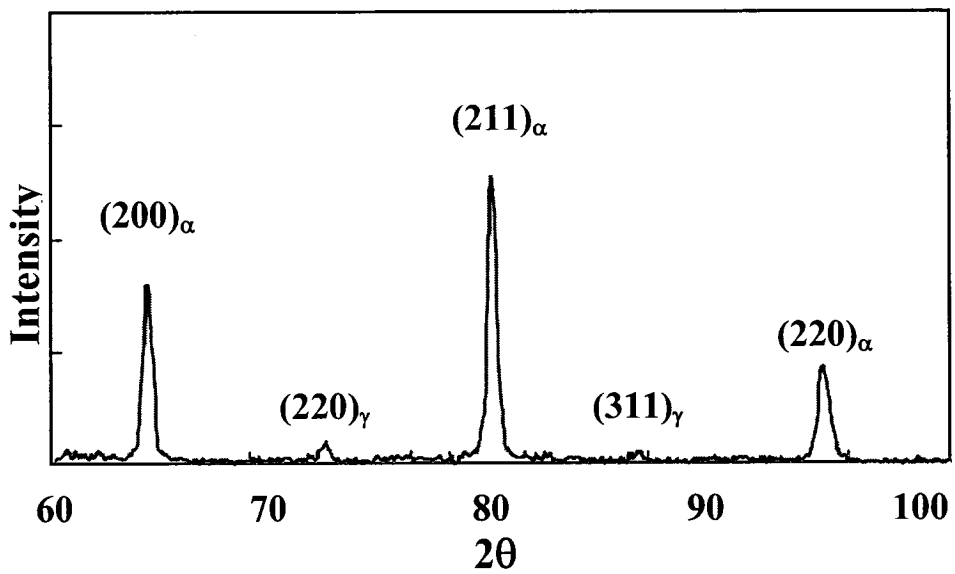

Figure 4.3Typical Fitted XRD Pattern of Ferrite- Austenite Dual Phase Structure.

$$V_\gamma = \frac{\dfrac{I_\gamma^{220}}{1.42I_\alpha^{200}+I_\gamma^{220}} + \dfrac{I_\gamma^{220}}{0.71I_\alpha^{211}+I_\gamma^{220}}}{4} + \frac{\dfrac{I_\gamma^{311}}{1.62I_\alpha^{200}+I_\gamma^{311}} + \dfrac{I_\gamma^{311}}{0.81I_\alpha^{211}+I_\gamma^{311}}}{4} \quad ..(4.6)$$

Here, $I_\gamma^{220}, I_\gamma^{311}$ are the integrated intensities of the X-ray beam diffracted by the crystallographic planes present in the retained austenite phase, while $I_\alpha^{200}, I_\alpha^{211}$ are the integrated intensities of the ferrite phase.

The carbon content in wt. % present in the retained austenite was calculated from the empirical formula, shown in Equation 4.6, given by Sugimoto and Nishiyama et al. [83, 84].

$$a_\gamma = 3.5467 + 4.67X10^{-3}\, wt.\%\, C_\gamma \ldots\ldots\ldots\ldots\ldots (4.6)$$

The volume fraction of tempered martensite in TMAS is assumed to be equal to the initial retained austenite volume fraction of the TRIP steel it was processed from, since Jeong et al and Ho et al [85, 86] have proved that a 69% cold rolling operation consumes all retained austenite particles and transform them to SIT martensite.

4.6 Mechanical Properties Assessment by Shear Punch Technique

4.6.1 Principles of Shear Punch Testing and Data Manipulation

A typical load vs. displacement curve for a polycrystalline metal produced by the shear punch is illustrated in Figure 4.4. It can be seen that the features of the load-displacement curve obtained from the shear punch test are similar to the ones obtained by conventional tensile testing. These include an elastic region, a point where there is a

deviation from elasticity, a plastic region, a region of plastic instability and finally fracture.

It is noteworthy that the stress state in the shear punch testing of engineering alloys has been reported to comprise primarily of a shear stress with contributions from compression, stretching, and bending in the deformation region between the punch and the die [53]. Hence, unlike tensile testing, the strain measurement for the shear punch test must be approximated by the punch displacement due to the characteristic loading configuration and the complex stress state in the specimen.

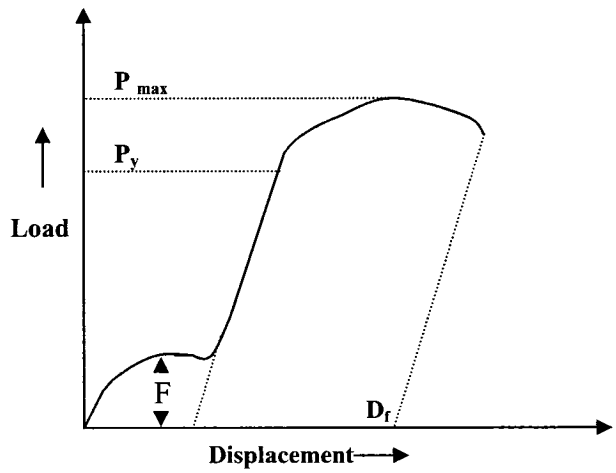

Figure 4.4 Schematic illustration of a typical load displacement curve for TRIP steels.

Other researchers [87, 88] have found that the load at the point of deviation from linearity, P_y, and the maximum load, P_{max}, correlate well with the uniaxial yield strength and ultimate tensile strength, respectively. By means of correlation factors, the effective stresses calculated from the shear punch test can be translated to uniaxial stresses. The tensile flow properties, including Yield Strength (YS), Ultimate Tensile Strength (UTS) and Total Elongation (El) can be determined using the following empirical equations.

$$\sigma_{eff} = \frac{P - F}{2\pi rt} = C\sigma \quad \text{..... (4.7)}$$

Where, σ is the tensile uniaxial stress (MPa), σ_{eff} is the effective stress in shear (MPa), P is either the yield or maximum load, F is the frictional load, r is the punch radius (mm), t is the specimen thickness (mm) and C is the correlation coefficient. The origin and calculation of the correlation factor C has been detailed extensively in earlier, publications [87, 88] in this work. The values obtained by the aforementioned researchers for the specific conditions were used by the author in this work (Refer to Appendix A for further information).

The total elongation is determined by the following empirical equation where El_{total} is the total elongation, t is the specimen thickness and d_f is the displacement at fracture.

$$El_{total} = \frac{d_f}{t} \quad \text{..... (4.8)}$$

It should be noted that although this approach has proved to be very good in obtaining tensile values from shear punch values, in order to obtain precise tensile properties, tensile tests should be performed.

It is noteworthy to remember that the shear punch tests were performed for four times on each sample (both TRIP and TMAS steels) and the mechanical properties values were averaged out from them. The results of the tests will be discussed in detail in Chapter 5.

CHAPTER 5

RESULTS

This chapter presents the experimental results obtained during the course of the research work. For the purpose of convenience and understanding, this chapter is separated into two major sections,

5.1. TRIP Steel Processing and Testing.
5.2. TMAS Processing and Testing.

5.1 TRIP Steel Processing and Testing

5.1.1 Retained Austenite Measurements.

The results for retained austenite measurement are shown in the order in which the experiments were carried out, starting with C(AL), H(AL) and H(CL) TRIP steels.

As mentioned before, for AL steels, the main method of varying the retained austenite content in the final microstructure was by TRIP annealing with different Intercritical Anneal (ICA) heat treatment parameters such as intercritical annealing temperature and time, keeping all the other parameters such as, bainitic hold temperature and time constant. In the case of H(CL) steels, the final retained austenite volume fraction in the

final structure was brought about by varying the bainite hold temperature and time, keeping all the other TRIP annealing parameters constant.

The tests were repeated to determine the range of error and repeatability of the experiments. All retained austenite volume fraction values reported in tables in the following sections are average values, and do not correspond to one single test.

5.1.1.1 C(AL) TRIP Steels

The retained austenite measurements by XRD made for C(AL) steels are given in Table 5.1

Table 5.1 - Initial retained austenite parameters of C(AL) TRIP steel after TRIP annealing.

Sample	V_γ	C_γ	$V_\gamma * C_\gamma$
A1	5.63	1.73	9.73
A2	5.65	1.74	9.83
A3	6.50	1.59	10.30
A4	5.09	1.53	7.78
V	4.25	1.52	6.87
C1	7.18	1.66	11.90

V_γ, C_γ - Volume fraction and carbon content of the retained austenite phase respectively

From the table, one can observe that changes in TRIP annealing parameters manifests itself as changes in the final retained austenite volume fraction. Figure 5.1 represents the relationship between final retained austenite volume fraction and intercritical annealing temperature. The accuracy of the X-ray diffraction technique utilizing Cu Kα radiation under high quality sample preparation and precise placement of the specimen with respect to the X-rays varies from ±10 to 15% for samples containing retained austenite values less than 5 Vol. % and reduces to ±5 - 8% for retained austenite content more than 5 Vol. % [89]. To achieve better results other X-ray sources such as Mo Kα and Cr Kα should be utilized. The error bars in this work were identified by performing X-ray analysis on three different samples annealed under the same TRIP annealing parameters. From Figure 5.1, it can be observed that the retained austenite volume fraction increases with increasing intercritical annealing temperature. This effect could

be due to the fact that at higher intercritical annealing temperatures the ratio of two phase austenite to ferrite is high. And more austenite can be retained from such high austenite fraction intercritical structure after the completion of the TRIP annealing [90]. However, there was no obvious change in the second phase (bainite) volume fraction with intercritical annealing temperature.

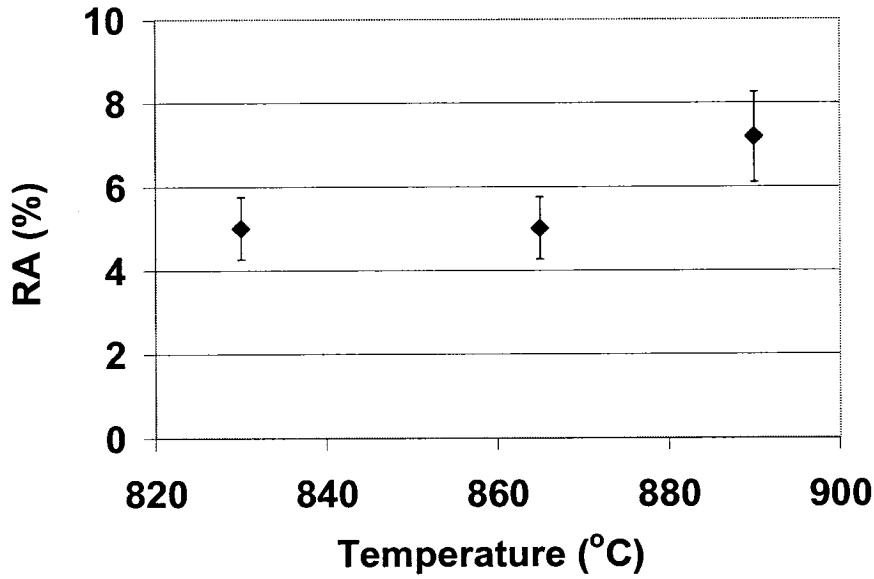

Figure 5.1 Variation of Retained Austenite Volume fraction with ICA Temperature.

It was also observed from the table 5.1, that the carbon concentration in the retained austenite phases is quite high compared to the values normally observed in literature ≈ 0.74 to 1.1% [91].

Figure 5.2 shows the variation of retained austenite volume fraction with increasing intercritical annealing (ICA) hold time. It can be seen that there is a modest increase in the retained austenite volume fraction when ICA hold time is increased from 350 to 550 seconds.

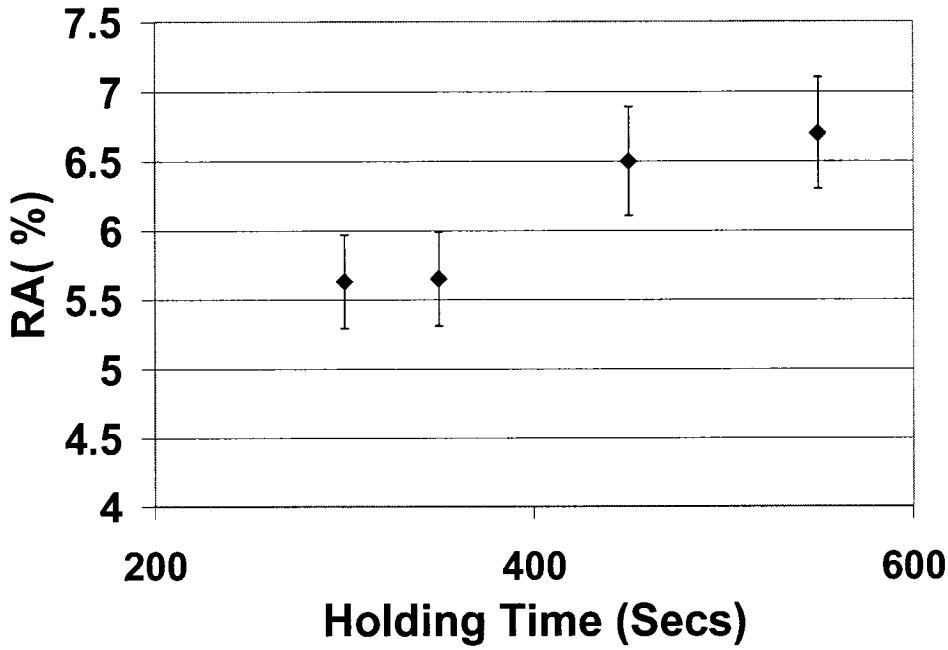

Figure 5.2 Variation of Retained Austenite Volume fraction with ICA Holding Time.

This increase in retained austenite fraction could be due to more austenite formed with time in the intercritical region. This improvement in retained austenite fraction with ICA time is also seen in the micrographs of Figures 5.3 (d), 5.3 (e), and 5.3 (f).

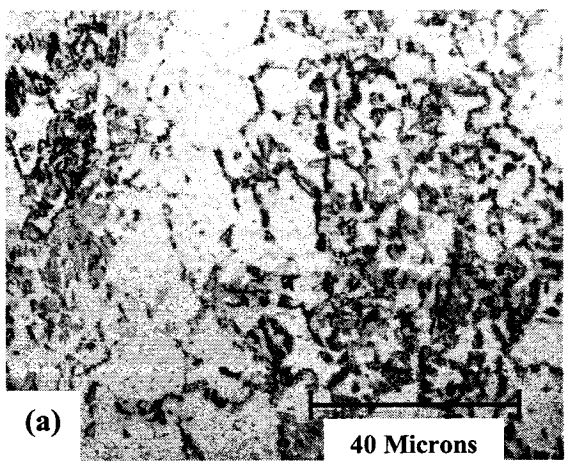

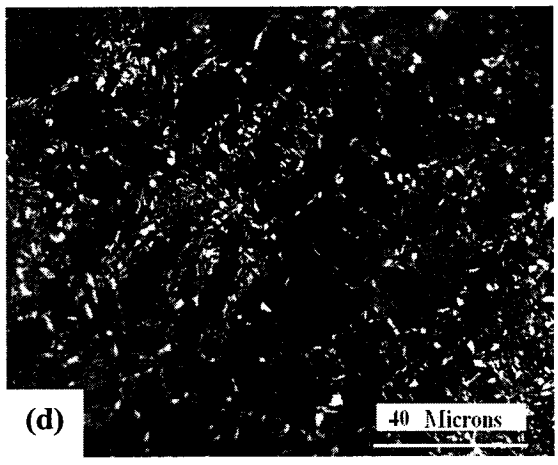

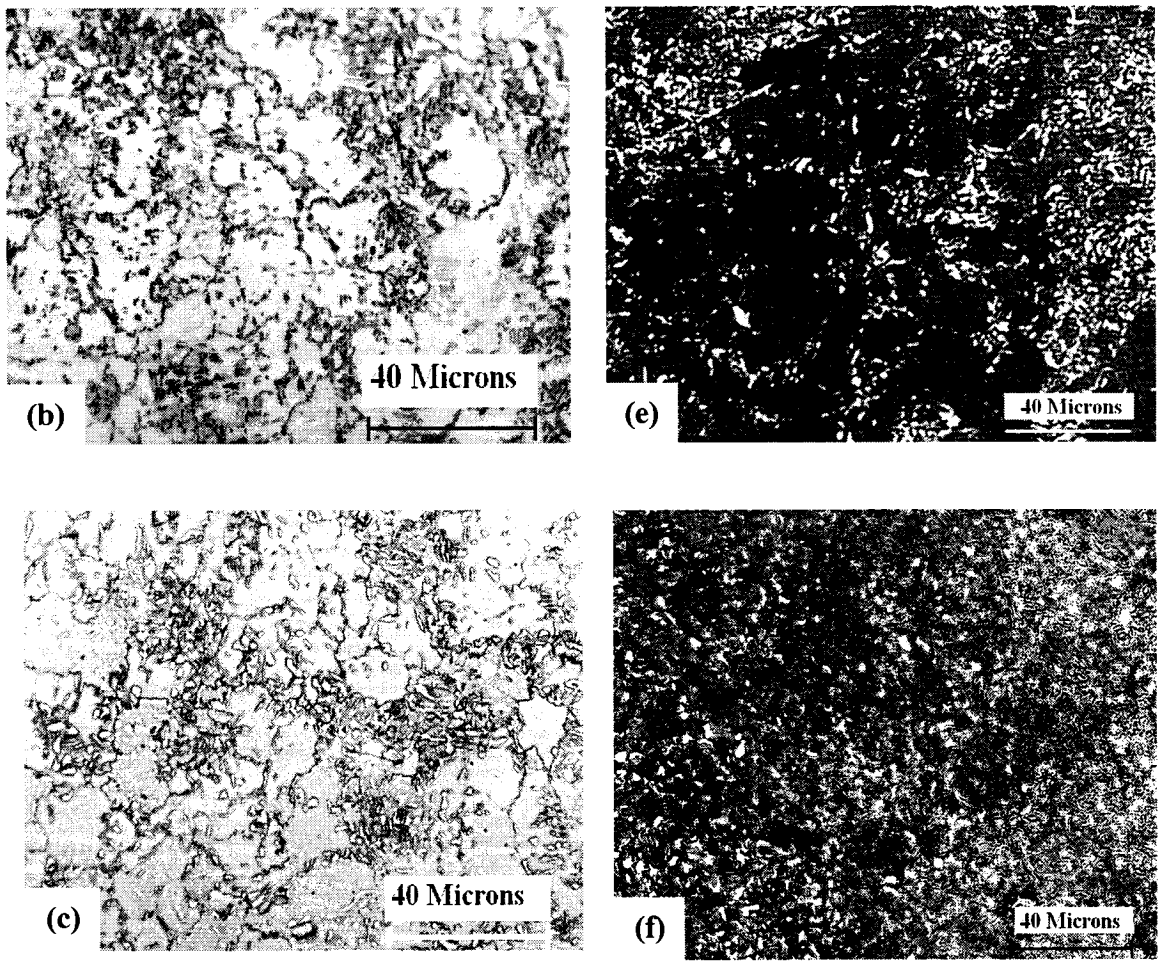

Figure 5.3 Microstructures of C(AL) samples; a, b, and c are 2% Nital etched microstructures and d, e, and f are LePera color etched microstructures of A1, A2, and A3 steels, respectively.

The figures are arranged in the order of holding time, from 300 to 450 seconds, respectively. The white particles in the microstructure represent the MA constituents (retained austenite + martensite, if any). The Figures are shown with their respective nital etches to reveal the ferritic grain boundaries, bainite and martensite, if any. It can be noticed from the nital etches, Figures 5.3 (a), 5.3 (b) and 5.3 (c), that bainite and MA is found along the ferrite grain boundaries. This is accordance with the trend observed in literature, which dictates that preferred site for austenite nucleation is at the ferrite grain boundaries and ferrite-bainite grain boundaries. It can also be observed that the

population of MA constituents increase as the ICA holding time is increased, which is in accordance with the XRD data.

When observed closely, one can see from Figure 5.3 a) the presence of banding in the structure. This banding in the mocrostructure is more clearly visible in a low magnification optical micrograph shown in Figure 5.4. It can be noticed that the retained austenite phase has a tendency to form and populate along these bands.

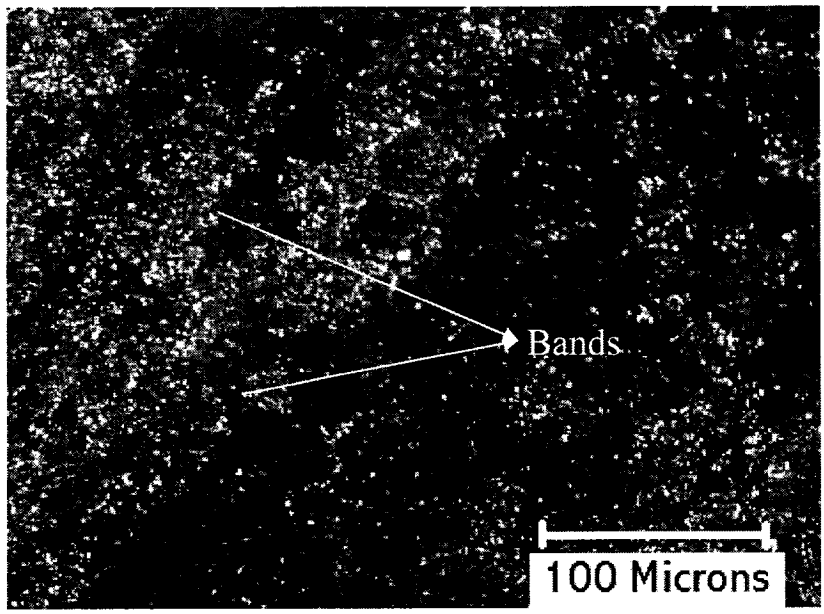

Figure 5.4 Optical micrograph of A1 sample etched with LePera color etchant showing the presence of bands.

It is generally thought that development of a banded structure becomes pronounced with increasing manganese content. This according to Kim et al. [92] is because the area where manganese and carbon are simultaneously segregated during casting are not completely homogenized, due to the reduced diffusion rate of carbon in the presence of manganese as well as the slow diffusion of manganese during homogenization. Thus they are elongated in a band type manner wherein retained austenite/bainite grains are intensively formed.

5.1.1.2 H(AL) TRIP Steels

Table 5.2 represents the initial retained austenite parameters observed in H(AL) steels.

Table 5.2 - Initial retained austenite parameters of H(AL)TRIP annealed AL TRIP steel.

Sample	V_γ	C_γ	$V_\gamma * C_\gamma$
HA1	7.35	1.10	8.0
HA2	7.65	1.30	9.9
HA3	8.10	1.40	11.3
HA4	8.30	1.45	12.0
HC1	8.50	1.40	11.9
HC2	8.80	1.51	13.2

V_γ, C_γ - Volume fraction and carbon content of the retained austenite phase respectively

Compared to the C(AL) specimens, it is immediately apparent that the level of retained austenite is, in general, much higher. However, the general effect of temperature and time is similar to C(AL) steels with regard to retained austenite volume fraction. The carbon concentration present in the retained austenite grains is still quite high and may strongly stabilize the retained austenite.

As mentioned before, highly stable retained austenite starts to undergo SIT transformation at very high strain levels or not SIT at all. Figure 5.5 and 5.6 represents the relationship between retained austenite volume fraction and ICA holding temperature and time, respectively.

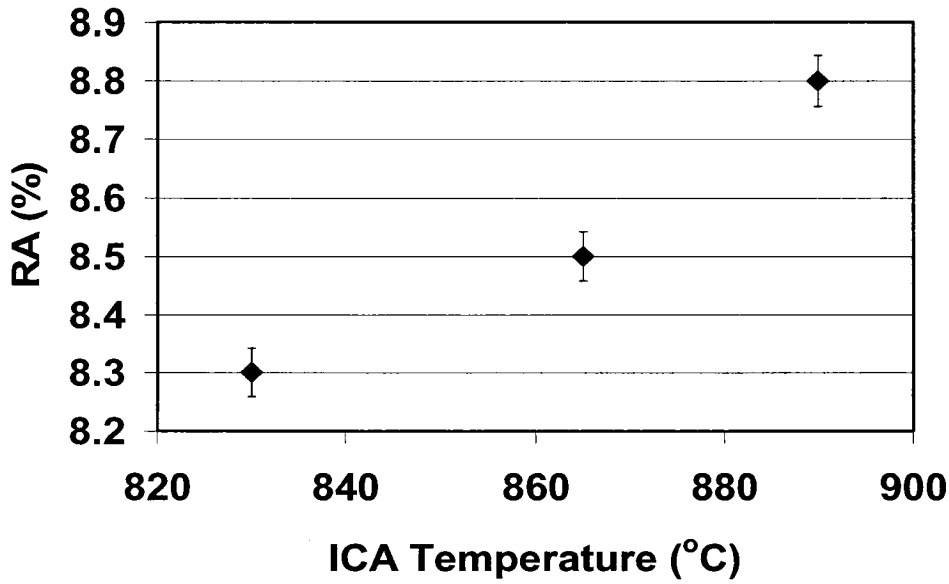

Figure 5.5 Variation of Retained Austenite Volume fraction with ICA Temperature.

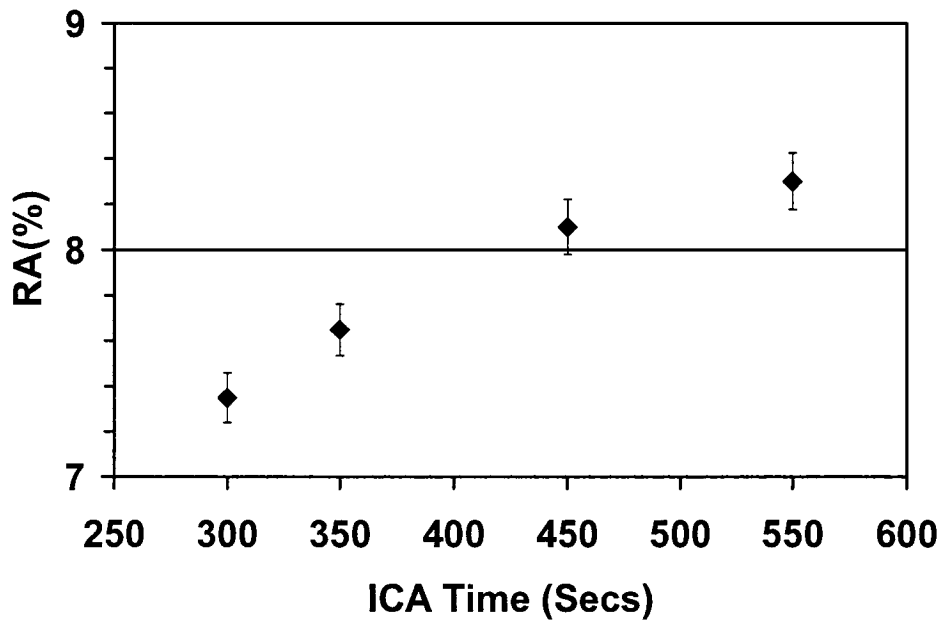

Figure 5.6 Variation of retained austenite volume fraction with ICA time.

The reasoning used to describe the phenomenon of increasing retained austenite volume fraction with increasing intercritical annealing temperature and time for C(AL) steels (Section 5.1.1.1) is applicable to H(AL) steels as well. Figure 5.7, contains

microstructures of H(AL) steels arranged in the order of increasing intercritical annealing time, and thus, increasing retained austenite fraction. The white colored phase seen in the color micrographs correspond to retained austenite, while the light brown phase is ferrite. The dark phases observed correspond to phases rich in carbon, such as lower bainite and/or martensite, if any present or pearlite, if any present.

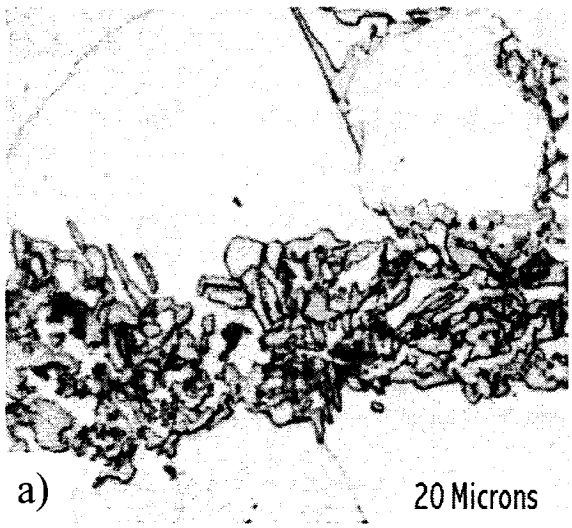

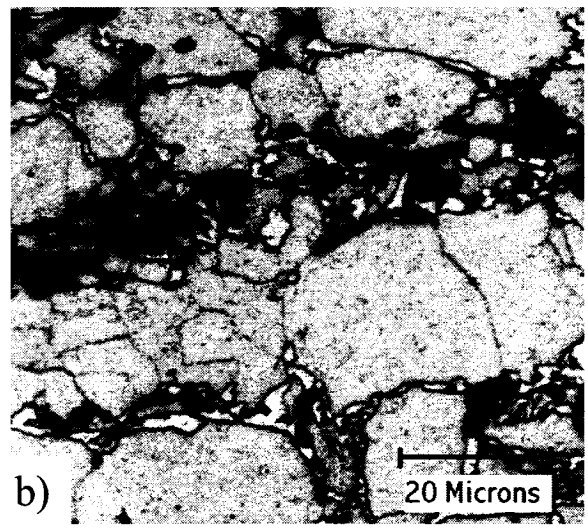

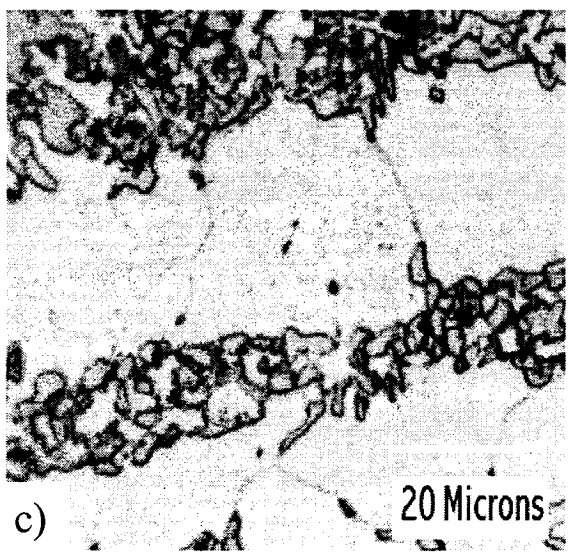

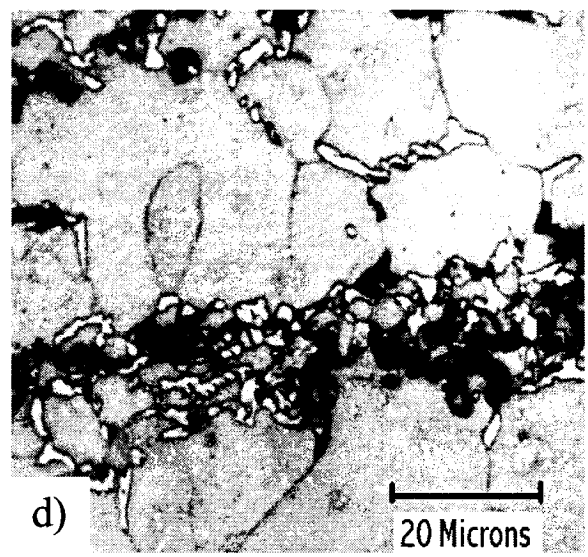

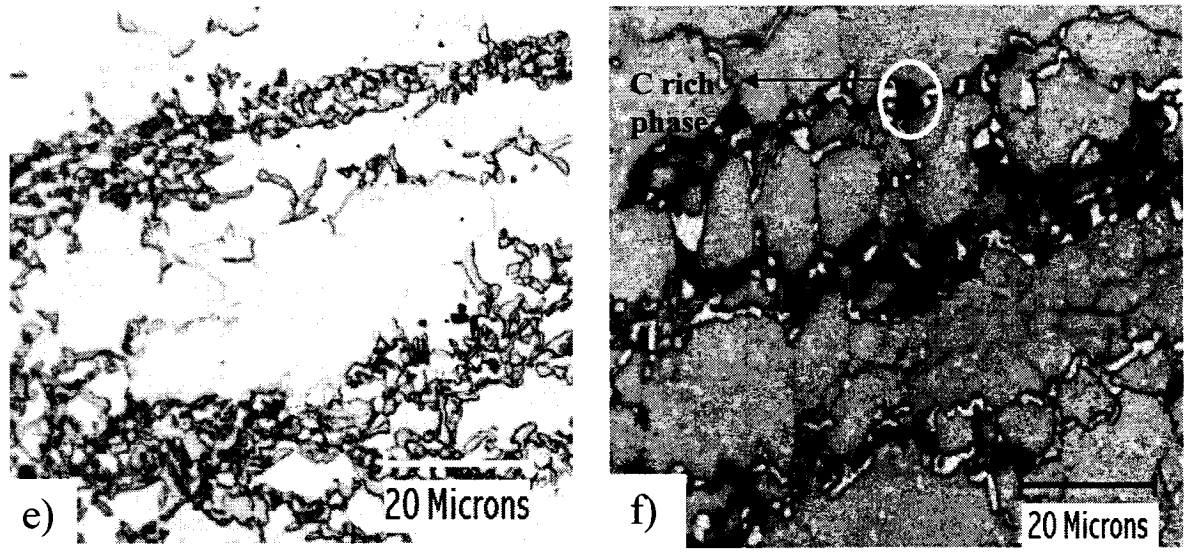

Figure 5.7 Microstructures of H(AL) steel samples: a, b, and c are 2% Nital etched microstructures and d, e, and f are 10% SMB color etched microstructures of HA1,HA2, and HA3 steels, respectively.

From Figure 5.7 a) and b), one can notice the presence of bands in the microstructure, similar to cold rolled and TRIP annealed AL TRIP steel. And similarly, the retained austenite phase has a tendency to form along the bands, as seen in Figure 5.8b. Comparing Figure 5.4 to 5.8a, the banding appears to be more predominant in H(AL) steels compared to C(AL) steels.

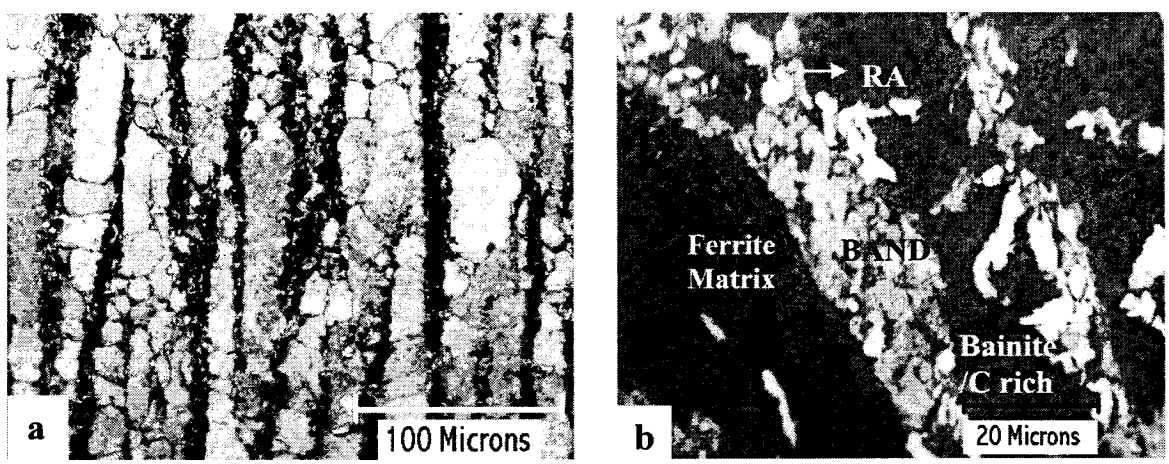

Figure 5.8 Optical micrographs HA1 sample showing banded structure, a) 10% SMB etch b) LePera etch.

The formation of retained austenite and bainite along the bands was also seen by Kim et al [92] in Al containing TRIP steel. He suggested that retained austenite and bainite tend to form preferentially along the bands due to manganese segregation along them. He also suggested that rafting and banding in the microstructure not only affects the retained austenite fraction and morphology but also affects mechanical properties. The black colored phases in the color etched microstructures in Figure 5.7 b, d, and f are perceived to be C rich. It has been observed by steel researchers in the past that super saturation of intercritical austenite during isothermal stage with excess carbon results in the precipitation of carbides rather than retention of such austenite particles at room temperature [93, 94, 95]. However, it is hypothesized that most of the black phase is not carbide, but carbon rich, perhaps a lower bainite.

Also, comparing Figures 5.7 and 5.3, it can be seen that the retained austenite grain sizes are slightly larger in the H(AL) steel 1-3 μm vs. 0.5 to 2 μm in C(AL) steel.

5.1.1.3 H(CL) TRIP Steels

Table 5.3 - Initial retained austenite parameters of H(CL) TRIP steel.

Sample	V_γ	C_γ	$V_\gamma * C_\gamma$
CL-2T	8.40	0.78	6.55
CL-3T	9.12	1.03	9.39
CL-4T	9.94	1.10	10.93
CL-5T	10.63	1.11	11.79
CL-6T	11.00	1.14	12.54
CL-7T	10.11	1.00	10.11
CL-8T	11.20	1.16	12.99
CL-9T	5.00	0.70	3.50

V_γ, C_γ - Volume fraction and carbon content of the retained austenite phase respectively

Table 5.3 shows the initial retained austenite parameters of the H(CL) TRIP steel. As mentioned before, the major technique employed to achieve maximum variation in

retained austenite for this steel was to change the bainitic hold temperature over a 150°C range, keeping other TRIP annealing parameters the same. The influence of bainitic hold temperature on final retained austenite volume fraction is show in Figure 5.9. It can be seen that with decreasing bainitic hold temperature, the amount of austenite retained increases significantly reaching a maximum of 11.2% at 350°C and then dropping to the lowest value of 5% at 300°C. The sudden drop in retained austenite level at temperatures below 350°C could be attributed to the decomposition of two phase austenite to martensite. A similar observation was made by Bouet et al [96]. The data point marked as 600s hold is the retained austenite measurement for sample CL-2T held for 600 seconds at the bainite hold temperature of 400°C.

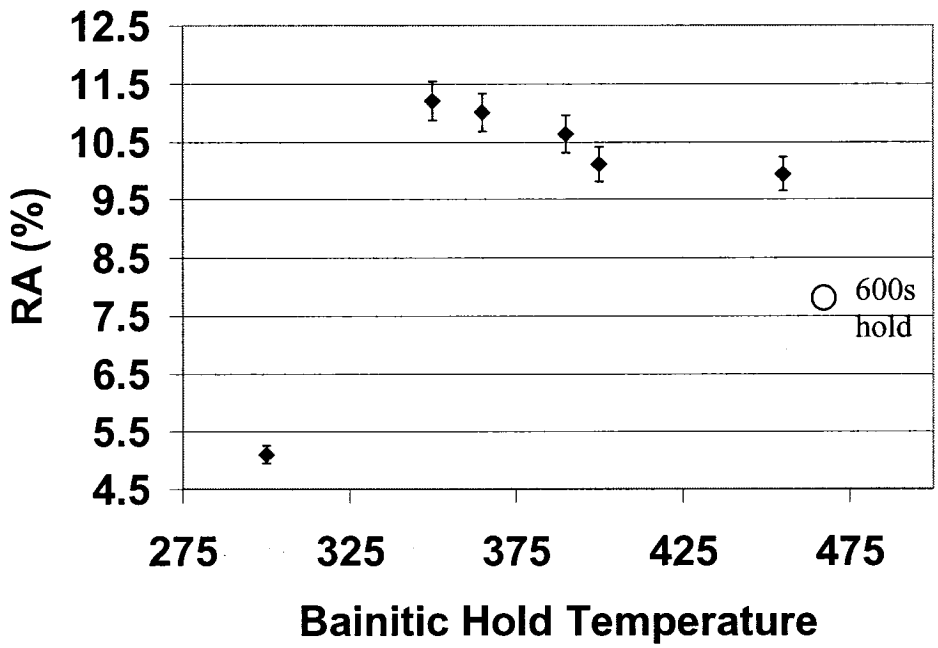

Figure 5.9 Variation of retained austenite volume fraction with bainitic hold temperature.

The effect of bainitic hold time on the microstructure is evident from Figure 5.10, which consists of H(CL) steel with different levels of retained austenite in the final structure, shown in the order of decreasing bainitic hold temperature. Unlike AL TRIP steels, the H(CL) steels exhibit an equiaxed microstructure, largely unbanded, with a relatively homogenous distribution of second phases namely, retained austenite and bainite.

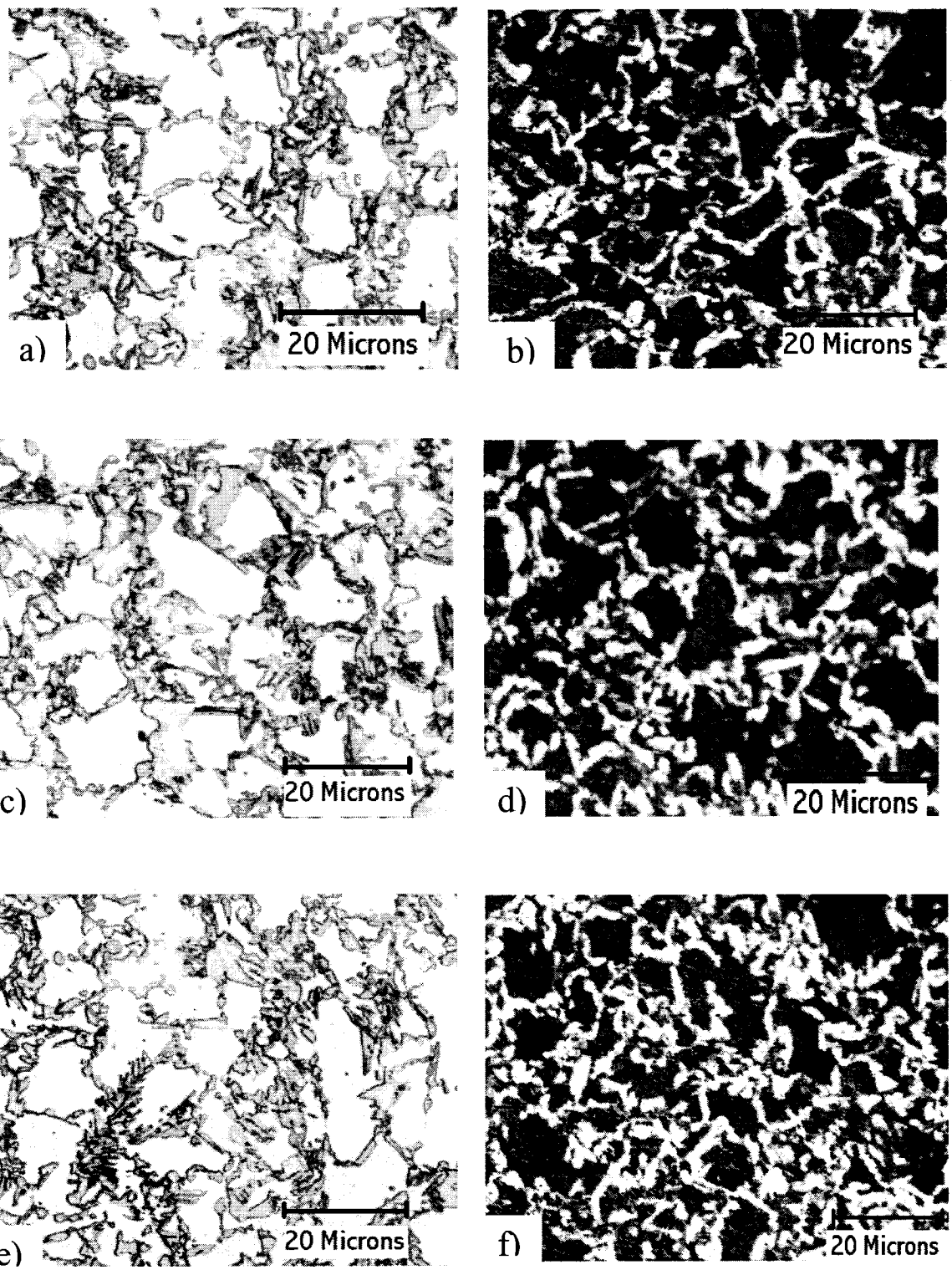
a)
20 Microns
b)
20 Microns
c)
20 Microns
d)
20 Microns
e)
20 Microns
f)
20 Microns

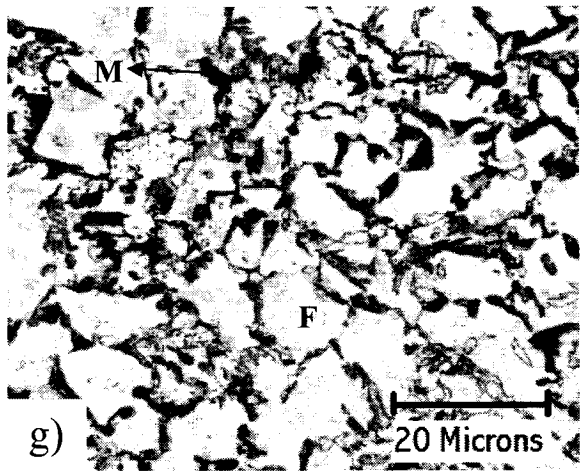

Figure 5.10 Microstructures H(CL) steel samples, a, c, e and f are 2% Nital etched microstructures and b, d, and f are LePera color etched microstructures of CL-4T, CL-5T, and CL-8T, respectively, and g is 2% nital etched microstructure of CL-9T steel.

Similar to AL steels, the retained austenite particles tend to form and cluster along the ferrite grain boundaries in H(CL) steels (Figure 5.10), but banding and rafting in the microstructure is not observed in this case. Moving along the microstructures from b to d in Figure 5.10, there is not much difference in the white phase, but from d to f, there is a noticeable increase, which is somewhat supported by the XRD work (Figure. 5.9). The MA particles are homogenously distributed throughout the microstructure. Such an apparent difference in the distribution of MA particles in the microstructure between the AL and classic steel is brought by non-simultaneous segregation of manganese and carbon during steel casting, which is usually observed with high aluminum containing AL steels [97]. Also, comparing Figures 5.10, 5.7 and 5.3, one can observe that retained austenite grain sizes are considerably bigger in the case of H(CL) steels, around 2 to 4 microns, compared to 0.5 to 2 microns and 1-3 microns in C(AL) and H(AL) steels respectively. Such changes in grain size and morphology are expected to have a strong influence on the final mechanical properties of the steels. As was seen in Figure 5.9, the retained austenite drops when the isothermal bainite temperature is 300 °C, probably due to the formation of martensite [98]. Figure 5.10 g reveals black grains present along the ferrite grain boundaries, which are probably martensite grains.

5.1.2 Mechanical Properties of TRIP steels

Experimental force vs. displacement curves of some of the TRIP (and TMAS) steels are exhibited in Appendix A. (Page 113) at the end of this thesis. Information on the mode of calculation of mechanical properties of the steels from shear punch tests is also presented briefly in the same section.

In the following, it is important to note that the retained austenite fractions quoted for each sample are average values and do not correspond to each individual sample. (In fact, it is reasonable to say that there is not much difference between the retained austenite fractions within each composition, apart from the classic trip composition held at the bainite transformation temperature of 300 °C)

Table 5.4 gives the values of Yield Strength (YS), Ultimate Tensile Strength (UTS), Total Elongation (%El) and Formability Index (F.I) of the steels under investigation. The names of the samples correspond to respective TRIP annealing treatments mentioned in Section 4.3.1.

Figure 5.11 shows the influence of retained austenite fraction on the UTS of the steels under investigation.

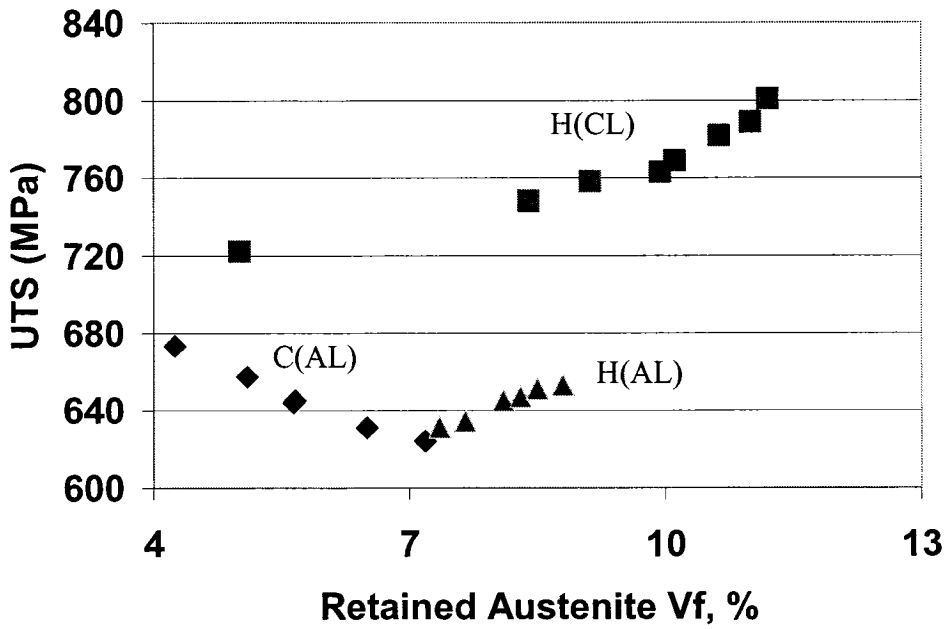

Figure 5.11 Variation of UTS of TRIP steels with retained austenite volume fraction. ***H(AL)*** *– Hot rolled and TRIP annealed high Al steel,* ***C(AL)*** *- Cold rolled and TRIP annealed high Al steel,* ***H(CL)*** *– Hot rolled and TRIP annealed classic TRIP steel*

Table 5.4 Mechanical Properties of C(AL) TRIP Steel.					
Sample	**V_γ**	**σy (MPa)**	**σu (MPa)**	**%El**	***F.I (MPa %)**
A1	5.63	436.0	643.7	32.8	21113.3
A2	5.65	433.0	645.0	33.0	21285.0
A3	6.50	424.8	631.0	35.5	22400.0
A4	5.09	456.5	657.4	33.1	21759.9
C1	7.18	414.0	624.0	39.0	24336.0
V	4.25	464.0	673.0	29.7	19988.1
Mechanical Properties of H(AL) TRIP Steel.					
Sample	**V_γ**	**σy (MPa)**	**σu (MPa)**	**%El**	***F.I (MPa %)**
HA1	7.35	421	631.2	34.0	21460.8
HA2	7.65	423	634.4	35.3	22394.3
HA3	8.10	422	645.0	36.1	23284.5
HA4	8.30	419	647.0	37.0	23939.0
HC1	8.50	427	651.2	38.4	25006.0
HC2	8.85	425	653.0	40.0	26120.0

Mechanical Properties of H (CL) TRIP Steel.					
Sample	V_γ	**σy (MPa)**	**σu (MPa)**	**%El**	***F.I (MPa %)**
CL-2T	8.40	459.0	748.0	35.4	26479.2
CL-3T	9.12	465.3	758.0	36.2	27439.6
CL-4T	9.94	467.0	763.0	38.0	28994.0
CL-5T	10.63	465.0	782.0	41.0	36062.0
CL-6T	11.00	469.2	789.0	44.0	34716.0
CL-7T	10.11	462.0	769.0	39.0	29991.0
CL-8T	11.20	471.0	801.0	46.0	36846.0
CL-9T	5.00	462.8	462.8	24.0	17328.0

It is apparent from Figure 5.12 that the UTS of H(AL) and H(CL) steels increase with increasing retained austenite fraction while it reduces for the C(AL) steels, the latter being in contrast to the literature findings. According to Zackay et al. [99], the postponing of necking and progressive work hardening is a direct consequence of the transformation of retained austenite to SIT martensite during deformation of TRIP steels. And, any increase in such transformable meta-stable retained austenite fraction brings a marked increase in both strength and ductility. But this is not the case with the C(AL) steels under investigation. The steels shows very low strength levels at high retained austenite values. For instance, with an increase of retained austenite fraction from 4% to 7%, the strength of the steel drops by almost 50 MPa from 675 MPa to 621 MPa.

Such an anomaly is believed to be the effect of retained austenite grain size, carbon concentration and the effect of phases surrounding the retained austenite grains, which have an influence on strain sensitivity of retained austenite present [100]. Details of this peculiar phenomenon will be discussed in the forthcoming chapter.

The UTS of the other two TRIP steels, H(AL) and H(CL) steels increase with increasing retained austenite, a trend which other steel researchers have observed in the past. This is assumed to be the effect of strain induced transformation of the retained austenite phase to martensite during deformation. This strain induced transformation of retained austenite to martensite offers progressive work hardening of the steel, which in turn manifests itself in the form of improved strength [101, 102], as observed in Figure 5.11.

But on closer inspection, one can observe that the strength levels achieved by the H(AL) steels are relatively modest compared to the H(CL) steels. For instance, in H(CL) steels, a change in retained austenite fraction by approximately 3% from 7.2% to 11.2 % brings about a change in UTS by 100 MPa, which is significantly higher compared to AL steels, where the corresponding change is only approximately 40 MPa. The reasons for such a difference in strength levels improvement will be discussed later. Higher carbon concentration in the

retained austenite in H(AL) steels (0.7 to 1.1 vs 1.1 to 1,5 wt%) is also believed to be a strong factor in poor mechanical response of the steel since this implies less strain induced transformation.

Figure 5.12 shows the relationship between retained austenite volume fraction and total elongation of the TRIP steels under investigation.

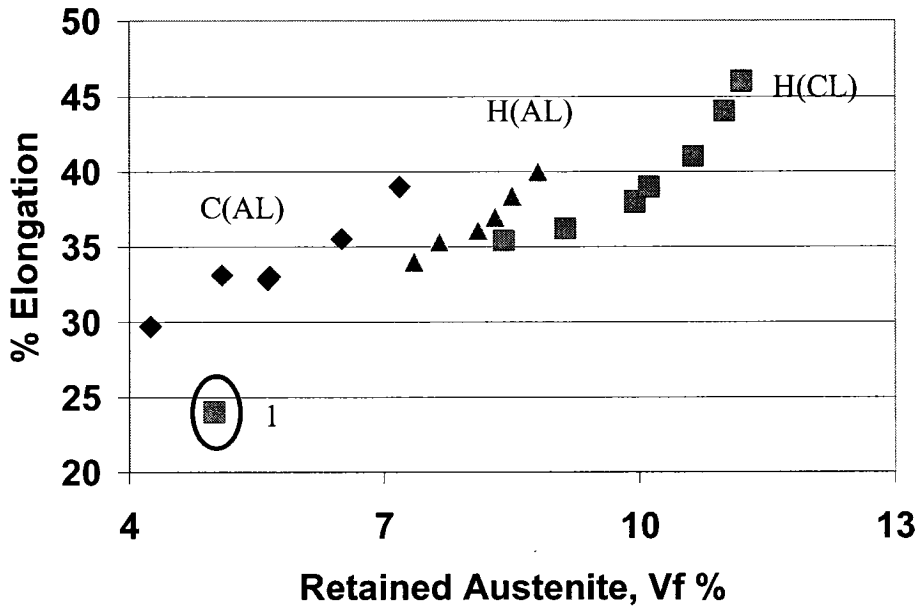

Figure 5.12 Variation of TRIP steel total elongations with retained austenite volume fraction. ***H(AL)*** *– Hot rolled and TRIP annealed,* ***C(AL)*** *- Cold rolled and TRIP annealed,* ***H(CL)*** *– Hot rolled and TRIP annealed CL steel*

It is clear from the figure that there is a definite increase in the total elongation of all the steels with increasing retained austenite volume fraction. This could be indicative of the fact that SIT of the retained austenite phase is taking place during straining resulting in increased strength and ductility. Over the limited range at which the three steels overlap in terms of retained austenite fraction, the C(AL) steels are clearly superior, with the other two steels behaving similar to each other. At the highest level of RA, the H(CL) steel seems to exhibit an increase in the rate of improvement in elongation with RA fraction, similar to the effect of

RA seen in the UTS results (Figure. 5.11). The reason that the H(AL) steel is worse than the C(AL) steel may be due to the presence of bands in the microstructure and coupled with high carbon concentration of retained austenite. Such loss in ductility due to banding in the microstructure has been observed by Kim et al [103] in past for chemically similar steels. However, this does not explain why the H(AL) steel is better than the H(CL) steel. However, the H(CL) steel does exhibit the largest retained austenite particle sizes, which are then relatively unstable, and may contribute to the inferior ductility compared to the H(AL) steel.

It is also interesting to note that the data point with the lowest value of elongation, circled and numbered as 1, corresponds to CL-9T steel which contained some amount of martensite in its microstructure in conjunction to a low RA fraction of 5%. The presence of hard martensite particles could be the reason behind poor elongation values exhibited by the steel.

Figure 5.13 clearly indicates that the formability index increases with retained austenite volume fractions for all the steels and conditions experimental steels.

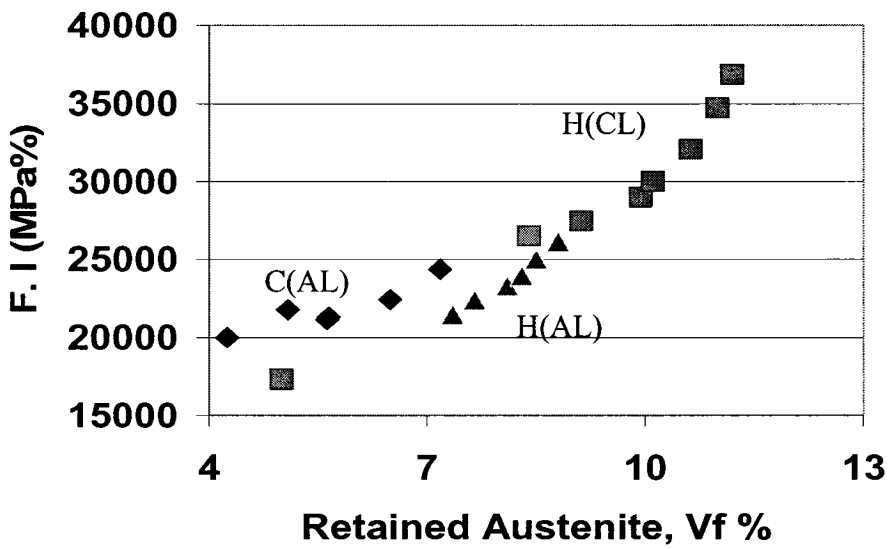

Figure 5.13 Variation of formability index of TRIP steels with retained austenite volume fraction. ***H(AL)*** *– Hot rolled and TRIP annealed,* ***C(AL)*** *- Cold rolled and TRIP annealed,* ***H(CL)*** *– Hot rolled and TRIP annealed CL steel.*

For the C(AL) steels, the rate of the increase is relatively low compared to the others. For instance, the formability index changes only by 5000 MPa% for a change in retained austenite volume fraction from 4% to 7%. On the other hand, the formability index of the H(CL) almost doubles from 17,000 MPa% to 30,000 MPa% for a similar increase in the retained austenite fraction from 5% to 8%. This is mainly because the C(AL) steels decrease in strength with increasing RA, unlike the H(AL) and H(CL) steels.

For the same RA volume fraction, H(AL) steels exhibit formability indices somewhat lower than the H(CL) steels. The reasons for such low formability indices are probably connected to the difference in strength levels.

To summarize, H(CL) steels exhibit better retained austenite retention capacity, and consequently the highest retained austenite levels, and the highest mechanical properties corresponding to these levels. The C(AL) steels exhibit the lowest austenite retention levels, but at these low RA values, the C(AL) steel exhibits the best elongation and formability values. The H(AL) steels are slightly better at retaining austenite compared to the C(AL) steels, but tend to be inferior to the C(AL) steels for the same level of RA in terms of elongation and formability. .

5.2 Results of TMAS Processing and Testing.

This section presents the results of processing on microstructural evolution and mechanical property of Tempered Martensite Assisted Steels (TMAS) obtained via cold rolling of TRIP steels and a subsequent subcritical annealing at 500°C for 1 hour. The subcritical annealing is designed to temper all the SIT martensite and to recrystallize the ferritic matrix. As mentioned in Section 4.5, the amount of tempered martensite in TMAS structure is equal to the amount of retained austenite in the prior TRIP microstructure, except in the case of the CL-9T steel which contained 5% RA and martensite due to quenching at isothermal bainitic

transformation temperature of 300°C. In the latter, the amount of martensite formed as a result of the TRIP annealing has not been measured.

5.2.1 Effect of cold rolling

Figure 5.14 presents the microstructures of cold rolled experimental TRIP steels.

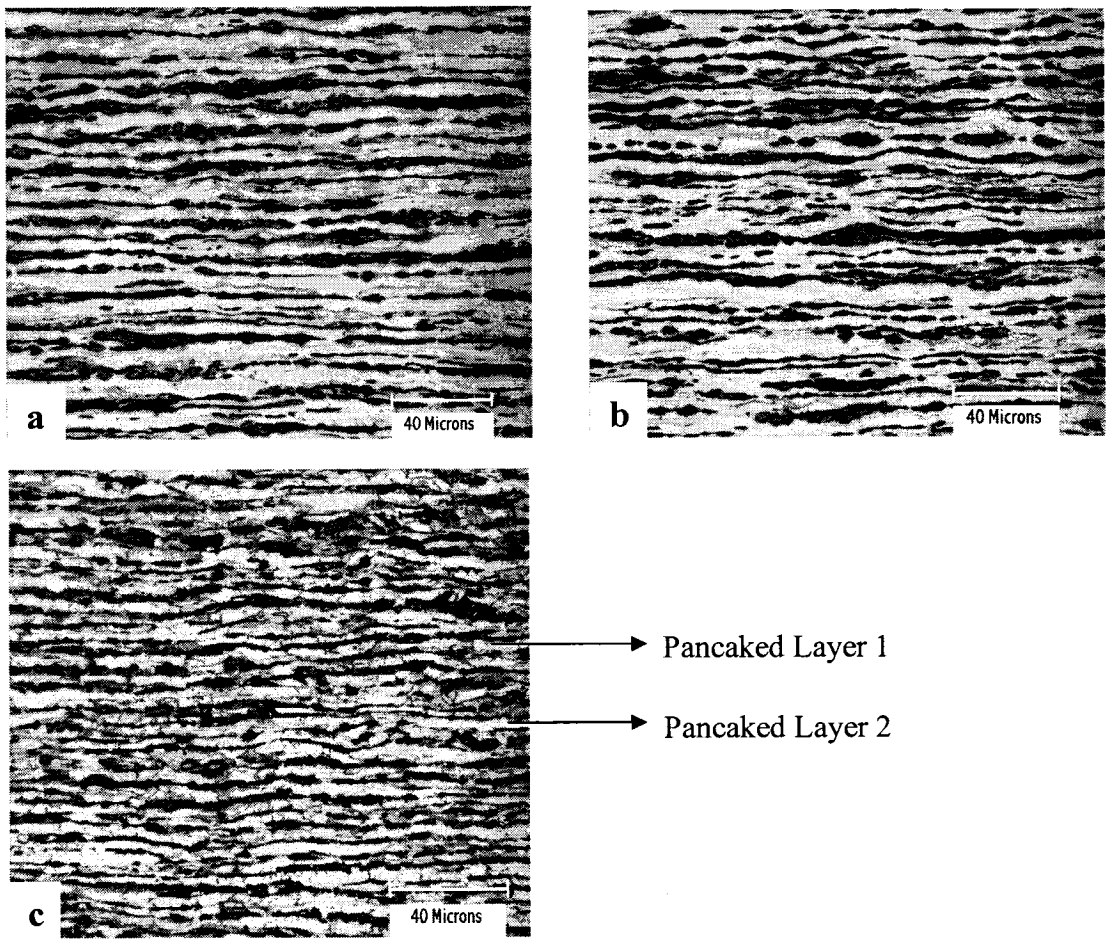

Figure 5.14 Cold rolled microstructures of TRIP steels, a) 2% Nital etched C(AL) steel, b) 2% Nital etched H(AL) steel, c) 2% Nital etched H(CL) steel.

Microstructures in Figure 5.14 show heavily pancaked structures which is a direct consequence of the cold rolling operation. The grains are flattened out and elongated along the rolling direction, resulting in a pancaked structure. Notice how the banding frequency (i.e.

width of the bands) varies from 5.14 a) to c). The lowest frequency is observed in the H(AL) steel (Figure 5.14 b) and the highest in H(CL) steel (Figure 5.14 c). This is, of course, a reflection of the prior microstructures. In general, the H(CL) steels have an equiaxed, fine TRIP structure compared to C(AL) and H(AL) steels which are severely banded and have large ferrite grains between the bands (Figure 5.8 a).

5.2.2 Microstructural Evolution of TMAS

5.2.2.1 C(AL) TMAS Structure

Figure 5.15 consists of the microstructures of A1, A3 and C1 TMAS, respectively. The microstructures are arranged in increasing order of tempered martensite fraction. However, no significant difference in the amount and distribution of second phase (bainite + tempered martensite) is apparent between the microstructures.

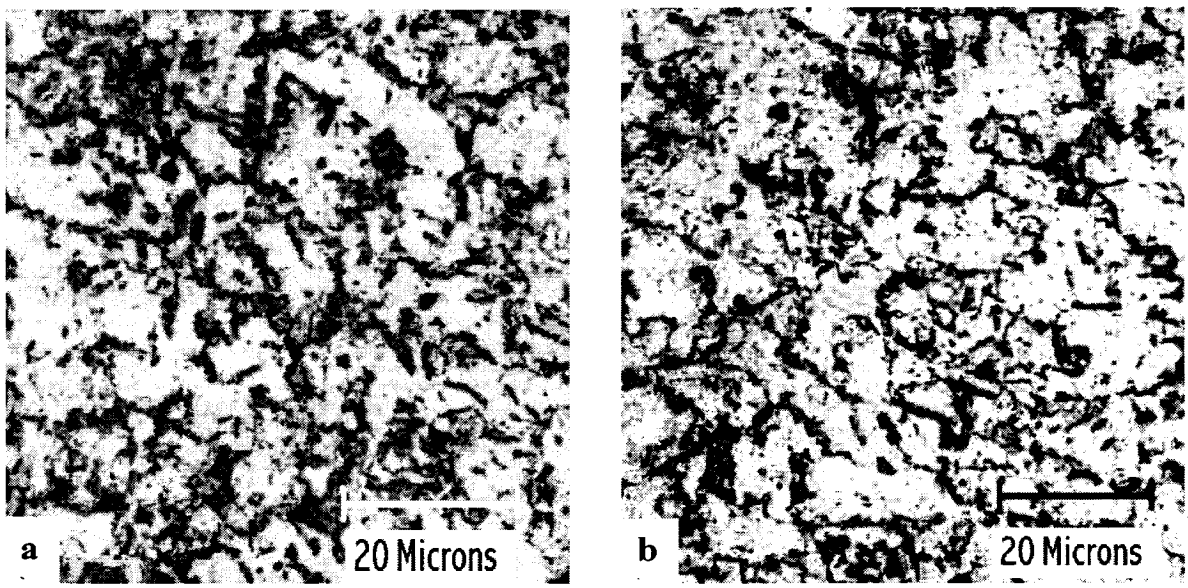

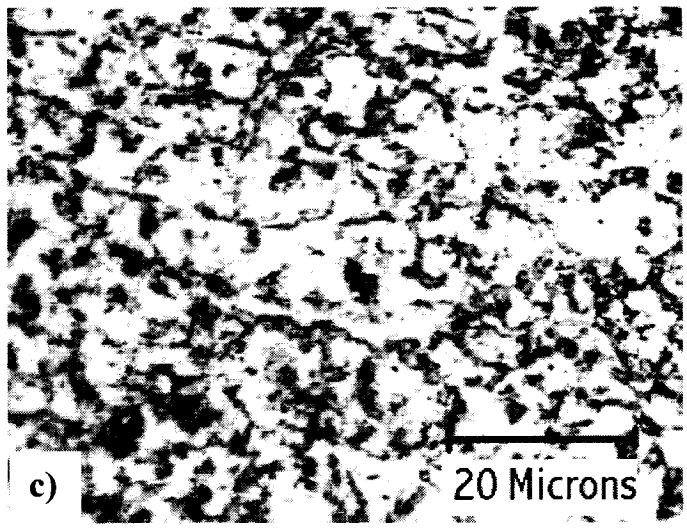

Figure 5.15 2% nital etched microstructures of a) A1 TMAS, b) A3 TMAS and c) C1 TMAS.

Comparison of Figure 5.15 to 5.14 clearly shows that the banded and the pancaked structure have been almost completely eradicated, indicating recrystallization of the ferrite and the bainite (the dark phase).

Jeong et al [104] made a similar observation with a chemically similar TMAS, and he suggested that tempering after cold rolling at subcritical temperatures ranging from 500°C to 600°C resulted in recrystallization and grain refinement. He also suggested that recrystallization and grain refinement of the cold rolled structure resulted in relatively high strength and formability whose values were close in range to the values achieved by commercial TRIP steels.

Figure 5.16 more clearly shows how the original cold rolled and TRIP annealed AL steel has been affected by the TMAS treatment. Here, the initial TRIP anneal after the first cold rolling was A3 (830 °C intercritical anneal, followed by 400 °C for 240s) leading to the structure shown in Fig. 5.16 (a), and the subcritical anneal after the second cold rolling was 500 °C for 1hour, giving Figure. 5.16 (b). The microstructures were taken from the same area in the

sample before and after cold rolling and subcritical annealing. There appears to be some grain refinement in TMAS compared to its prior TRIP structure, and a reduction in the degree of banding. There appears to be more second phase, but this may be an etching effect. The average ferrite grain size of the prior TRIP structure was 20 microns, while the average grain size of the TMAS was only around 14 microns. This grain refinement is expected to have an influence on the final mechanical properties of the TMAS.

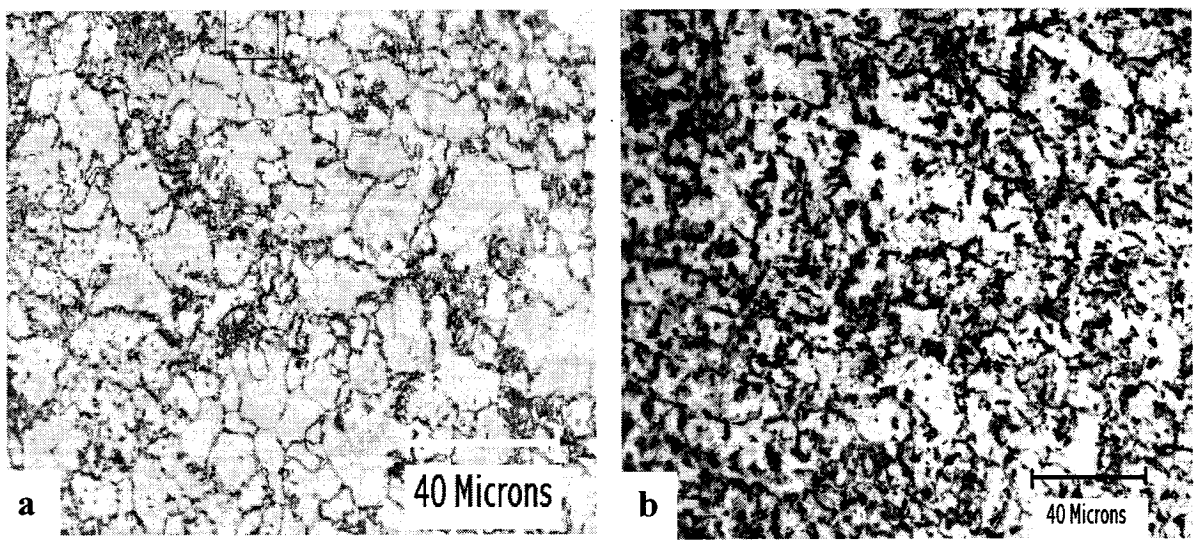

Figure 5.16 Comparative microstructure of A3 C (AL) TRIP and TMAS.

5.2.2.2 H(AL) TMAS Structures

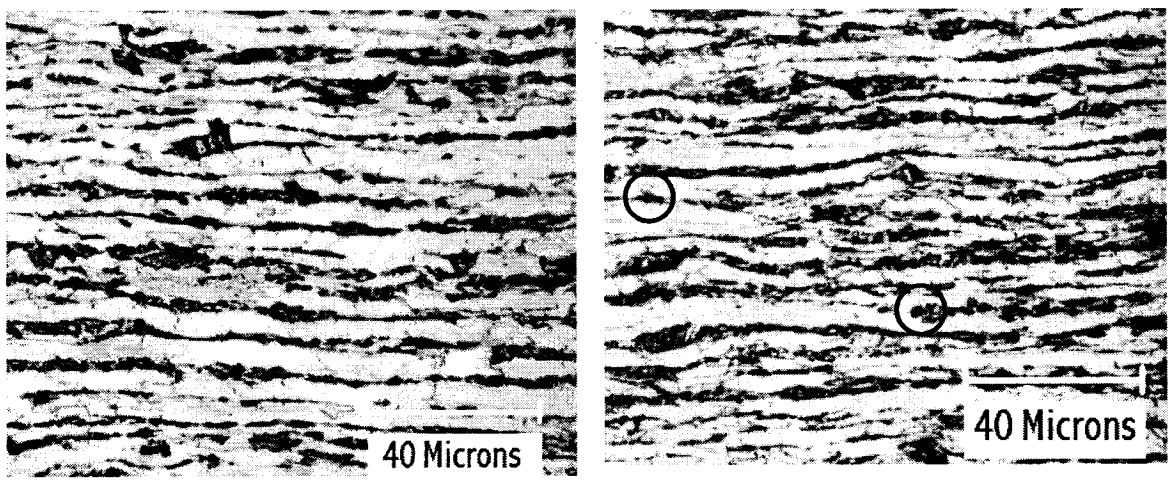

Figure 5.17 2% nital etched microstructures of a) HA1 TMAS, b) HA3 TMAS

This steel has retained much of the pancaked characteristics of the cold rolled microstructure, suggesting that the extent of recrystallization is much reduced compared to the C(AL) steel above. However, it is clear that ferrite has recrystallized to some extent and there are some signs of recrystallization, or some sort of microstructural change, in the second phase (bainite bands).

5.2.2.3 *H(CL) TMAS Structures.*

The H(CL) TMAS exhibit microstructures very similar to the ones seen with H(AL) steels (Figure 5.17). There are clear signs of recrystallization in the ferrite layers. The second phase seems to have been much more affected by the subcritical anneal compared to the H(AL) TMAS specimens. The spheroid-like 'chains' (circled) are probably the remnants of very thin pancaked second phase layers. There are some signs of this in the H(AL) TMAS structures (Figure 5.17b), but not as extensively as seen here. This suggests, perhaps, that the bainite of the classic TRIP steel is more readily 'recrystallized' than the bainite of the high Al TRIP steel. Or the morphology of the bands is more amenable to recrystallization.

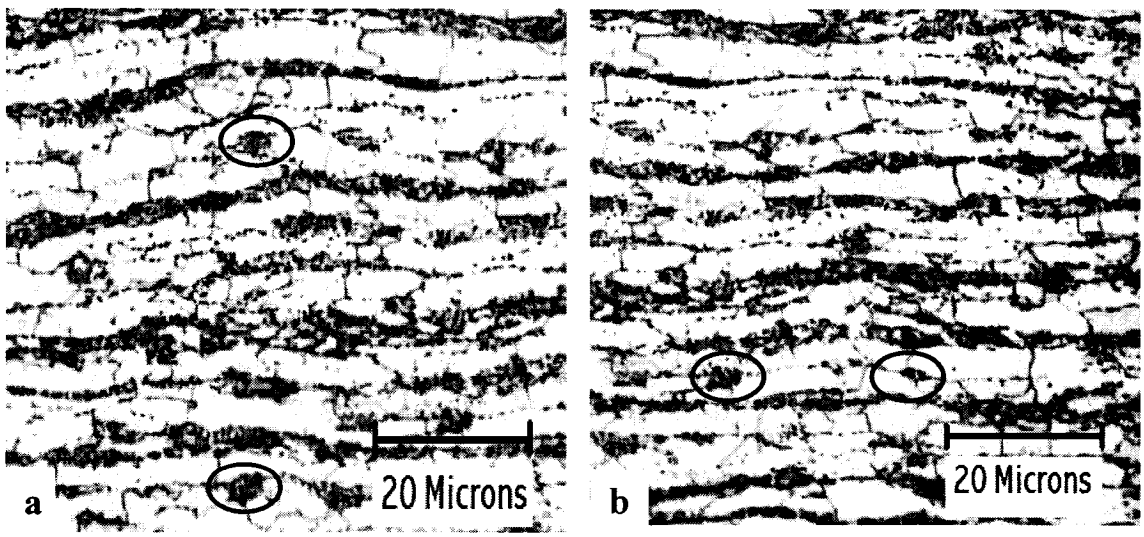

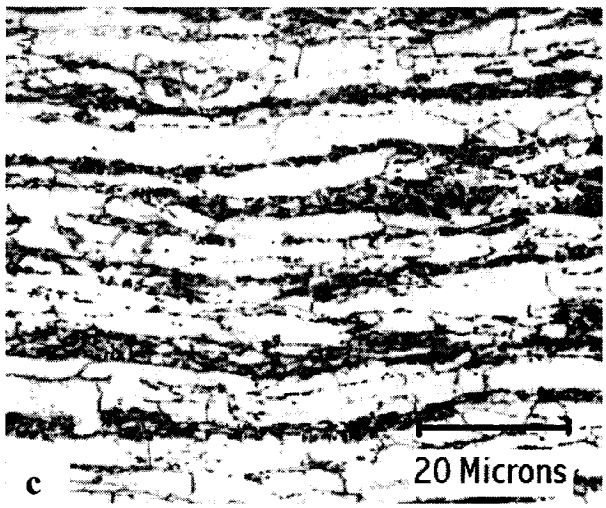

Figure 5.18 2% nital etched microstructures of a) CL-4T TMAS, b) CL-5T TMAS and c) CL-8T TMAS

The micrographs in Figure 5.18 are arranged in the order of increasing tempered martensite fraction. Moving from Figure 5.18 a) to c), there does not seem to be a significant difference between the microstructures, except for the number of recrystallized grains and the spheroids of secondary phases. For instance, there appears to be more degree of recrystallization in CL-4T steel compared to CL-8T, although this could be etching effect of a local microstructural variation. Decrease in the number of recrystallized grains with increasing fraction of tempered martensite can be attributed to the pinning effect of tempered martensite particles, inhibiting recrystallization and grain growth.

5.2.3 Mechanical Properties of TMAS.

Table 5.5 gives the mechanical properties of all TMAS. The names of the samples in the table correspond to the TRIP steels they were obtained from and their respective tempered martensite fractions. It is clearly apparent from the table, that any variation in the tempered martensite volume fraction brings significant changes in the mechanical properties of the steel. Figure 5.19 represents the relationship between UTS and tempered martensite volume fraction of all the experimental TMAS.

Table 5.5 Mechanical Properties of C(AL) TMAS					
Sample	**V_α**	**σy (MPa)**	**σu (MPa)**	**%El**	***F.I (MPa %)**
A1	5.63	809.0	874.0	22.3	19490.2
A2	5.65	812.6	876.7	21.8	19112.0
A3	6.50	833.5	882.0	19.7	17375.4
A4	5.09	773.0	847.0	23.0	19481.0
C1	7.18	814.0	893.0	18.4	16431.2
V	4.25	809.0	874.0	23.8	20801.2
Mechanical Properties of H(AL) TMAS					
Sample	**V_α**	**σy (MPa)**	**σu (MPa)**	**%El**	***F.I (MPa %)**
HA1	7.35	711	881.0	22.8	20086.8
HA2	7.65	714	885.0	21.4	18939.0
HA3	8.10	721	892.2	20.9	18646.9
HA4	8.30	719	895.0	19.2	17184.0
HC1	8.50	715	901.0	18.4	16578.4
HC2	8.85	720	912.0	18.0	16416.0

Mechanical Properties of H(CL) TMAS					
Sample	**V_α**	**σy (MPa)**	**σu (MPa)**	**%El**	***F.I (MPa %)**
CL-2T	8.4	682	891	24	21384
CL-3T	9.12	689	902	22.8	20565.6
CL-4T	9.94	694	912	21	19152
CL-5T	10.63	696	921	19.7	18143.7
CL-6T	11	691	933	18.4	17167.2
CL-7T	10.11	683	919	20	18380
CL-8T	11.2	694	941	17.9	16843.9
CL-9T	5	672	924	26	21424

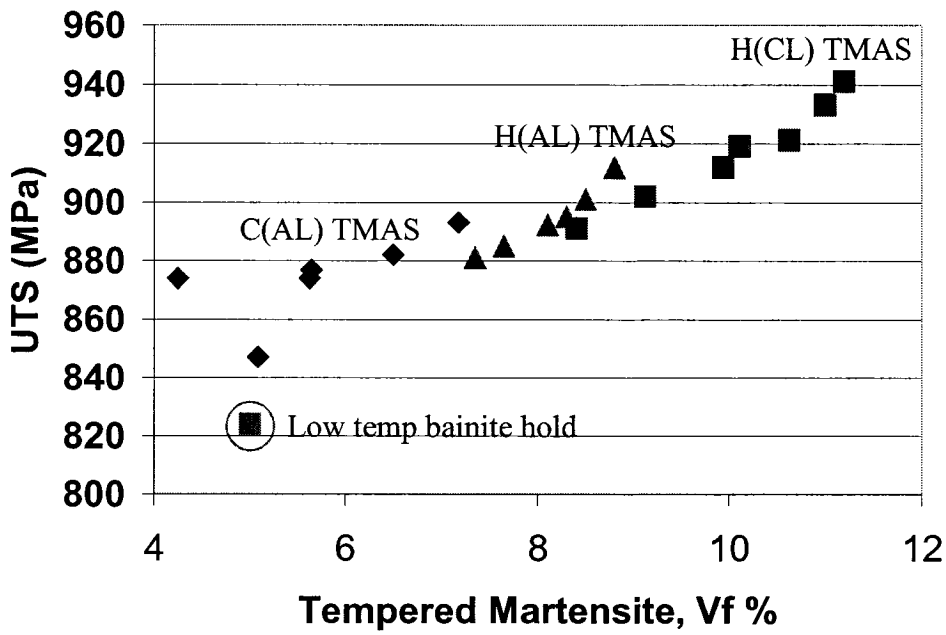

Figure 5.19 Variation of TMAS UTS with tempered martensite volume fraction.

The UTS of almost all of the TMAS appears to be *solely* controlled by the amount of tempered martensite (i.e. the amount of retained austenite prior to cold rolling), and increases with increasing tempered martensite fraction. This is in contrast to the steels in the TRIP annealed condition (Figure. 5.11) where the UTS were not only controlled by the retained austenite, but by other factors. In particular, note the difference in UTS of the high Al steels vs. the classic TRIP for the same retained austenite level in Figure. 5.11 has been totally eradicated by the TMAS treatment. The only exception to this observation is the 5% retained austenite Cl-9T H(CL) steel, which was generated by quenching to a low bainite hold temperature. This steel in the TMAS condition exhibits a relatively low UTS for a given prior retained austenite level and does not seem to belong to the population defined by the other steels.

Figure 5.20 addresses the relationship between total elongation and tempered martensite volume fraction.

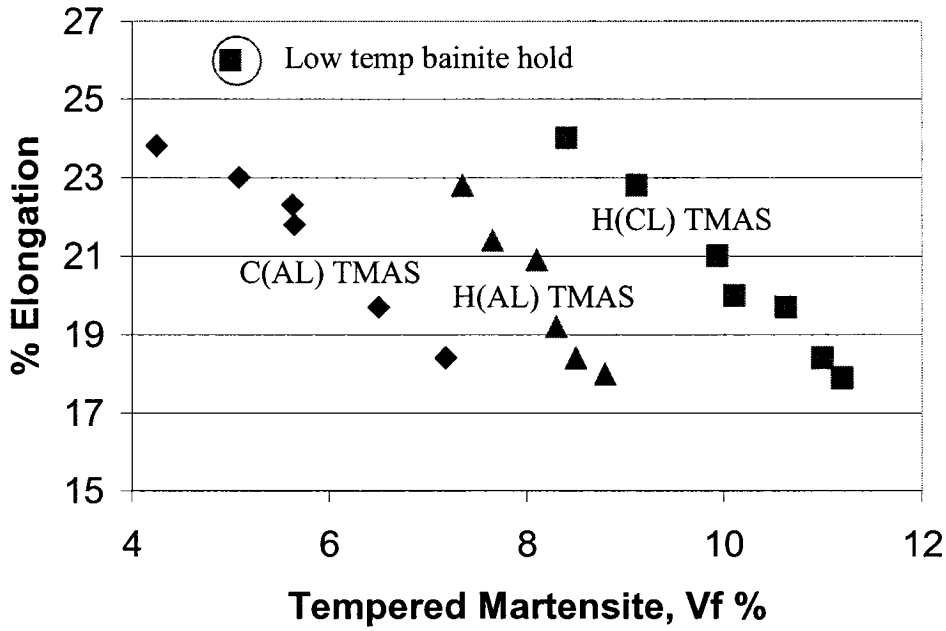

Figure 5.20 Variation of TMAS total elongations with tempered martensite volume fraction.

This sort of behavior is in accordance with general trend observed with conventional high strength materials, where any increasing strength comes at the price of decreasing ductility and formability [105]. Unlike the effect on UTS, TMAS processing appears to have accentuated the differences between the steels. In fact one can notice that there are now three very clearly delineated populations of behavior revealed in Figure. 5.20, compared to the TRIP annealed versions of these steels, Figure. 5.12, where the steels are less well separated into their respective microstructures and prior processing conditions. Again the 5% retained austenite CL-9T H(CL) steel, which was generated by quenching to a low bainite hold temperature seems to not belong to the TMAS generated from the classic TRIP steels.

Figure 5.21 represents the influence of tempered martensite volume fraction on the formability index values of TMAS.

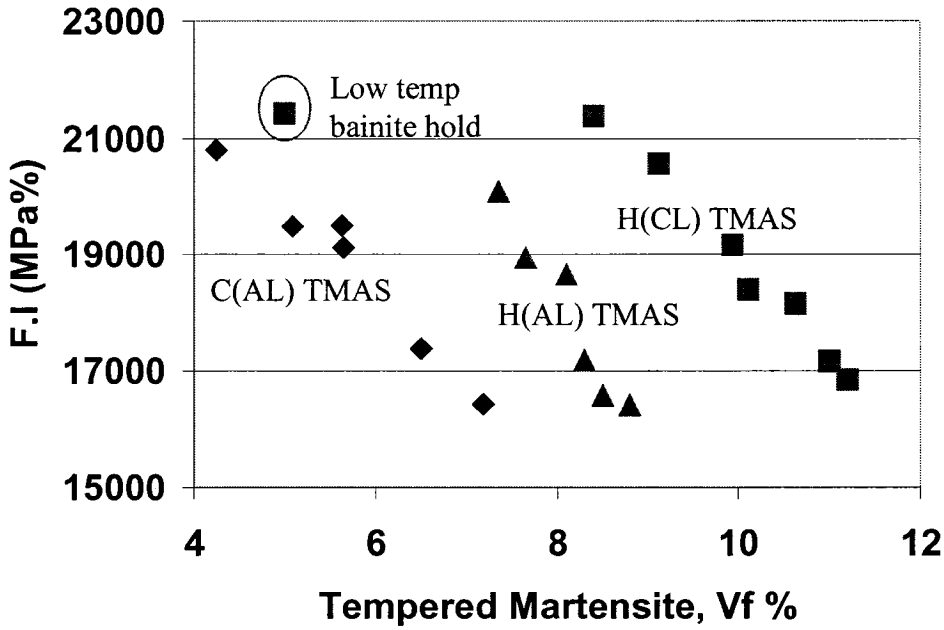

5.21 Variation of TMAS formability index with tempered martensite volume fraction.

The formability index of the steels follows a similar trend observed with the steels' total elongation, which is not surprising since, on the basis of total elongation, all the TMAS belong to different populations. It can be clearly seen from the figure that any increase in tempered martensite fraction decreases the formability index of the steels. The formability index values accentuate the observation that the low bainite hold version of the classic TRIP steel is very different compared to the other classic TRIP steels in the TMAS condition.

CHAPTER 6

Discussion

6.1 TRIP Steel Processing

6.1.1 Effect of Intercritical Annealing Parameters on Retained Austenite Fraction: H(AL) and C(AL) steels

It is noteworthy to remember that *only* the aluminum containing TRIP steel were subjected to changes in intercritical annealing parameters. Changing the intercritical parameters such as temperature and holding time varied the degree of austenite retention in these steel.

6.1.1.1 Effect of Intercritical Annealing Temperature

As was illustrated in Figures 5.1 and 5.5, an increase in the intercritical annealing temperature from 830°C through 890°C resulted in an increase in retained austenite volume fraction, where a maximum was observed for both the steels at 890°C.

With respect to the estimate of Jeong et al [106], based on a calculated phase diagram for high Al TRIP steels, at intercritical annealing temperatures of 830, 865 and 890°C the amount of relative intercritical phase distribution of ferrite to austenite is 70:30, 40:60

and 45:55, respectively. Ho et al [107] reported that the ferrite fractions were over estimated by a factor of 2 to 3% by the FACTSAGE software at intercritical temperatures ranging from 780°C onward. The same software was used by Jeong et al [108] for predicting the equilibrium temperatures of 0.16%C- 2% Al- 1.5%Mn TRIP steel and the results from his work are used in this work. This means, at 890°C the volume fraction ratio of austenite to ferrite is 47:53 and not 45:55 denoted by the software.

As mentioned in the literature review, some researchers [109, 110] postulate that the highest fraction of retained austenite and best mechanical properties are observed when TRIP steels are intercritically annealed at a volume fraction ratio of 60% austenite to 40% ferrite, while others say [111, 112] the best results are achieved when intercritically annealed at a temperature where the volume fraction ratio of austenite to ferrite is 50:50.

In this study, the highest retained austenite content was observed for both C(AL) and H(AL) steels at 890°C, where the relative volume fraction ratio of two phase austenite to ferrite was 45:55. If the estimates of Jeong (with the Ho 'correction') regarding the amount of austenite in the intercritical region are assumed to be correct, then, with respect to the fraction of austenite, the maximum occurs at 890°C, which corresponds to 47% austenite. Increasing this intercritical austenite to 60% by intercritically annealing at 865 °C reduces the retained austenite. This is in close agreement with the postulates proposed by the aforementioned researchers who claim that austenite retention is maximized at 50% intercritically formed austenite. [111, 112]

Though the final retained austenite fraction increases with increasing intercritical annealing temperature, the range of increase in both the steels is less than or equal to 1% and is very well in the range of possible experimental errors. It is clear that intercritical annealing temperatures used in this work do not alter the final retained austenite fraction significantly, presumably because they do not alter the intercritically formed austenite to a large enough extent. A similar observation was made by Parish et

al [113], and, in fact, there is considerable agreement that the intercritical annealing temperature does not strongly affect the properties.

Kim et al [114] reported that the best way to achieve good strength-ductility balance coupled with a good retained austenite fraction is to set the intercritical annealing temperature in such a way so that the stability of the two phase austenite is increased by keeping the fraction of the two phase austenite as low as possible to promote higher solubility of alloying elements in the austenite. With higher intercritical temperatures, even though the fraction of two phase austenite increases, the solubility of alloying elements in the austenite and stability of the austenite decreases. In other words the final retained austenite content of TRIP steels not only depends on the intercritical annealing temperature but also the solubility of alloying elements in two phase austenite and its stability. So increasing the ICA temperature does not necessarily guarantee any significant increase in final retained austenite volume fraction. This is in complete accordance with the results observed in this work, section 5.1.1.1 and 5.1.1.2, where an increase in temperature by almost 100°C brought negligible change to the final retained austenite fraction. However, in this work, the overriding reason for the negligible effect of intercritical annealing temperature is because there is little change in the retained austenite at the end of TRIP processing,

6.1.1.2 Effect of Intercritical Annealing Hold Time

An increase in intercritical holding time also results in the increase of the final retained austenite volume fraction, as illustrated in Figure 5.2 and 5.6. This is in accordance with the trend observed in the literature [115]. It has been reported that longer holding times homogenize the microstructure and offer more time for the ferrite, pearlite and cementite present in the initial microstructure to efficiently transform to intercritical austenite [116]. However, very long holding times also initiate grain coarsening and are detrimental to the final properties [117]. So by increasing the holding time up to a stipulated limit can improve the final retained austenite fraction, which is exactly what

is observed in Figure 5.2 and 5.6, where increasing holding times brings about an increase in retained austenite fraction. Again, the increase is quite small, of the order of 1%.

6.1.1.2 Effect of Isothermal Annealing Temperature on Retained Austenite Fraction

Only the retained austenite content in H(CL) steels was modified by altering the isothermal annealing parameters, especially the temperature. Changing the isothermal hold temperature from 475°C to 350°C resulted in an increase in retained austenite fraction, where a maximum was observed. Decreasing the temperature further shifted the trend in opposite direction. The retained austenite fraction plummeted to a very low value of around 5% at 300°C.

As mentioned in the literature review, in general, the bainite transformation stage dictates the level of retained austenite and transformation of austenite to bainite is a strong function of temperature. At higher bainite temperatures, more of the intercritical austenite transforms to bainite and there is less austenite to retain on cooling to room temperature. In addition the bainite formed is coarse and the remaining enriched austenite tends to form as films between the bainitic ferrite laths. So, bainite morphology affects the stability of the retained austenite [118].

Here, to a first approximation, decreasing temperatures decrease the rate of transformation of the intercritical austenite, changes the bainite morphology from coarse to fine and promote C segregation to the remaining austenite, both tending to increase the retained austenite. Figure 6.1 is the microstructure of CL-4T steel isothermally bainite transformed at 455°C showing coarse bainite and inter-lamellar film type retained austenite. This is in accordance with the trend observed by the aforementioned researcher.

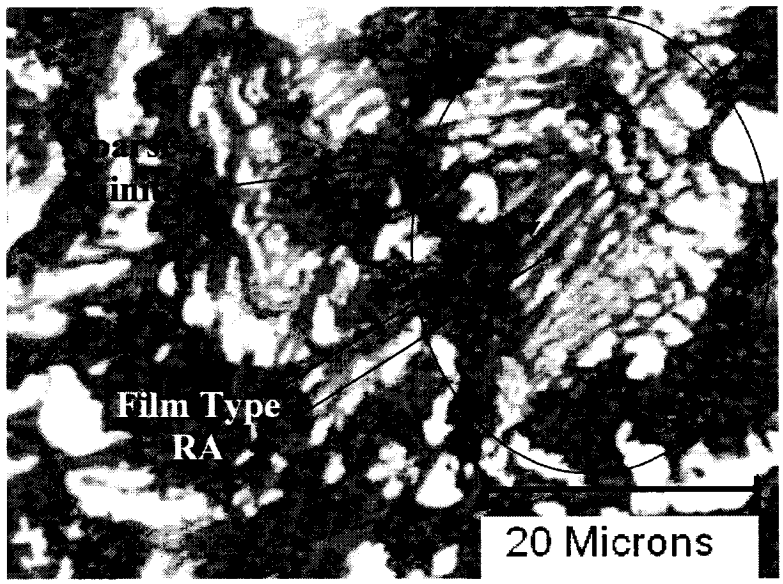

Figure 6.1 CL 2T TRIP steel with bainitic inter-lamellar film type retained austenite. LePera color etched. IBT temperature = 455°C

Thee results in this work (Figure. 5.9) correspond quite well to the plateau region that was revealed by Traint and Pichler et al. [119, 120] in Fig. 2.8. Therefore, it is likely that, for the classic steel H(CL) used in this work, lowering the temperature from 350 to, say 325 °C would greatly increase the retained austenite. However, note that Figure. 2.8 does not show the drastic drop seen at 300 °C in Fig. 5.9.

M. Bouet at al [121] suggested that carbide precipitation is caused by the destabilization of the structure following increased super saturation of retained austenite with C at low isothermal annealing temperatures. With increasing C super saturation the remaining two phase austenite present in the isothermal stage becomes unstable and starts to decompose into ferrite and carbide. This reduces the final retained austenite fraction. So the reduction in retained austenite fraction with decreasing isothermal temperature observed in this work may be associated to the formation of carbide precipitation. However, the microstructure in this work appeared to reveal the presence of martensite. In other words, 300 °C is somewhat below the Ms temperature for the intercritically

formed austenite. As will be shown in the discussion of the mechanical properties, this seems to be a much more likely reason for the sudden reduction in retained austenite. It also seems reasonable that the highest possible level of retained austenite for a given intercritical anneal temperature would be formed just above the Ms temperature. However, this type of retained austenite may not produce the best *TRIP* properties, but in terms of *TMAS*, the situation may be different.

6.2 Effect of Retained Austenite Fraction on Mechanical Properties of TRIP Steels

As mentioned before, TRIP steels combine increasing strength values with increasing ductility, which is in complete contrast to conventional steels. This enhancement in strength and ductility is brought by the SIT of metastable retained austenite to martensite during deformation. Martensite, apart from being a very strong phase, the transformation of retained austenite to martensite is accompanied by a volume expansion and results in localized increase in strain hardening coefficient during straining. These mechanisms delay the onset of necking and leads to higher uniform and total elongation [122]. In general, it has been established by a number of researchers that any increase in retained austenite fraction brings about an increase in strength and ductility [123-125], although, as noted above, this depends on the stability of the retained austenite.

It was shown in section 5.1.2.1 and in Figure 5.11 that with increasing retained austenite volume fraction the UTS of H(AL) and H(CL) steels increases while it decreases for H(CL) steels. H(AL) and H(CL) steels clearly follow the trend set by literature while CAL steels follow the reverse behavior.

This contrast can be attributed to the high stability of the retained austenite against strain induced transformation, which can be attributed to the much higher C level and much finer austenite particle size. As was seen in Table 5.1, the carbon concentration

of the fine size retained austenite in C(AL) steels is coupled with high carbon concentration in excess if 1.5%. According to Reisner et al. [126], C concentration determines the chemical driving force for the transformation of retained austenite to martensite. Very high carbon concentration leads to high retained austenite stability. Consequently, such highly stable retained austenite particles do not undergo TRIP and an increase in this type of retained austenite will not increase the strength. As well, Chen et al. [127] reported that, for a P containing TRIP steel, retained austenite particles less than 1 μm hardly transformed into martensite, even if necking occurred. Consequently, fine retained austenite particles had only a negligible effect on strength values.

The high C level and fine particle size in C(AL) TRIP steels are, in turn, a function of the pre-TRIP processing microstructure. Unlike H(AL) and H(CL) steels, C(AL) steels have an initial microstructure of deformed ferrite, bainite and martensite (which was retained austenite before cold rolling) obtained via cold rolling a TRIP microstructure. Another study, concerning intercritical annealing of a dual phase structure revealed that the martensitic grains start to transform to low carbon martensite by ejecting carbon out into the surrounding phase in the form of epsilon carbide [128]. Subsequently, austenite grains start to form preferably at intercritical temperature at these carbon rich regions especially at martensite interlath boundaries and martensite-carbide boundaries [129]. In the case of CAL steels, perhaps, austenite might have started forming at these fine epsilon carbides-ferrite boundaries and/or martensite-carbide boundaries during the course of the intercritical annealing. It should be noted that epsilon carbide, $Fe_{2.4}C$, packs more carbon than cementite. The resulting intercritical austenite would be very rich in carbon and fine in size. The corresponding austenite nucleation sites in H(AL) and H(CL) steels would be ferrite/cementite boundaries, which has lower C concentrations and are bigger in size compared to epsilon carbide. Thus, the carbon levels in the retained austenite present in C(AL) TRIP steels may be higher than if the starting microstructure had been ferrite and pearlite. Hanzaki et al., [130] showed that retained austenite particles with higher carbon concentrations increasingly tends to

decompose into carbides and ferrite during cooling from isothermal stage resulting in low final retained austenite fraction. This may explain why C(AL) steels suffer from low retained austenite fraction values.

Alternatively (or additionally), the microstructural features of the nucleation sites in the C(AL) steels tend to be much finer than the corresponding sites in the hot rolled steels, therefore producing a finer retained austenite particle size in the C(AL) steel. The finer intercritically formed austenite may accelerate the bainite transformation, thus leading to less retained austenite, and may also contribute to higher the higher C level.

It should also be mentioned that an increasing proeutectoid ferrite volume fraction in the pre-TRIP structure has also been found to increase the C in retained austenite [131], but the ferrite volume fractions were not measured in this work.

The high carbon concentration in the retained austenite present in C(AL) steels coupled with the fine retained austenite particles size increased the stability of the retained austenite against strain induced transformation.

Now that it is established that the retained austenite particles in C(AL) steel did not undergo TRIP transformation and did not contribute toward strength. The reason for decreasing strength with increasing retained fraction can be explained as follows. For the fixed ferrite volume fraction in the microstructure, the change in retained austenite volume fraction is inversely related to the change in bainitic volume fraction. The stronger bainitic phase tends to act as secondary strengthening agent in the steel microstructures. Consequently, samples with relatively low retained austenite volume fraction tend to be stronger because of higher volume fraction of the stronger bainitic phase. But this increase in strength comes at the cost of ductility, similar to conventional high strength steels. This would explain why the ductility of the C(AL) steels increased with increasing retained austenite fraction, as shown in Figures 5.11 and 5.12.

Though HAL steels did show an increasing trend of strength and ductility with increasing retained austenite fraction, the extent of this increase was small and was in the same level of strength and ductility values of the C(AL) steels that did not undergo TRIP transformation, Figure 5.13. In fact, for similar retained austenite levels, the H(AL) steels tend to exhibit poorer ductility and strength. The reason for such low values of strength and ductility even after undergoing TRIP transformation can be explained on the basis of the final TRIP microstructure of HAL steels.

As was seen in Figures 5.7 and 5.8, the TRIP microstructures of H(AL) steels were severely banded and had an inhomogeneous distribution of ferritic grain size throughout the microstructure, see Figure 5.8 a and b. Retained austenite particles clustered along the bands due to high saturation of Mn along them. The retained austenite particles in H(AL) steels showed a higher than normal carbon concentration, approximately from 1.1 to 1.4% (Table 5.2) due to the combined action of Mn and Al along the bands in inhibiting carbide formation and promoting carbon saturation of austenite [132]. This excessive carbon saturation may have resulted in some of the retained austenite decomposing to carbide and ferrite during cooling from isothermal stage and consequently may have lowered the final retained austenite fraction.

Kim et al [132] also showed that banding and rafting of microstructures have a detrimental effect on uniform and total elongation. Also, some of the retained austenite particles are encompassed by thick platelets of bainite and carbide as shown in Figures 5.8 and 6.2. These platelets of thick bainite and carbide stabilize the retained austenite particles and resist the shear transformation that accompanies the transformation of retained austenite to martensite during deformation. As a result, these retained austenite particles probably did not undergo TRIP and did not account for strength and ductility.

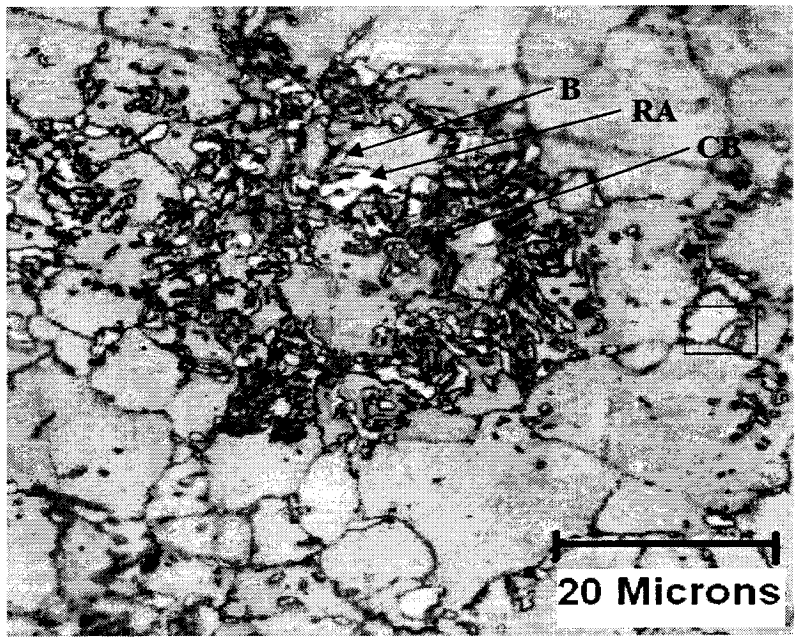

Figure 6.2 Optical micrographs HA1 sample showing retained austenite (RA) encompassed by bainite (B) and carbon rich particles (CB)

The strength and ductility of H(CL) steels increase with increasing volume fraction of retained austenite and the levels are much higher compared to C(AL) and H(AL) steels, Figures 5.11 and 5.12. This is probably because much of the retained austenite is contributing to TRIP, and the microstructure is much more uniform, at least compared to the HAL structure.

This enhanced strength-ductility balance also increases the formability indices of H(AL) and H(CL) TRIP steels, as seen in Figure 5.14. As was noted in section 5.1.2.1, the increase in formability indices with retained austenite fraction in C(AL) steels is marginal compared to the other two steels. Since, TRIP transformation of retained austenite phase did not occur in any of the C(AL) steels, the increment in ductility and hence formability is solely due to the loss of the stronger bainitic phase with increasing retained austenite fraction. Hence, this is no match to the improvement in formability by TRIP effect as observed in other two steels, and consequently the increase in formability is marginal in C(AL) steels.

6.3 Effects of Cold Rolling

As represented in Figure 5.14, the cold rolling operation resulted in pancaking of the microstructure resulting in elongation of grains along the rolling direction. Ho et al [133] performed a similar cold rolling operation on chemically similar TRIP steels to address the extent of retained austenite consumption into SIT martensite during deformation. It was reported that the 69% thickness reduction cold rolling operation consumed all the retained austenite particles and converted them into SIT martensite. Also, Jeong et al [134] performed a similar cold rolling operation to process TMAS from chemically similar TRIP steels. He also reported that a 69% thickness reduction cold rolling transformed all retained particles to martensite. From the above, it can be assumed without any doubt that the 69% thickness reduction cold rolling operation performed in this work would have transformed all of the retained austenite phase into martensite and pancaked the ferritic matrix in conjunction. To summarize, the microstructure of the steels after cold rolling consists of severely deformed ferritic matrix with deformed bainite and SIT martensite distributed throughout the microstructure.

6.4 TMAS Processing

Microstructures of the C(AL), H(AL) and H(CL) TMAS were shown in Figures 5.15, 5.17 and 5.18. As mentioned in Section 5.2.2, the TMAS microstructures of C(AL) steels appear recrystallized with secondary phases distributed throughout the microstructure in a regular fashion, while the H(AL) and H(CL) steels do not show such signs of extensive recrystallization.

Jeong et al [134] suggested that at subcritical annealing temperatures in the range of 500°C to 600°C, a number of fine carbide particles precipitate within the ferritic matrix during the early period of holding at subcritical annealing temperature in addition to SIT martensite undergoing tempering at the same instance, Figure 6.3. The white particles seen in the micrograph are epsilon carbide particles with rich carbon content. But,

ripening and coarsening of these carbide particles follow immediately after the precipitation.

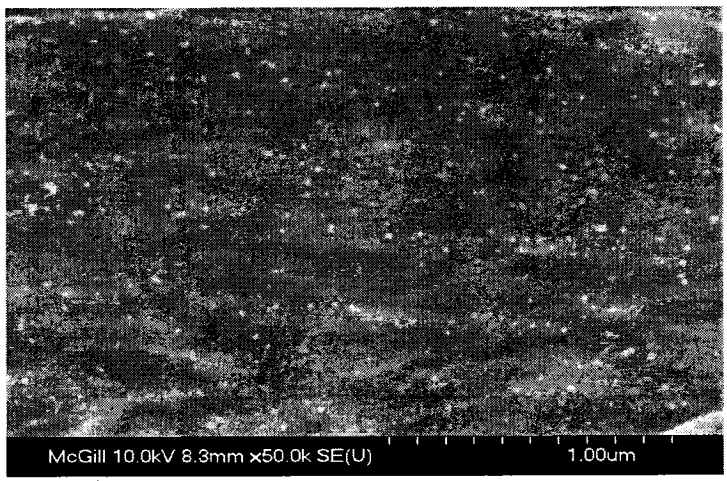

Figure 6.3 SEM micrograph of Al containing TMAS showing nucleation of fine carbides after subcritically annealing at 500°C [135]

He also made a strong note that even at a high subcritical annealing temperature of 500°C; the SIT martensite particles did not undergo any recrystallization, though they were softening due to tempering. As a result, these tempered martensite particles were pinning up a huge fraction of the deformed ferritic matrix from undergoing recrystallization. However, since these martensite particles are mainly within the bainite bands, it is not clear how these would affect the recrystallization of the ferrite bands.

Nevertheless, Jeong's observations appear to be in accord with the results observed for the H(AL) steel where the ferritic matrix did not undergo any substantial recrystallization and a significant amount of the cold rolled structure was preserved even after tempering at 500°C. It is believed that the highly irregular prior TRIP structure of H(AL) steels resulted in a pancaked structure with thick bainitic bands preventing recrystallization from occurring homogenously during tempering. Poor recrystallization response was observed by Kim et al., [135] for chemically similar steel with bands in the microstructure, even at high intercritical temperatures. No reason was

specifically stated for the poor recrystallization response. This is in accordance with the results observed for HAL steels. Note that the possible effect of Al precipitates cannot be eliminated, especially in view of the very high Al levels in the H(AL) steel, although Jeong et al [137] were not able to find any Al bearing precipitates.

C(AL) TMAS on the other hand, have homogenous microstructures; see Figure 5.15, which contradicts the suggestions made by Jeong et al [136, 137] about the preservation of the cold rolled structure even after tempering at 500°C, since microstructural inhomogenities are absent. One other possibility by which the absence of extensive recrystallization can be explained is through the presence and amount of tempered martensite present. As listed in Table 5.4, the tempered martensite volume fractions present in C(AL) TMAS are very low and are limited in range compared to H(AL) and H(CL) steels. Consequently, it can be suggested that there were few unrecrystallized tempered martensite particles pinning up the ferritic matrix from undergoing complete recrystallization. As a result, the ferritic matrices in C(AL) TMAS were able to undergo extensive recrystallization with ease compared to H(AL) and H(CL) where the matrices were pinned up by a large fraction of tempered martensite particles, for the same subcritical heat treatment temperature and time.

6.5 Effect of Tempered Martensite Volume Fraction on Mechanical Properties of TMAS

The mechanical properties of TMAS strongly depend on the volume fraction of tempered martensite particles distributed in their microstructure. This is analogous to DP steels where the mechanical properties are dependent on martensite volume fraction. But the two steels differ from each other to a great extent on the basis how these martensitic particles are introduced. When DP steels are intercritically annealed and quenched, whatever intercritical austenite that was present in two-phase region will transform into martensite [138]. But in the case of TMAS, the martensite particles are

introduced through the SIT retained austenite during cold rolling of TRIP steels. However, the martensite particles present in both steels account toward the variation in mechanical properties. The results shown in section 5.2.3 will be discussed in the following passages. Given the limited availability of literary resources on TMAS processing and testing, the mechanical properties of these steels will be compared with reference to DP and other advanced steels hitherto.

It was noticed from Figure 5.19 that the UTS of all the three types of TMAS, namely, C(AL), H(AL) and H(CL) TMAS increased with increasing volume fraction of tempered martensite. This is entirely expected. What is somewhat less predictable is that all the values more or less fall on the same curve, which is in complete contrast to these steels in the TRIP condition, where they exhibited three distinct behaviors (Figure 5.11).

The differences in deformation behavior that led to the differences seen in the UTS behavior of these steels under TRIP condition were postulated to be the retained austenite characteristics, and the banded structure. Certainly, TMAS has eliminated the different ways in which retained austenite responded to deformation, vis a vis SIT vs. non SIT vs. some SIT. In TMAS, all the retained austenite has been transformed to tempered martensite. This may well be the main reason why these TMAS has rendered these steels 'similar'. The effect of banding, which was postulated to be very detrimental to UTS is now seen in the H(CL) TMAS structure, as well as the H(AL) TMAS structure. However, the C(AL) TMAS exhibits no banding, and it is therefore difficult to explain why it appears to belong to the same population as the other two TMAS steels.

Another point of interest is the CL-9T H(CL) TMAS with the very low retained austenite prior to cold rolling. Recall that the low retained austenite was thought to be due to transformation of some of the intercritical austenite to martensite. If this is true, then the true amount of tempered martensite in the TMAS structure is higher than the

retained austenite amount prior to cold rolling. Whatever is the true value of the tempered martensite, the UTS is much lower than expected from all the other steels and microstructures. This may be because martensite formed on quenching would have a lower C content, and would temper faster, therefore generating a much softer tempered martensite compared to the SIT produced martensite. This implies that the ductility of this steel would be 'abnormally' high, and this appears to be the case (Figure 5.20).

Looking more globally at the TMAS elongation results (Figure 5.20), TMAS appears to have increased or at least maintained the differentiation between the three series of steels (compare Figure 5.20 with Figure 5.12). Perhaps the condition of the proeutectoid ferrite is affecting the ductility more than it affects the strength. For example, the H(CL) TMAS, which shows the best ductility performance, exhibited more recrystallization than the H(AL) TMAS. However, the C(AL) TMAS seems to have undergone the most recrystallization, has the worst ductility. The recrystallized structure, seems to have many relatively coarse particles, however (Figure. 5.15), and these may be very detrimental to ductility.

Formability indices of all the three types of TMAS decreases with increasing fraction of tempered martensite in the microstructure. This is an expected outcome, since formability index, as mentioned earlier, is a product of UTS and total elongation and any substantial decrease in total and uniform elongation reduces the formability indices of the steels, as noted by Engl et al [139] for conventional HSLA steel. But on a closer look at tables 5.4 and 5.5, one can observe that the formability indices of TMAS are in close range with the formability indices of TRIP steels. This is further illustrated in Figure 6.4 which is a graphical representation of variation of formability index of TRIP and TMAS with retained austenite and tempered martensite fraction, respectively.

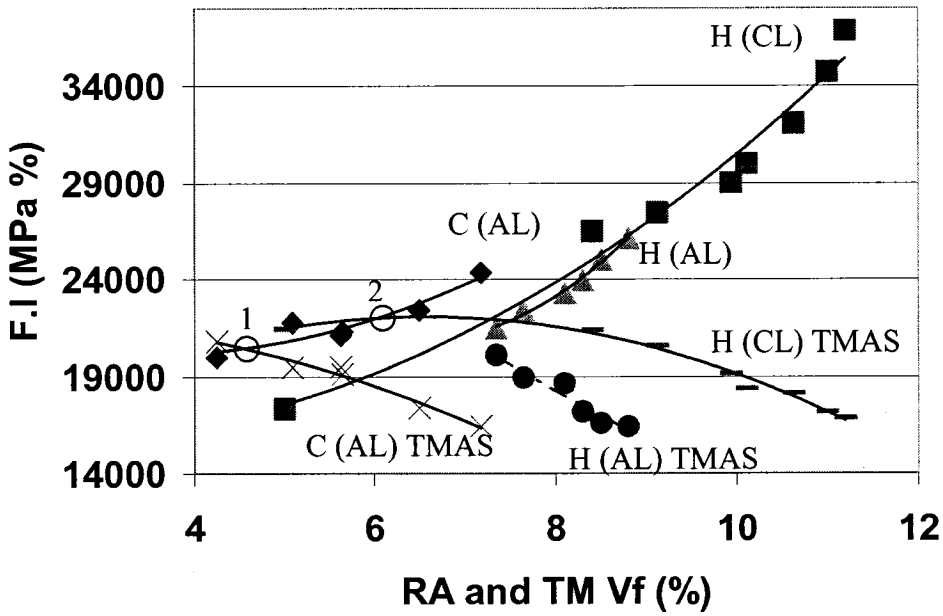

Figure 6.4 Comparison of FI between TMAS and TRIP. 1 and 2 are points of intersection between curves of TRIP and TMAS

From this figure one can notice the points of intersection, shown by a circle between curves of TRIP and TMAS, exhibiting the same formability index. Though they have the same formability index, at those points the strength levels associated with the steels are very different. For example, at intersection point 1, both C(AL) TRIP and C(AL) TMAS have the same formability index of 21000 MPa%, but C(AL) TRIP has an UTS of only 640 MPa while C(AL) TMAS has an UTS of 875 MPa. There is an obvious difference in strength by 235 MPa for the same formability index, which is very significant.

This is a remarkable quality because such high formability values are not generally observed at such high strength levels for conventional high strength steels. Table 6.1 was adopted from Schumann et al., [140] which presents the average mechanical properties of a number of conventional materials used predominantly in the automotive industry.

Table 6.1 Mechanical Properties of Conventional Steels

Steel Grade	YS (MPa)	TS (MPa)	%El (%)	FI (MPa %)
DP 500	345	540	26	14040
DP 600	350	620	26	16120
TRIP 700	390	725	24	17400
TRIP 800	450	800	27	21600

Figure 6.5 further explains the significant differences in strength between TMAS and TRIP. It is very clear from the Figure that at any given volume fraction of RA, there is a significant difference in strength of 150 MPa between TMAS and TRIP. Of particular note is the retained austenite in the C(AL) steel. In the TRIP condition, the retained austenite did not enhance the mechanical properties. However, tempered martensite particles present after TMAS contributed strongly towards the mechanical properties, especially strength. Thus, it can be clearly noted that tempered martensite particles do not have any stability constraints which may prevent contributions to strength, as is the case of retained austenite TRIP steels.

Comparison of TMAS properties to commercial TRIP steel properties listed in Table 6.1 indicates that for the same formability range of 21000 MPa%, TMAS offers in excess of 900 MPa strength compared to only 800 MPa in the case of TRIP 800. Due consideration has to be given to the fact that TRIP 800 is one of the strongest, if not the strongest of all automotive steel available in today's market. Since steel crashworthiness strongly depends on UTS [141], TMAS with better strength than TRIP steels should promote better crashworthiness without compromising formability.

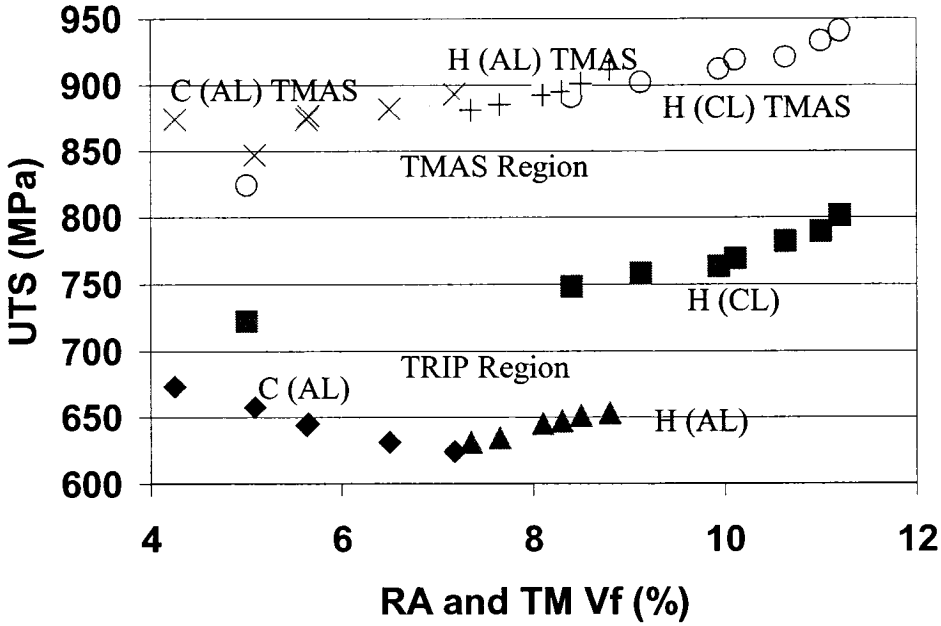

Figure 6.5 Comparison of strength between TMAS and TRIP.

Figure 6.6 is a schematic representation of the revised strength-formability graph adopted from Chapter 1 with the inclusion of TMAS produced in this work. One can see that TMAS exhibits good strength-formability balance, overlapping significantly with TRIP, DP and Martensitic steels, which is a significant contribution, but not significant enough to push the maximum strength-formability balance boundary set by the TRIP steel

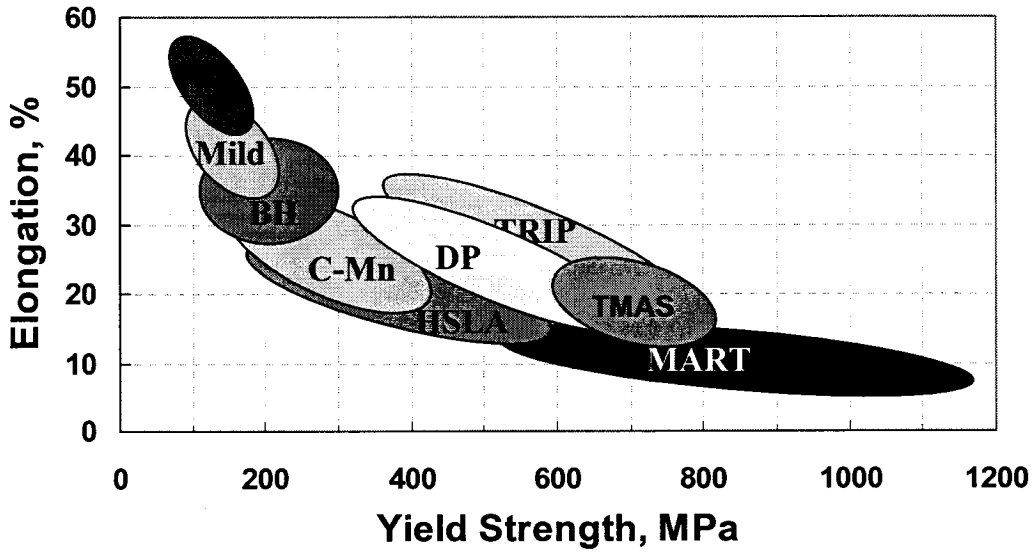

Figure 6.6 Schematic representation of strength-ductility balance of conventional automotive steels, including TMAS

CHAPTER 7

Conclusions

Classic TRIP steel and Al TRIP steel strips were processed into respective Tempered Martensite Assisted Steels (TMAS). The influence of retained austenite and tempered martensite particles on mechanical properties of TRIP and TMAS were studied, respectively. The conclusions are summarized below.

1. Two different TRIP steels, 1) a Si containing "classic" H(CL) TRIP steel and 2) Al containing TRIP steels with two different initial conditions, C(AL) and H(AL), were TRIP annealed with different parameters to achieve different levels of retained austenite volume fraction in the final structure.

2. After TRIP annealing, C(AL) TRIP steels exhibited the least values of retained austenite volume fraction and range, while H(CL) exhibited the most and H(AL) TRIP steels occupied the middle grounds between C(AL) and H(CL) TRIP steels.

3. The retained austenite particles in C(AL) TRIP steels were very fine in size, approximately 0.5 to 2 μm compared to 1 to 3 and 2 to 5 μm in H(AL) and H(CL) TRIP steels, respectively.

4. Small grain size and low values of retained austenite volume fraction of C(AL) TRIP are associated to the following reasons.

- *Complex starting microstructure:* C(AL) TRIP steels had a starting microstructure of deformed ferrite, bainite and SIT martensite compared to ferrite and pearlite in H(CL) and H(AL) TRIP steels. During intercritical annealing preferential nucleation of fine intercritical austenite occurred along epsilon carbides-ferrite boundaries, which has higher C content than ferrite-cementite boundaries. Austenite particles retained from such fine intercritical austenite were excessively rich in carbon concentration, greater than 1.6% vs. 0.7 to 1.4%. of H(AL) and H(CL) steels.

- *Precipitation of carbides during cooling and/or extensive bainite formation:* Retained austenite particles with excessive carbon concentration decomposed into carbides and ferrite during cooling from isothermal stage lowering the final retained austenite volume fraction. Alternatively (or additionally) the finer intercritically formed austenite may have accelerated the bainite transformation, thus leading to less retained austenite, and may also contribute to higher the higher C level.

5. Excessive carbon concentration and very fine grain size of retained austenite in C(AL) steels resulted in absolutely no SIT of retained austenite to martensite during mechanical testing. Consequently, the highly stable retained austenite particles did not contribute toward the mechanical properties, especially strength and formability. The strength of the C(AL) TRIP steels decreased with increasing retained austenite fraction due to the loss of the stronger bainitic phase. Conversely, the total elongation and formability increased with increasing retained austenite fraction.

6. H(AL) TRIP steels microstructure exhibited severe banding and rafting with ferritic grains in excess of 20 microns in size between the bands.

- Retained austenite particles clustered along the bands due to high saturation of Mn along them. The retained austenite particles in H(AL) steels showed a higher than normal carbon concentration, approximately from 1.1 to 1.4% due to the combined action of Mn and Al along the bands in inhibiting carbide formation and promoting carbon saturation of austenite. This excessive carbon saturation resulted in some of the retained austenite decomposing to carbides and ferrite during cooling from isothermal stage and consequently lowered the final retained austenite fraction.

- Some of the retained austenite particles along the bands were encapsulated by thick platelets of bainite and carbide, making them less amenable to SIT during testing. Consequently the mechanical properties, especially strength and total elongation did not increase significantly with increasing fraction of retained austenite, since some of the retained austenite particles did not undergo SIT.

7. In H(CL) TRIP steels:

   - The retained austenite morphology changed from bainitic interlath film type to isolated islands encapsulated by bainitic grains with decreasing isothermal bainite temperature.

   - At very low isothermal temperatures, especially below 325°C, most of the intercritical austenite converted into martensite during quenching to isothermal temperature from intercritical region.

8. In general,

   - H(CL) steels exhibit better retained austenite retention capacity, and consequently the highest retained austenite levels, and the highest mechanical properties corresponding to these levels.

- The C(AL) steels exhibit the lowest austenite retention levels, but at these low RA values, the C(AL) steel exhibits the best elongation and formability values.
- The H(AL) steels are slightly better at retaining austenite compared to the C(AL) steels, but tend to be inferior to the C(AL) steels for the same level of RA in terms of elongation and formability.

9. Subcritical heat treatment of the cold rolled TRIP structure initiated recrystallization of the ferritic matrix, tempering of SIT martensite.

- Compared to H(AL) and H(CL) TMAS, recrystallization of the ferritic matrix in C(AL) TMAS was comparatively more complete due to minimum availability of tempered martensite particles which act as grain boundary pinning agents.
- The ferritic matrix in H(AL) and H(CL) steels owing to their higher tempered martensite fraction did not undergo significant recrystallization and much of the cold rolled structure was preserved. In comparison the H(CL) steels were more amenable to recrystallization.
- However, it is not clear of how these martensite particles present mainly within the bainite bands, would affect the recrystallization of the ferrite bands.

10. With increasing tempered martensite volume fraction the UTS of TMAS increases significantly while the total elongation and formability index of TMAS decreased.

11. The TMAS obtained CL-9T TRIP sample containing martensite created due to quenching in the isothermal region has the lowest value of strength and abnormally high value of total elongation due to faster tempering and softening

of low carbon 'quenched' martensite compared to 'SIT' martensite with higher carbon in other TMAS samples.

12. Though the formability indices of TMAS decreases with increasing fraction of tempered martensite, the formability index values are in close range with the values observed for TRIP, DP and other high strength automotive steels.

13. For a given formability index value, TMAS offers better strength values compared to TRIP steels (a minimum difference of approximately 150MPa), and consequently can offer better crashworthiness.

14. TMAS exhibit mechanical properties that overlap with TRIP, DP and high strength martensitic steels, but it fails to push the strength-ductility balance threshold set by TRIP steels.

15. TMAS with its excellent combination of strength and formability has the potentials to replace TRIP and other high strength steels in automotive applications.

REFERENCES

1. M. D. Meyer, D. Vanderschueren and B. C. D Cooman, ISIJ International, Vol. 39, No.8, 1999, 813.
2. P. J. Jacques, P. H. Hartlet and F. Delannay, Int. Conf. on TRIP-Aided High Strength Ferrous Alloys, Ghent, 2002, 129.
3. B. Mintz, International Materials Review, Vol. 46, 2001, 169.
4. T. Jeong, S. Yue and E. Es-sadiqi, MS&T Conference Proceedings, 2004, 725.
5. C. M. Parish, Master's Thesis, University of Pittsburg, Pittsburg, 2003, 8.
6. V. F. Zackay, E. R. Parker, D. Fahr and R. Bush, Trans. Am. Soc. Mat., Vol. 60, 1967, 252.
7. C. M. Parish, Master's Thesis, University of Pittsburg, Pittsburg, 2003, 9.
8. L. Laquerbe, J. Neutjens, Ph. Harlet, F. Caroff and P. Cantinieaux, 41st MWSP Conf. Proc. ISS, Vol. 37, 1999, 89.
9. M. L. Brandt, PhD Thesis, Northwestern University, Illinois, 1997, 18.
10. B. Mintz, International Materials Review, Vol. 46, 2001, 169.
11. J. Mahieu, B.C. De Cooman, J. Maki and S. Claessens, Iron and Steel Maker, Vol. 29, 2002, 29.
12. H. C. Chen, H. Era and M. Shimizu, Metallurgical Transactions A, Vol. 20A, 1989, 437.
13. J. Zhao, O. Matsumara, Y. Sakuma and Y. Ishii, ISIJ International, Vol. 32, No. 10, 1992, 1110.
14. Y. Sakuma, O. Matsumara and H. Takeshi, Metallurgical Transactions A, Vol. 22A, 1991, 489.
15. P. Jacques, X. Cornet, P. Harlett, J. Ladriere and F. Delannay, Metallurgical Transactions A, Vol. 29A, 1998, 2383.

16. A. Z. Hanzaki, PhD Thesis, McGill University, Montreal, 1994, 38.
17. P. J. Jacques, P. H. Hartlet and F. Delannay, Int. Conf. on TRIP-Aided High Strength Ferrous Alloys, Ghent, 2002, 129.
18. H. B. Ryu, J. G. Speer and J. P. Wise, Metall. And Mat. Trans. A, Vol. 33A, 2002, 2811.
19. H. T. Fei, Master's Thesis, McGill University, Montreal, 2003, 21.
20. A. Pichler, P. Stiaszny, R. Potzinger, R. Tikal and E. Werner, 40th MWSP Conference Proceedings, Pittsburg, 1998, 259.
21. A. P. Coldren, G. Tither, A. Conford and J. R. Hiam, Formable HSLA and DP Steels, ed. A. D. Davenport, TMS/AIME, Warrendale, PA, 1979, 205.
22. H. C. Chen, H. Era and M. Shimizu, Metallurgical Transactions A, Vol. 20A, 1989, 437.
23. S. Traint, A. Pichler, P. Stiaszny and F. A. Werner, 42nd MWSP Conf. Proc., 2000, 549.
24. A. Z. Hanzaki, P. D. Hodgson and S. Yue, Metallurgical Transactions A, Vol. 28A, 1997, 2405.
25. A. D. Chiro, Master's Thesis, McGill University, Montreal, 1997, 91.
26. M. P. Bouet, Master's Thesis, McGill University, Montreal, 1999, 68.
27. A. Z. Hanzaki, PhD Thesis, McGill University, Montreal, 1994, 124.
28. A.N Vaisilakos, J. Ohlert, K. Giasla, G. N. Haidemenopoulos and W. Bleck, Int. Conf. on TRIP aided high strength ferrous alloys, 2002, 277.
29. M. P. Bouet, Master's Thesis, McGill University, Montreal, 1999, 54.
30. W. C. Jeong, D. K. Matlock and G. Krauss, Mat. Science and Eng. A, 165, 1993, 1.
31. A. Itami, M. Takashi and K. Ushioda, ISIJ International, Vol. 35, No. 9, 1995, 1121.
32. S. J. Kim, C. G. Lee. I. Choi and S. Lee, Metallurgical and Materials Transcations A, Vol. 32A, 2001, 505.
33. W. Bleck, Int. Conf. on TRIP aided high strength ferrous allys, GRIPS, Ghent, 2002, 13.
34. D. C. Ludwigson and A. J. Berger, J. Iron and Steel Inst., 207, 1969, 63.

35. A. Itami, M. Takashi and K. Ushioda, ISIJ International, Vol. 35, No. 9, 1995, 1121.
36. A. J. DeArdo, M. Gray and L. Meyer, Niobium, Proc. of Int. Symp. 1981, 685.
37. J. Y. Koo and G. Thomas, Formable HSLA and DP Steels, ed. A. D. Davenport TMS/AIME, Warrendale, PA, 1979, 256.
38. M. F. Ashby, Materials Selection in Mechanical Design, Butterworth-Heinemann, 1999, 421.
39. R. B. G. Yeo, Trans. Metall. Soc. AIME, 227, 1963, 884.
40. A. J. Goldman and W. Robertson, Acta. Metall., 12, 1974, 1265.
41. A. J. Goldman and W. Robertson, Acta. Metall., 13, 1965, 391.
42. G. R. Speich, A. J. Schwoeble and W. C. Leslie, Metallurgical Transactions A, 3A, 1972, 2031.
43. M. P. Puls and S. J. Kirkaldy, Metallurgical Transactions A, Vol. 3A, 1972, 2777.
44. T. Wada, H. Wada, J. F. Elliot and J. Chipman, Metallurgical Transcations A, Vol. 3A, 1972, 1657.
45. A. D. Chiro, Master's Thesis, McGill University, Montreal, 1997, 91.
46. S. S. Hansen and B. F. Bramfitt, Proc. Inter. Conf. on Steel Rolling, ISIJ, 1980, 1297.
47. J. B. Gilmour, G. R. Purdy and J. S. Kirkaldy, Trans. TMS/AIME, 1964, 1025.
48. P. J. Jacques, E. Girault, A. Mertens, B. Verlinden, J. V. Humbeck and F. Delannay, ISIJ International, Vol. 41, 2001, 1068.
49. S. Traint, A. Pichler, P. Stiaszny and F. A. Werner, 42nd MWSP Conf. Proc., 2000, 549.
50. A. D. Chiro, Master's Thesis, McGill University, Montreal, 1997, 91.
51. A. Pichler, P. Stiaszny, R. Tikal, E. Werner and R. Potzinger, 40th MWSP Conf. Proc., 1998, 259.
52. I. Tsukatani, S. I. Hashimoto, T. Inoue, ISIJ International, Vol. 31, 1991, 992.
53. R. W. K. Honeycombe, 'Steels: Microstructure and Properties', ASM, University of Cambridge, London, England, 1982, 55.
54. S. Zaefferer, J. Ohlert and W. Bleck, Acta Mat. Vol. 52, 2004, 2765.

55. A. D. Chiro, Master's Thesis, McGill University, Montreal, 1997, 91.

56. J. B. Gilmour, G. R. Purdy and J. S. Kirkaldy, Trans. TMS/AIME, 1964, 1025.

57. J. Immamura and T. Furukawa, Nippon steel Technical Report Overseas, 10, 1977, 103.

58. K. I. Sugimoto, N. Usui, M. Kobayashi and S. I. Hashimoto, ISIJ International, Vol. 32, No. 12, 1992, 1311.

59. Z. Nishiyama, Martensitic Transformation, Academia Press, 1978,.

60. K. Sugimoto, M. Misu, M. Kobayashi and H. Shirashawa, ISIJ International, Vol. 33, 1993, 775.

61. T. V. Rajan, C. P. Sharma and A. Sharma, Heat Treatment: Principles and Techniques, Prentice Hall India, New Delhi, 1999, 114.

62. T. V. Rajan, C. P. Sharma and A. Sharma, Heat Treatment: Principles and Techniques, Prentice Hall India, New Delhi, 1999, 117.

63. M. Sudo, I. Tsukatani, Z. Shibata, Metallurgy of Continuous-Annealed Sheet Steel, Dallas, 19, 1982.

64. G. R Speich, R. L. Miller, Fundamentals of Dual-Phase Steels, Chicago, 279, 1981

.

65. T. Waterschoot, M. DeCooman and S. Vandeputte, Metallurgical Transactions A, Vol. 34A, No. 3A, 781.

66. M. De. Meyer, D. Vanderschueren and B. C. De Cooman, ISIJ International, Vol. 39, No.8, 1999, 813.

67. T. Jeong, S. Yue and E. Es-sadiqi, MS&T Conference Proceedings, 2004, 725.

68. T. Jeong, Master's Thesis, McGIll University, Montreal, 2005, 48.

69. S. Traint, A. Pichler, P. Stiaszny and F. A. Werner, 43 MWSP Conf. Proc., ISS, Charlotte, 2001, 411.

70. A. Pichler, P. Stiaszny, R. Tikal, E. Werner and R. Potzinger, 40th MWSP Conf. Proc., 1998, 259.

71. G. N. Haidemenepoulos and A. N. Vasilokos, Steel Resecarh, Vol. 67, 1996, 513.

72. A. Z. Hanzaki, P. D. Hodgson and S. Yue, ISIJ International, Vol. 35, 1995, 79.

73. L. Laquerbe, J. Neutjens, Ph. Harlet, F. Caroff and P. Cantinieaux, 41st MWSP Conf. Proc. ISS, Vol. 37, 1999, 89.
74. T. Jeong, S. Yue and E. Es-sadiqi, MS&T Conference Proceedings, 2004, 725.
75. H. Ho, Master's Thesis, McGill University, Montreal, 2004, 75.
76. S. Traint, A. Pichler, P. Stiaszny and F. A. Werner, 42nd MWSP Conf. Proc., 2000, 549.
77. A. Pichler, P. Stiaszny, R. Tikal, E. Werner and R. Potzinger, 40th MWSP Conf. Proc., 1998, 259.
78. J. Mahieu, B.C. De Cooman, J. Maki and S. Claessens, Iron and Steel Maker, Vol. 29, 2002, 29.
79. K. W. Andrews, ISIJ International, Vol. 20, No. 3, 1965, 721.
80. Y. Sakuma, O. Matsumara, O. Akisue, ISIJ International, Vol. 31, No. 11, 1991, 1348.
81. T. Jeong, S. Yue and E. Es-sadiqi, MS&T Conference Proceedings, 2004, 725.
82. M. D. Meyer, D. Vanderschueren and B. C. D Cooman, ISIJ International, Vol. 39, No.8, 1999, 813.
83. K. Ishida and T. Nishizawa, Trans. Jpn. Inst. Met., Vol. 15, 1974, 225.
84. K. I. Sugimoto, N. Usui, M. Kobayashi and S. I. Hashimoto, ISIJ International, Vol. 32, No. 12, 1992, 1311.
85. T. Jeong, S. Yue and E. Es-sadiqi, MS&T Conference Proceedings, 2004, 725.
86. H. Ho, Master's Thesis, McGill University, Montreal, 2004, 75.
87. A. M. Elwazri, P. Wanjara and S. Yue, Canadian Metallurgical Quarterly, Vol. 45, No.1, 33.
88. G. E. Lucas, Journal of Nuclear Materials, 117, 1983, 327.
89. L. Zhao, N. H. V. Dijk, E. Bruck, J. Sietsma and S. V. Zwaag, Materials Science and Engineering A, 313, 2001, 145.
90. S. J. Kim, C. G. Lee. I. Choi and S. Lee, Metallurgical and Materials Transcations A, Vol. 32A, 2001, 505
91. M. P. Bouet, Master's Thesis, McGill University, Montreal, 1999, 54.

92. S. J. Kim, C. G. Lee. I. Choi and S. Lee, Metallurgical and Materials Transcations A, Vol. 32A, 2001, 505.
93. A. Z. Hanzaki, PhD Thesis, McGill University, Montreal, 1994, 124.
94. A. D. Chiro, Master's Thesis, McGill University, Montreal, 1997, 50.
95. M. P. Bouet, Master's Thesis, McGill University, Montreal, 1999, 68.
96. M. P. Bouet, Master's Thesis, McGill University, Montreal, 1999, 54.
97. S. J. Kim, C. G. Lee. I. Choi and S. Lee, Metallurgical and Materials Transcations A, Vol. 32A, 2001, 505.
98. M. P. Bouet, Master's Thesis, McGill University, Montreal, 1999, 54 -55.
99. V. F. Zackay, E. R. Parker, D. Fahr and R. Bush, Trans. Am. Soc. Mat., Vol. 60, 1967, 252.
100. C. M. Parish, Master's Thesis, University of Pittsburg, Pittsburg, 2003, 31.
101. A. Z. Hanzaki, PhD Thesis, McGill University, Montreal, 1994, 124.
102. S. J. Kim, C. G. Lee. I. Choi and S. Lee, Metallurgical and Materials Transcations A, Vol. 32A, 2001, 505.
103. S. J. Kim, C. G. Lee. I. Choi and S. Lee, Metallurgical and Materials Transcations A, Vol. 32A, 2001, 505.
104. T. Jeong, S. Yue and E. Es-sadiqi, MS&T Conference Proceedings, 2004, 725.
105. A. Z. Hanzaki, PhD Thesis, McGill University, Montreal, 1994.
106. T. Jeong, Master's Thesis, McGIll University, Montreal, 2005, 42.
107. H. Ho, Master's Thesis, McGill University, Montreal, 2004, 75.
108. T. Jeong, Master's Thesis, McGIll University, Montreal, 2005, 43-44.
109. J. H. Cheng, PhD Thesis, Pohang University of Science and Tech., Pohang, 1994, 64.
110. Y. Sakuma, ISIJ International, Vol. 27, 1987, 570.
111. C. G. Lee et al, J. Kor. Inst. Metall. Mater., Vol. 36, 1998, 1382.
112. S. J. Kim, C. G. Lee, I. Choi, J. Kor. Inst. Metall. Mater., Vol. 37, 1999, 774.
113. C. M. Parish, Master's Thesis, University of Pittsburg, Pittsburg, 2003, 96.
114. S. J. Kim, C. G. Lee. I. Choi and S. Lee, Metallurgical and Materials Transcations A, Vol. 32A, 2001, 505.

115. M. L. Brandt, PhD Thesis, Northwestern University, Illinois, 1997, 88.

116. S. V. Zwaag, Int. Conf. on TRIP-aided High Strength Ferrous Alloys, Ghent, 2002, 141.

117. S. J. Kim, C. G. Lee. I. Choi and S. Lee, Metallurgical and Materials Transcations A, Vol. 32A, 2001, 505.

118. B. Mintz, International Materials Review, Vol. 46, 2001, 169.

119. S. Traint, A. Pichler, K. Hauzenberger, P. Stianszy, E. Werner, Int. Conf. on TRIP aided high strength ferrous alloys, 2002, 121.

120. A. Pichler, P. Stianszy, R. Potzinger, R. Tikal, F. Werner, 40th MWSP Conf., 1998, 259.

121. M. P. Bouet, Master's Thesis, McGill University, Montreal, 1999, 54.

122. C. M. Parish, Master's Thesis, University of Pittsburg, Pittsburg, 2003, 31.

123. B. Ehrhardt, B. Engl, T. Gerber and U. Schrieven, Proc. SAE World Congress, 1998, 1377.

124. T. Jeong, Master's Thesis, McGill University, Montreal, 2005, 66.

125. N. C Goel, J. P Chakravarthy, K. Tangri, Met. Trans A, V18A, 1987, 5.

126. G. Reisner, F. D. Fischer, E. Werner, K. Tanaka, G. Cailletaud and T. Antretter, International Journal of Plasticity, Vol. 16, 2000, 723.

127. H. C. Chen, H. Era and M. Shimizu, Metallurgical Transactions A, Vol. 20A, 1989, 437.

128. A. P. Coldren, G. Tither, A. Conford and J. R. Hiam, Formable HSLA and DP Steels, ed. A. D. Davenport, TMS/AIME, Warrendale, PA, 1979, 205.

129. K. Ishida and T. Nishizawa, Trans. Jpn. Inst. Met., Vol. 15, 1974, 225.

130. D. S. Leem, Y. D. Lee, J. H. Jun and C. S. Choi, Scripta Materialia, V45, 2001, 767.

131. H. Ho, Master's Thesis, McGill University, Montreal, 2004, 70.

132. S. J. Kim, C. G. Lee. I. Choi and S. Lee, Metallurgical and Materials Transcations A, Vol. 32A, 2001, 505.

133. H. Ho, Master's Thesis, McGill University, Montreal, 2004, 79.

134. T. Jeong, Master's Thesis, McGill University, Montreal, 2005, 68.

135. S. J. Kim, C. G. Lee, I. Choi, J. Kor. Inst. Metall. Mater., Vol. 37, 1999, 774.

136. T. Jeong, Master's Thesis, McGill University, Montreal, 2005, 68.

137. T. Jeong, Master's Thesis, McGill University, Montreal, 2005, 67 - 68.

138. D. T. Llewellyn and D. J. Hilis, Iron and Steelmaking, Vol. 23, No. 6, 1996, 471.

139. B. Engl, B. Ehrhardt, T. Gerber and U. Schrieven, Proc. SAE World Congress, 1998, 1377.

140. T. W. Schumann, Proc. SAE World Congress, 1998, 1383.

141. K. Ishida and T. Nishizawa, Trans. Jpn. Inst. Met., Vol. 15, 1974, 225.

APPENDIX A

As has been mentioned before, the shear punch test is similar to a blanking operation. During the test, the load P on the punch and the tool (i.e. actuator) displacement d are both recorded.

The yield strength of test materials in this work was calculated from the load vs. displacement curve by ascertaining the initial point of non-linearity along the elastic loading line and plugging in the load at that point into the formula,

$$Y.S = \frac{P_{Y.P}}{2\pi\, c_y\, 0.75\, t} \quad \text{..... (A-1)}$$

Where, Y.S is the yield strength of the test sample, $P_{Y.P}$ is the load at the initial point of non-linearity in the load vs. displacement curve (Yield Point), C_y is the yield strength correlation coefficient, in this case, it is 0.644, t is the sample thickness and finally the constant 0.75 is the average of the radii of the punch and the die. Similarly, for the measurement of the UTS, the load $P_{Y.P}$ and correlation factor C_y in equation A-1 has to be replaced with P_{max} and C_{UTS}, respectively. Where, P_{max} is the maximum load attained in the test before fracture and C_{UTS} is the UTS correlation coefficient, which is 0.799 in this work.

The total elongation of the test specimen after the test is calculated using the following equation.

$$T.E = \frac{d_f}{C_e t} \quad \text{..... (A-2)}$$

Where, T.E is the total elongation of the test sample, d_f is the displacement at fracture and C_e is the elongation correlation co-efficient and t is the sample thickness, respectively. The value of C_e used in this work is 2.482.

A typical experimental force vs. displacement curve of A4 C(AL) sample is shown in Figure A-1.

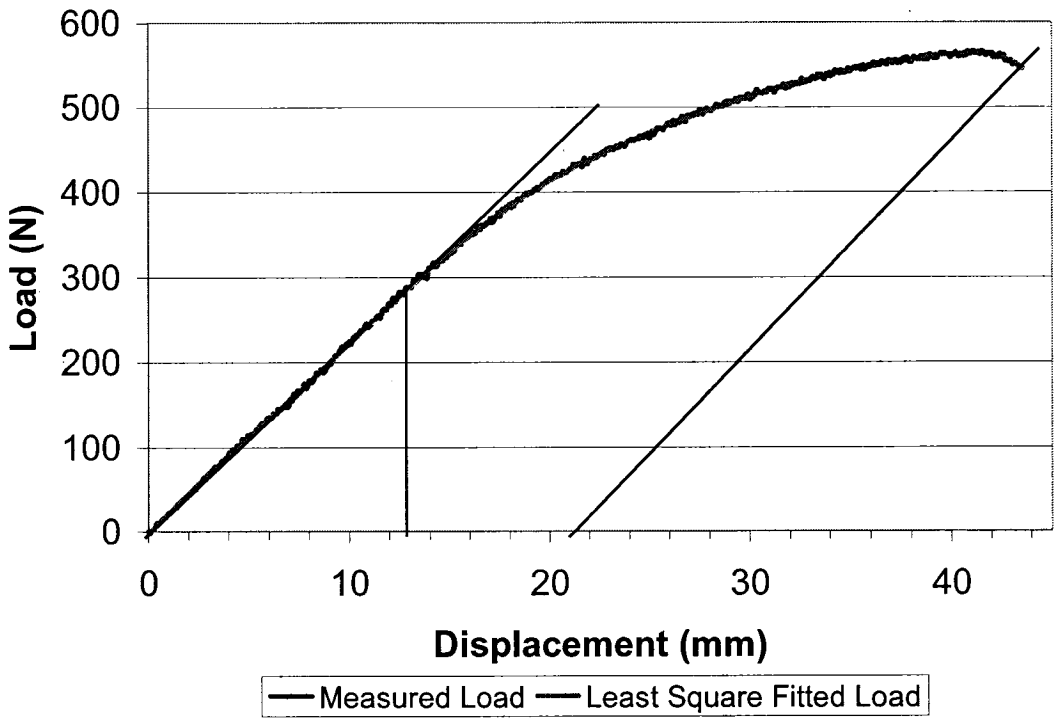

Figure A-1. Experimental load vs. displacement curve of A4 C(AL) TRIP steel sample.

The most obvious difference between this curve and Fig. 4.4., which showed a schematic of an expected shear punch curve, is the absence of the so-called frictional load. There has been some work at McGill (unpublished) that indicates that the friction load may be an artifact associated with alignment of the tool and the die. In any case, F is taken as being zero. The noise from the data acquisition system makes the measured load noisy and finding the characteristic points, such as yield point and maximum load

from the curve is difficult. To avoid the noise, the measured load is replaced and/or superposed with a least square fitted load obtained through data regression. From this new curve, one can ascertain the point of non-linearity by drawing a line in sync with elastic loading part of the curve, as shown in Figure A-1. Figure A-2 provides the representative load vs. displacement curves of a few other TRIP and TMAS steels.

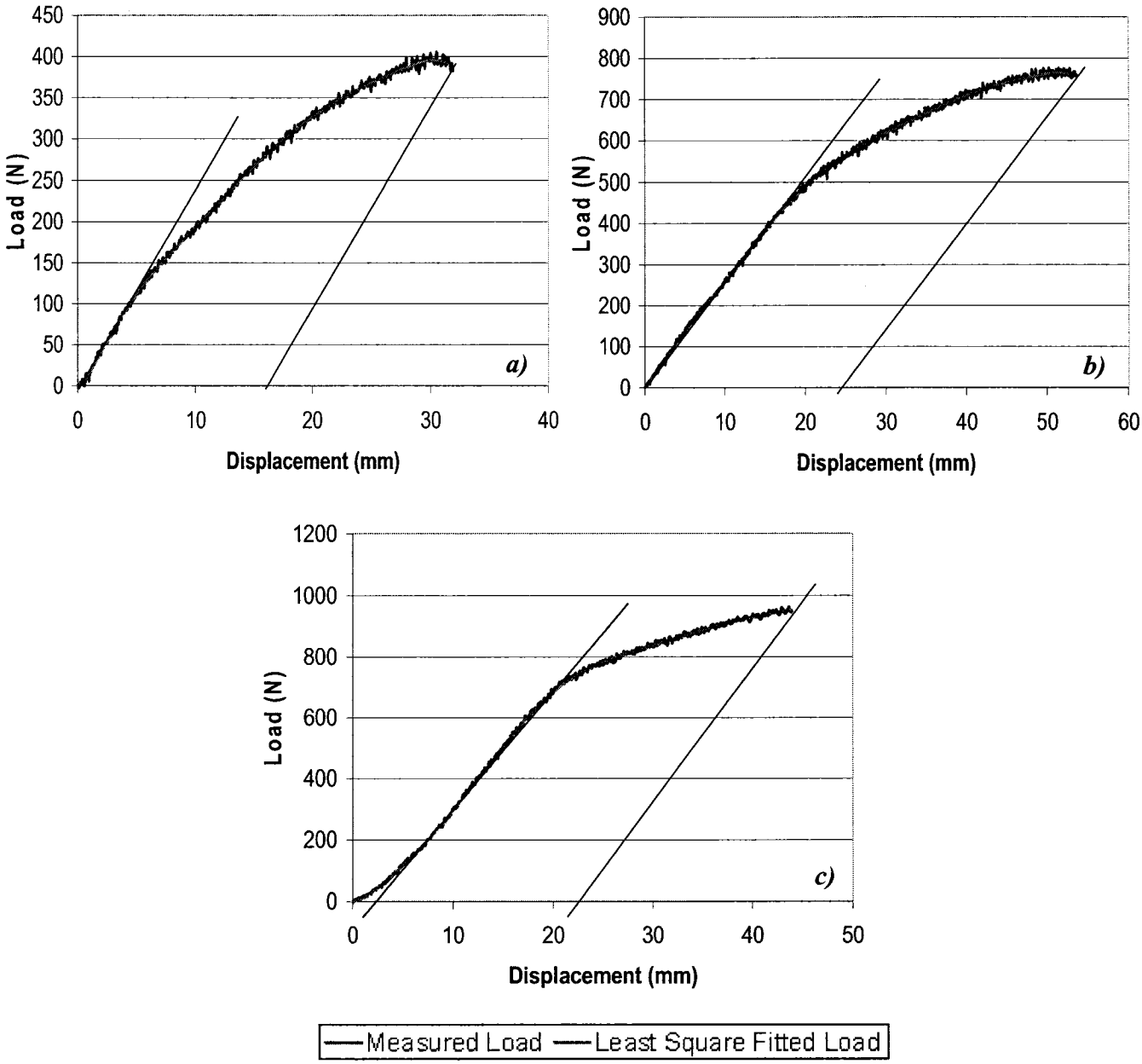

Figure A-2. Experimental load vs. displacement curves of a) A1 C(AL) TRIP b) CL-2T H(CL) TRIP and c) CL-2T TMAS samples.